

Deployment Strategies for High Accuracy and Availability Indoor Positioning with 5G

Jesper Ahlander and Maria Posluk

Master of Science Thesis in Electrical Engineering
**Deployment Strategies for High Accuracy and Availability Indoor Positioning
with 5G:**

Jesper Ahlander and Maria Posluk
LiTH-ISY-EX--20/5303--SE

Supervisors: **Gustav Lindmark**
ISY, Linköping University
Fredrik Gunnarsson
Ericsson AB
Sara Modarres Razavi
Ericsson AB
Deep Shrestha
Ericsson AB

Examiner: **Fredrik Gustafsson**
ISY, Linköping University

*Division of Automatic Control
Department of Electrical Engineering
Linköping University
SE-581 83 Linköping, Sweden*

Copyright © 2020 Jesper Ahlander and Maria Posluk

Abstract

Indoor positioning is desired in many areas for various reasons, such as positioning products in industrial environments, hospital equipment or firefighters inside a building on fire. One even tougher situation where indoor positioning can be useful is locating a specific object on a shelf in a commercial setting.

This thesis aims to investigate and design different network deployment strategies in an indoor environment in order to achieve both high position estimation accuracy and availability. The investigation considers the two positioning techniques downlink time difference of arrival, DL-TDOA, and round trip time, RTT. Simulations of several deployments are performed in two standard scenarios which mimic an indoor open office and an indoor factory, respectively.

Factors having an impact on the positioning accuracy and availability are found to be deployment geometry, number of base stations, line-of-sight conditions and interference, with the most important being deployment geometry. Two deployment strategies are designed with the goal of optimising the deployment geometry. In order to achieve both high positioning accuracy and availability in a simple, sparsely cluttered environment, the strategy is to deploy the base stations evenly around the edges of the deployment area. In a more problematic, densely cluttered environment the approach somewhat differs. The proposed strategy is now to identify and strategically place some base stations in the most cluttered areas but still place a majority of the base stations around the edges of the deployment area.

A robust positioning algorithm is able to handle interference well and to decrease its impact on the positioning accuracy. The cost, in terms of frequency resources, of using more orthogonal signals may not be worth the small improvement in accuracy and availability.

Acknowledgments

We would like to begin by thanking Ericsson for providing us with the opportunity to write this thesis. A special thanks is directed to our supervisors Deep Shrestha, Sara Modarres Razavi and Fredrik Gunnarsson at Ericsson for your constant support, guidance and helpful discussions. You always took your time answering our many questions and helping us when we were confused.

We also want to express our gratitude to our supervisor at Linköping University, Gustav Lindmark, and our examiner, Fredrik Gustafsson, for all valuable input and proofreading.

Finally, we say thank you to our families for the support and to all of our friends for making our time at Linköping University amazing.

*Linköping, June 2020
Jesper Ahlander and Maria Posluk*

Contents

Notation	xi
1 Introduction	1
1.1 Background	1
1.2 Problem Formulation	2
1.3 Limitations	2
1.4 Related Work	3
1.5 Thesis Outline	4
2 Theoretical Background	5
2.1 Positioning Performance Requirements and Metrics	5
2.2 Issues with Indoor Positioning	7
2.3 Positioning Techniques	8
2.3.1 Downlink Time Difference of Arrival	8
2.3.2 Multi-cell Round Trip Time	9
2.4 Cramér-Rao Lower Bound	10
2.4.1 Downlink Time Difference of Arrival	11
2.4.2 Multi-cell Round Trip Time	12
2.5 Geometric Dilution of Precision	12
2.6 Orthogonality	13
2.7 Positioning Reference Signal	14
3 Methodology	17
3.1 Positioning Simulator	17
3.1.1 System Level Simulation	17
3.1.2 Link Level Simulation	18
3.1.3 Time of Arrival Estimator	18
3.1.4 Position Estimator	18
3.1.5 New Functionalities	18
3.2 Deployment Parameters	19
3.2.1 System Level Simulation	19
3.2.2 Link Level Simulation	20
3.3 Link Level Study	21

3.4	Indoor Open Office Study	21
3.4.1	Deployment Scenarios	21
3.4.2	Cramér-Rao Lower Bound Investigation	26
3.4.3	Geometry	27
3.4.4	Interference	27
3.4.5	Line-Of-Sight	29
3.5	Indoor Factory Study	29
3.5.1	Deployment Scenarios	30
3.5.2	Geometry	32
3.5.3	Line-Of-Sight	32
3.5.4	Fallback Positioning Technique	32
4	Simulation Results	35
4.1	Link Level Study	35
4.2	Indoor Open Office Study	37
4.2.1	Theoretical and Simulated Positioning Accuracy	37
4.2.2	Line-Of-Sight	49
4.2.3	Geometry	51
4.2.4	Worst Position Estimates	53
4.2.5	Interference	55
4.3	Indoor Factory Study	59
4.3.1	Simulated Positioning Accuracy	59
4.3.2	Line-Of-Sight	61
4.3.3	Worst Position Estimates	63
4.3.4	Fallback Positioning Technique	70
5	Discussion and Analysis	73
5.1	Indoor Open Office	73
5.1.1	Theoretical and Simulated Positioning Accuracy	73
5.1.2	Geometry	74
5.1.3	Line-Of-Sight	75
5.1.4	Interference	76
5.2	Indoor Factory	77
5.2.1	Simulated Positioning Accuracy	77
5.2.2	Worst Position Estimates	78
5.3	Deployment Strategies for Positioning Accuracy and Availability	78
6	Conclusions and Future Work	81
6.1	Conclusions	81
6.2	Future work	82
A	Additional Results	87
A.1	Indoor Open Office	88
A.1.1	Cramér-Rao Lower Bound	88
A.1.2	Line-Of-Sight	94
A.1.3	Worst Position Estimates	100
A.1.4	Interference	102

A.2	Indoor Factory	105
A.2.1	Line-Of-Sight	105
A.2.2	Worst Position Estimates	106
Bibliography		109

Notation

ABBREVIATIONS

Abbreviation	Description
1G	First Generation
2D	Two Dimensional
3D	Three Dimensional
3GPP	Third Generation Partnership Project
5G	Fifth Generation
AWGN	Additive White Gaussian Noise
BS	Base Station
CDF	Cumulative Distribution Function
CID	Cell ID
CIR	Channel Impulse Response
CRLB	Cramér Rao Lower Bound
DL-TDOA	Downlink Time Difference Of Arrival
FCC	Federal Communications Commission
FDM	Frequency Division Multiplexing
FIM	Fisher Information Matrix
GDOP	Geometric Dilution Of Precision
GNSS	Global Navigation Satellite System
InF	Indoor Factory
InF-DH	Indoor Factory - Dense High
InF-SH	Indoor Factory - Sparse High
IOO	Indoor Open Office
ISD	Inter-Site Distance
LMF	Location Management Function
LOS	Line-Of-Sight
LTE	Long-Term Evolution
NLOS	Non-Line-Of-Sight
OFDM	Orthogonal Frequency Division Multiplexing
OTDOA	Observed Time Difference Of Arrival
PDP	Power Delay Profile
PRS	Positioning Reference Signal
RMSE	Root Mean Square Error
RSTD	Reference Signal Time Difference
RTT	Round Trip Time
SINR	Signal-to-Interference-plus-Noise Ratio
SNR	Signal-to-Noise Ratio
TDOA	Time Difference Of Arrival
TOA	Time Of Arrival
UE	User Equipment

1

Introduction

This chapter presents some background to motivate why this thesis work has been conducted. The purpose is described, after which the problem formulation and limitations are stated. Finally, previous works related to the area is explored.

1.1 Background

Localisation in cellular networks was in the beginning considered as an optional feature. Since then, from *First Generation* (1G) in the 1980's to *Fifth Generation* (5G) today, the localisation methods have gone from almost non-existent and covering outdoor-only scenarios to now achieving up to sub-meter level accuracy in indoor environments [9]. When a *User Equipment* (UE) is located outdoors, the *Global Navigation Satellite System* (GNSS) can be supported by the cellular networks to enable meter-level accuracies. Therefore, when indoor requirements for positioning emergency calls became mandatory the case of studying positioning scenarios with indoor users was initiated since it had not been investigated and applied thoroughly up until then [21].

The principle of indoor positioning is based on a UE being placed somewhere in an indoor environment where a deployment of several *Base Stations* (BSs) is present. An indoor BS is often referred to as a node or cell. There is always a trade-off between how accurate the position estimation can be and how complex and costly the BS deployment planning is [25]. Indoor and outdoor positioning differs since the indoor environment contains more obstacles and therefore often leads to multipath propagation, higher *Non-Line-Of-Sight* (NLOS) probability and longer delay spread. The environment, in [21] defined as either indoor urban or deep indoor, is also characterised by very limited or no GNSS support at all, which means that alternative solutions are needed for positioning compared to relying on GNSS as in outdoor urban or rural environments.

The *Third Generation Partnership Project* (3GPP) sets the standards in telecommunication [8] and the United States *Federal Communications Commission* (FCC), amongst others, regularly issues requirements related to communication and performance a few years ahead. One requirement FCC stated is how accurate the position estimation of UEs must be in case of emergency calls to 911, more specifically how large percentage of the UEs should be positioned with an error less than 50 m in the horizontal plane with any radio access technology. For the years 2017, 2018, 2020 and 2021 the requirements from FCC were mandated for 40%, 50%, 70% and 80% of the UEs [1, 21].

Except for emergency calls, indoor positioning is today desired in many other areas for various reasons, such as positioning products in industrial environments, hospital equipment or firefighters inside a building on fire [9, 18]. One even tougher situation where indoor positioning can be useful is locating a specific object on a shelf in a commercial setting. All these use cases require more precise position estimation compared to outdoor positioning [6].

With this in mind there is a constant urge for telecommunication companies to continuously improve their indoor positioning techniques in order to meet FCC's requirements concerning emergency service situations, while simultaneously providing opportunities for usage in other upcoming areas of application. Seeing that this topic is relatively unexplored there are a lot of possible improvements lying ahead which can contribute to obtaining better position estimation accuracy.

1.2 Problem Formulation

This thesis aims to investigate and design different network deployment strategies in an indoor environment in order to achieve both high position estimation accuracy and availability. The results are then to be analysed for the purpose of understanding how accuracy and availability relates to different deployments. The questions to consider for accomplishing the objective are as follows

1. How does network deployment affect the position estimation accuracy and availability in two standard 3GPP scenarios when considering a limited number of deployments?
2. How does orthogonality and resource consumption affect the position estimation accuracy and availability?

1.3 Limitations

One limitation in this thesis is to investigate positioning only in a 5G context and only in an indoor environment. The indoor environment is limited to the two standard 3GPP scenarios called *Indoor Open Office* (IOO) and *Indoor Factory* (InF). There are several positioning methods available and in this thesis only *Downlink Time Difference Of Arrival* (DL-TDOA) and *Round Trip Time* (RTT) are considered, with DL-TDOA as the main study item. To investigate these positioning methods

in an indoor environment, simulations are made where only the deployment aspect of positioning is considered. Main focus will therefore lie on investigating deployment strategies and not on solving the actual positioning problem.

1.4 Related Work

Extensive research concerning positioning systems has been conducted over the years. Main focus has been on outdoor scenarios but recently the indoor environment has become increasingly interesting because of federal regulations and new areas of applications as mentioned in Section 1.1. Much work has been made with regard to improving the position accuracy, not necessarily for 5G but still within the cellular context using current and proposed new methods.

In [22] the authors investigated the horizontal and vertical positioning accuracy for two 3GPP *Three Dimensional* (3D) scenarios from Release 13 utilising two *Long-Term Evolution* (LTE) positioning methods, *Observed Time Difference Of Arrival* OTDOA and *Cell ID* (CID). Before 5G, DL-TDOA was called OTDOA but they are the same technique. The first scenario included an outdoor deployment with a mix of macro cells and small cells whereas the second scenario consisted of an outdoor deployment with macro cells and an indoor deployment with small cells. In both cases the OTDOA method showed promising results and could meet the FCC requirement for localising indoor UEs, yielding best result in the case with an added indoor deployment. The CID based method performed surprisingly well in the indoor deployment scenario both concerning horizontal and vertical accuracies. Consequently, the authors made the conclusion that an increasingly wider deployment of indoor cells proves very effective for indoor positioning.

Another positioning technique available that relies on time measurements besides DL-TDOA is RTT. The performance of Ericsson's RTT positioning method is presented for a commercial *Wideband Code Division Multiple Access* (WCDMA) network in [27], where UEs were present in different outdoor and indoor environments. The results displayed a 95% availability and 67% of the UEs having a radial distance error within 78 m. Based on the results the authors concluded that RTT can act as a fallback method emergency service positioning.

How the geometry affects the position determination in a *Two Dimensional* (2D) scenario is investigated in [17] where the *Geometric Dilution Of Precision* (GDOP) is studied. The GDOP helps stating how the position estimate is influenced by the measurement error. By placing all available BSs in a polygon the lowest GDOP will be achieved at the centre of the polygon, meaning the centre is the most favourable UE position when doing position estimation. The GDOP will increase further away from the centre of the polygon, especially when moving outside the polygon.

In [24] the authors perform a GDOP analysis of several scenarios where the BSs are evenly placed on a circle. A single UE is located either on the circumference of the circle, along radials within and beyond the circle or near a BS. They derive analytical expressions and compare the result with simulations. What they can show is a good agreement between theory and simulation except when the UE

position is too close to a BS. This disparity occurs due to the ranging errors being a significant proportion of the range.

When estimating positions using time of arrival techniques comes a non-linear estimation problem which can be solved by different means. The authors concluded in [19] that the choice of algorithm matters and can promote better positioning performance. In [23] the authors propose a new iterative method for detection of the first channel tap in an estimated *Channel Impulse Response* (CIR), which is used to determine *Time Of Arrival* (TOA), and compare it to the commonly used non-iterative method. The proposed algorithm is proven to outperform the non-iterative threshold-based method while also being more robust, thus supporting better position estimates.

1.5 Thesis Outline

The theoretical background on which this thesis is based is presented in Chapter 2. It includes brief explanations of some indoor positioning aspects and two positioning techniques. Additional useful theory for analysing positioning performance is also covered. Chapter 3 contains descriptions of the positioning simulator, the deployment parameters and the process of studying the two 3GPP standard scenarios. Thereafter, theoretical and simulation results from all conducted investigations are visualised in Chapter 4. In Chapter 5 the results presented in Chapter 4 are discussed and analysed. Finally, in Chapter 6, the questions asked in the beginning of the thesis is answered by drawing conclusions from the results and discussions. At last, future work on the subject is proposed.

2

Theoretical Background

Relevant theoretical background on the work conducted in this thesis is presented in this chapter and it starts with mentioning some performance requirements and issues related to indoor positioning. Moving on, the positioning techniques and additional useful theory for analysing positioning performance are explained. Lastly, the *Positioning Reference Signal* (PRS) is described.

2.1 Positioning Performance Requirements and Metrics

When analysing the performance of a positioning method it is not sufficient to only observe the accuracy, more aspects are relevant. The authors bring up six different performance metrics in [18] that are worth considering in wireless indoor positioning systems.

Accuracy

The most prominent performance requirement in positioning is accuracy, or positioning error, which is usually expressed as the mean distance error. This metric is the Euclidean distance between the true position and the estimated position of the UE. Generally, higher accuracy means better system but there still is a compromise to be made between accuracy and other characteristics.

Precision

Location precision differs from accuracy in a way that while accuracy focuses on the mean distance error, the precision considers the consistency of the system. It measures the position method's robustness by showing the variation in

performance over multiple trials. When presenting and comparing the precision of different positioning methods the *Cumulative Distribution Function* (CDF) is a useful tool. The CDF is based on the percentile format, thus a CDF plot visualises how large fraction or percentage of the total error lies within a certain limit. One example is that, assuming the accuracy of two positioning techniques are equal, one would prefer the option which reaches higher probability values faster.

Complexity

Software, hardware and operation factors altogether contribute to the complexity of a positioning system and in [18] the authors put emphasis on the software complexity, which translates to computational complexity. The computations performed by the positioning algorithm can either take place in the network or on the UE. If it is carried out on the network side, where there exists sufficient power supply and powerful processing capability, the calculation will be faster. On the other hand, if the same calculation was to be carried out on the UE the effects of complexity would be noticeable, in terms of longer computation time, due to limited battery life and the lack of strong processing power. Therefore, a low complexity positioning algorithm would be preferred when the computations are made by the UE.

Robustness

Robustness is an important aspect when considering performance since even though some signals may not be available, the positioning method must still function normally. Reasons to receiving many bad signals or having a reduced number of available signals are for example blocked signal paths or harsh environments creating problems.

Scalability

The positioning must function properly independent of the scope and that is measured using the scalability characteristic. When the distance between the receiver and transmitter increases, the positioning performance typically degrades. The authors mention that a positioning system needs scalability on two axes which are geography and density [18]. The density scale implies the number of units present per unit geographic area and the geography scale means the area covered. An area densely populated with UEs might cause congested signal channels and demand more position calculations while a large geographic coverage needs an expanded communication infrastructure.

Cost

The last performance metric is cost, which for a positioning system depends on several factors. Amongst the most important ones are money, space, time and energy. Every system has a price, therefore the money factor. The supplier also has to consider the measuring unit density which is a space cost. When using a

positioning system, installation and maintenance is required and that relates to the time factor. Finally, some UEs are energy passive, capable of an unlimited lifetime whereas others have a limited lifetime until recharging is needed.

2.2 Issues with Indoor Positioning

Some issues that can have an impact on position estimation accuracy are presented in this section. The issues presented are caused by measurement geometry, network synchronisation, incorrect parameters stored for antenna coordinates, network planning and the radio environment [10].

Deployment Geometry

The geometry of the deployment affects the accuracy and is often characterised by a parameter called GDOP. GDOP tells how much the UE/BS relative geometry affects the positioning error and the smallest error is achieved when the BS are symmetrically placed around the UE [10]. The theory behind GDOP is further explained in Section 2.5.

Incorrect Parameters

In a telecommunication network the coordinates of the antennas are needed when computing the hyperbolic lines used when estimating UE positions. The position estimation technique will be further explained in Section 2.3. The coordinates of the antennas mounted on different BSs should together with the UE be expressed in the same coordinate system. If a BS participating in a UE positioning process uses an incorrect coordinate system for the antenna coordinates, the position estimation will not be correct. Errors in the antenna coordinates will result in a proportional increment of UE positioning error [10].

Network Planning

Network planning aims to avoid making signals collide and also to keep them orthogonal since they will interfere with each other otherwise. To get orthogonality, there is need for a planning pattern which will remove the risk of having the same frequency in the same site, in adjacent cells, or in cells pointing at each other [10]. An explanation of orthogonality is given in Section 2.6.

Radio Environment

Environmental phenomena that affect the position estimation accuracy are for instance NLOS conditions, multipath propagation and shadow-fading. Multipath propagation is caused by reflection, diffraction and scattering of the transmitted signal because of obstacles in the environment, resulting in the signal taking different paths before it is received. This means the transmitted signal will be received from different directions and with different delays. Moreover, the multipath propagation will result in fading of the signal. This has a significant impact

on the TOA estimation, one step in the position estimation chain, and can lead to large errors in the position estimation accuracy. If there are many measurements available, it is possible to detect and reduce large bias errors from the position calculations if some of the measurements suffer from less multipath and NLOS propagation [10].

Network Synchronisation

For a positioning technique such as DL-TDOA, the synchronisation between the BSs is vital for the position estimation accuracy. Each nanosecond translates to approximately 0.3 m of ranging error if the signal is propagating with the speed of light. This could mean large errors in the position estimation since the hyperbolic lines used for UE position estimation will be more uncertain. As the synchronisation error increases, the UE position estimation error also gradually increases [10].

2.3 Positioning Techniques

There are several positioning methods that can be used in a telecommunication network, that is, a network where BSs and UEs wirelessly are exchanging information. Using wireless communication leads to bandwidth limitations and synchronisation problems that must be considered in the methods used. The positioning methods either depend on waveform observations, timing observations or power observations [12]. In this report, focus will lie on methods that are based on timing observations, more specifically DL-TDOA and RTT.

In a timing observation model the position to be estimated is calculated using observed travel times of a signal. Often it is easier to interpret the time as a distance and from here on all measured times are therefore multiplied by the speed of light to obtain measurement in meters.

The positioning methods are based on nonlinear models with assumed explicit additive noise. For this case, a general measurement equation at time t has the form

$$y_t = h(\theta_t) + e_t, \quad (2.1)$$

where y_t is the measurement, $h(\theta_t)$ is a nonlinear measurement model and e_t is the measurement noise [13]. All recently mentioned variables are vector-valued. The variable $\theta_t = [x_t \ y_t \ z_t]^T$ is the 3D position of the UE. In general, the function $h(\theta_t)$ will implicitly depend on the known and constant 3D positions of the N BSs, $p^i = [x^i \ y^i \ z^i]^T$, $i = 1, \dots, N$. This thesis will only cover the static case, meaning everything will be studied at a single time instance and therefore all time indices will be omitted from the upcoming equations.

2.3.1 Downlink Time Difference of Arrival

A *Time Difference Of Arrival* (TDOA) measurement is obtained by taking the difference between two TOA measurements. The TOA technique, which measures

the travel time of a signal between a BS and a UE, works best in an entirely synchronous network. Normally, the UE clock is not synchronised with the BS clock, meaning this clock bias will occur as a nuisance parameter [13]. The expression for a TOA observation, y_{TOA}^i , based on BS i in an asynchronous network is

$$y_{\text{TOA}}^i = |\theta - p^i| + \delta^i + e^i, \quad i = 1, \dots, N, \quad (2.2)$$

with δ^i being the unknown clock bias between the UE and BS i .

There are two different ways to implement the TDOA method in a telecommunication network and that is to specify a network direction, either downlink or uplink. DL-TDOA makes use of TOA measurements from the downlink signal, that is, the time for the signal to travel from a BS to the UE. The downlink signal that is used is called PRS and will be further described in Section 2.7. From Equation (2.2) and assuming all BSs are synchronised a DL-TDOA observation, $y_{\text{DL-TDOA}}^{i,j}$, based on a reference BS i and any other BS j is then expressed as

$$y_{\text{DL-TDOA}}^{i,j} = |\theta - p^i| - |\theta - p^j| + e^i - e^j, \quad 1 \leq i \leq N, \quad j = 1, \dots, N, \quad j \neq i. \quad (2.3)$$

In Equation (2.3) the clock bias has been cancelled out due to the assumption of the BSs being synchronised. This measurement model further assumes *Line-Of-Sight* (LOS) measurements. With a NLOS measurement, a positive offset is included in $y_{\text{DL-TDOA}}^{i,j}$ due to a longer signal path. The offset is not taken into consideration in the position estimation, meaning Equation (2.3) does not completely hold in NLOS conditions. The DL-TDOA measurement is also known as a *Reference Signal Time Difference* (RSTD) measurement [10, 13]. All the RSTD measurements are sent to the *Location Management Function* (LMF) for further computations, resulting in a position estimate of the UE [2]. The position estimation accuracy depends on how accurate the RSTD measurements are, which in turn depends on the network synchronisation accuracy and the BS locations [13].

2.3.2 Multi-cell Round Trip Time

In RTT positioning, the RTT measurement corresponds to the travel time of the signal from a BS to the UE and back to the BS. The latency between the uplink and downlink signals is also included in the measurement. As opposed to DL-TDOA, the signal used with the RTT technique is usually not the PRS. When utilising measurements from multiple BSs while conducting the position estimation the technique is called multi-cell RTT [15]. For simplicity, it will be referred to as only RTT in the rest of the thesis. An RTT measurement, y_{RTT}^i , based on BS i is the sum of an uplink and a downlink TOA measurement [20, 27],

$$y_{\text{RTT}}^i = 2|\theta - p^i| + e^{\text{TOA, uplink}} + e^{\text{TOA, downlink}}, \quad i = 1, \dots, N. \quad (2.4)$$

As with DL-TDOA, the measurement model for RTT assumes LOS. The measurements are then sent to the LMF in order to finally receive a position estimate of the UE. Since both the uplink and the downlink signals are used for every BS, no common clock is needed in the telecommunication network when RTT is used for position estimation [11].

2.4 Cramér-Rao Lower Bound

It is often useful to state a lower bound on the variance for any unbiased estimator and the *Cramér-Rao Lower Bound* (CRLB) serves that purpose. An estimator is said to be unbiased if it on average yields the true value of the unknown parameter, mathematically fulfilling the criterion

$$\mathbb{E}[\hat{\theta}] = \theta, \quad a < \theta < b \quad (2.5)$$

where θ is the parameter to be estimated, $\hat{\theta}$ is the estimate and a and b are the upper and lower limit of θ , respectively. One can motivate that an estimator is a *Minimum Variance Unbiased* (MVU) estimator if it, for all values of the unknown parameter, achieves the CRLB. In an opposite way it can function as a benchmark to which the performance of other unbiased estimators can be compared, meaning it is impossible to find an unbiased estimator with a variance less than the bound [14]. In this thesis, θ in Equation (2.5) is the vector with the x , y and z positions of the UE.

In order to compute the CRLB one needs to first determine the *Fisher Information Matrix* (FIM), $\mathcal{I}(\theta)$, which with the current assumptions is given by

$$\mathcal{I}(\theta) = \mathbb{E}[\nabla_{\theta}^T \ln p_E(y - h(\theta)) \nabla_{\theta} \ln p_E(y - h(\theta))], \quad (2.6)$$

where

$$\nabla_{\theta} \ln p_E(y - h(\theta)) = \left[\frac{\partial \ln p_E(y - h(\theta))}{\partial x} \quad \frac{\partial \ln p_E(y - h(\theta))}{\partial y} \quad \frac{\partial \ln p_E(y - h(\theta))}{\partial z} \right] \quad (2.7)$$

and $p_E(y - h(\theta))$ is the likelihood function of the given error distribution [13]. When the measurement noise is of the type *Additive White Gaussian Noise* (AWGN), the FIM becomes

$$\mathcal{I}(\theta) = H^T(\theta) R^{-1}(\theta) H(\theta), \quad (2.8)$$

where R is the noise covariance matrix and with

$$H(\theta) = \nabla_{\theta} h(\theta). \quad (2.9)$$

One can also note that the information is additive for independent observations [12], meaning M observations will result in the following expression for $\mathcal{I}(\theta)$

$$\mathcal{I}(\theta) = \mathcal{I}_{1:M}(\theta) = \sum_{t=1}^M \mathcal{I}_t(\theta), \quad (2.10)$$

where $\mathcal{I}_t(\theta)$ is the FIM at time t . Independent of how $\mathcal{I}(\theta)$ is calculated, CRLB is finally given by

$$\text{Cov}(\hat{\theta}) \geq \mathcal{I}^{-1}(\theta). \quad (2.11)$$

The relation in Equation (2.10) implies what may be intuitive, that more information results in a lower bound [13, 14].

In positioning studies, plotting the positioning error in meters is a relevant performance metric and it is achieved by calculating the *Root Mean Square Error* (RMSE) [13]. A lower bound for the RMSE of an estimator is obtained by ultimately taking the square root of the trace of CRLB

$$\text{RMSE} = \sqrt{\mathbb{E}[(x - \hat{x})^2 + (y - \hat{y})^2 + (z - \hat{z})^2]} \geq \sqrt{\text{Cov}(\hat{\theta})} \geq \sqrt{\text{tr}(\mathcal{I}^{-1}(\theta))}. \quad (2.12)$$

When only the 2D UE position is of interest, a lower bound for this for this error can be obtained from the FIM as

$$\text{RMSE} = \sqrt{\mathbb{E}[(x - \hat{x})^2 + (y - \hat{y})^2]} \geq \sqrt{\mathcal{I}_{1,1}^{-1}(\theta) + \mathcal{I}_{2,2}^{-1}(\theta)}, \quad (2.13)$$

with $\mathcal{I}_{1,1}^{-1}(\theta)$ and $\mathcal{I}_{2,2}^{-1}(\theta)$ being the two first diagonal elements of \mathcal{I}^{-1} .

2.4.1 Downlink Time Difference of Arrival

In this section the analytical expression for CRLB using DL-TDOA is derived while still keeping to the definitions and assumptions made in previous sections. When studying CRLB no signal or network direction is involved, hence DL-TDOA will here be referred to as TDOA.

According to Equations (2.1) and (2.3), the following applies when BS number 1 is used as reference

$$h_{\text{TDOA}}(\theta) = \begin{pmatrix} |\theta - p^1| - |\theta - p^2| \\ |\theta - p^1| - |\theta - p^3| \\ \vdots \\ |\theta - p^1| - |\theta - p^N| \end{pmatrix}. \quad (2.14)$$

Computing H_{TDOA} according to Equation (2.9) for $h_{\text{TDOA}}(\theta)$ gives

$$H_{\text{TDOA}} = \begin{pmatrix} \frac{x-x_1}{d_1} - \frac{x-x_2}{d_2} & \frac{y-y_1}{d_1} - \frac{y-y_2}{d_2} & \frac{z-z_1}{d_1} - \frac{z-z_2}{d_2} \\ \frac{x-x_1}{d_1} - \frac{x-x_3}{d_3} & \frac{y-y_1}{d_1} - \frac{y-y_3}{d_3} & \frac{z-z_1}{d_1} - \frac{z-z_3}{d_3} \\ \vdots & \vdots & \vdots \\ \frac{x-x_1}{d_1} - \frac{x-x_N}{d_N} & \frac{y-y_1}{d_1} - \frac{y-y_N}{d_N} & \frac{z-z_1}{d_1} - \frac{z-z_N}{d_N} \end{pmatrix}, \quad (2.15)$$

where the distance, d_j , between the UE and BS j is defined as

$$d_j = \sqrt{(x - x_j)^2 + (y - y_j)^2 + (z - z_j)^2}, \quad j = 1, \dots, N. \quad (2.16)$$

The measurement noise covariance matrix R becomes

$$R = \begin{pmatrix} \sigma_1^2 + \sigma_2^2 & \sigma_1^2 & \dots & \sigma_1^2 \\ \sigma_1^2 & \sigma_1^2 + \sigma_3^2 & \dots & \sigma_1^2 \\ \vdots & \vdots & \ddots & \vdots \\ \sigma_1^2 & \sigma_1^2 & \dots & \sigma_1^2 + \sigma_N^2 \end{pmatrix}, \quad (2.17)$$

where σ_i^2 is the measurement noise variance from BS i . The FIM is obtained by inserting Equations (2.15) and (2.17) into Equation (2.8), which when inserted into Equation (2.11) results in CRLB for TDOA. From this, using Equation (2.13), the 2D RMSE is obtained for the position θ of the UE.

2.4.2 Multi-cell Round Trip Time

In this section the analytical expression for CRLB using RTT is derived while, as in the TDOA case, still keeping to the definitions and assumptions made in previous sections.

According to Equations (2.1) and (2.4), the following applies

$$h_{RTT}(\theta) = 2 \begin{pmatrix} |\theta - p^1| \\ |\theta - p^2| \\ \vdots \\ |\theta - p^N| \end{pmatrix}. \quad (2.18)$$

Computing H_{RTT} according to Equation (2.9) for $h_{RTT}(\theta)$ gives

$$H_{RTT} = 2 \begin{pmatrix} \frac{x-x_1}{d_1} & \frac{y-y_1}{d_1} & \frac{z-z_1}{d_1} \\ \frac{x-x_2}{d_2} & \frac{y-y_2}{d_2} & \frac{z-z_2}{d_2} \\ \vdots & \vdots & \vdots \\ \frac{x-x_N}{d_N} & \frac{y-y_N}{d_N} & \frac{z-z_N}{d_N} \end{pmatrix}, \quad (2.19)$$

where d_j is defined as in Equation (2.16). The measurement noise covariance matrix R becomes

$$R = \begin{pmatrix} \sigma_1^2 & 0 & \dots & 0 \\ 0 & \sigma_2^2 & \dots & 0 \\ \vdots & \vdots & \ddots & \vdots \\ 0 & 0 & \dots & \sigma_N^2 \end{pmatrix}. \quad (2.20)$$

FIM is obtained by inserting Equations (2.19) and (2.20) into Equation (2.8), which when inserted into Equation (2.11) results in CRLB for RTT. From this, using Equation (2.13), the 2D RMSE is obtained for the position θ of the UE as in the TDOA case.

2.5 Geometric Dilution of Precision

GDOP is an expression describing the effect coming from geometry on the relationship between positioning error and measurement error [26]

$$\text{GDOP} = \frac{\text{Positioning error}}{\text{Measurement error}}. \quad (2.21)$$

The range, d_i , from a UE to the i th BS is defined as in Equation (2.16) and is obtained by multiplying the corresponding TOA measurement with the speed

of light. If the available measurements are range differences they can be made independent to each other by utilising the concept of pseudo-ranges, PR_i ,

$$PR_i = d_i + \rho, \quad i = 1, \dots, N, \quad (2.22)$$

where ρ is an arbitrary range offset [17]. Assuming random, independent, zero-mean noise with equal variance for all measurements, the matrix H_{GDOP} is written as

$$H_{GDOP} = \begin{pmatrix} \frac{\partial PR_1}{\partial x} & \frac{\partial PR_1}{\partial y} & \frac{\partial PR_1}{\partial \rho} \\ \frac{\partial PR_2}{\partial x} & \frac{\partial PR_2}{\partial y} & \frac{\partial PR_2}{\partial \rho} \\ \vdots & \vdots & \vdots \\ \frac{\partial PR_N}{\partial x} & \frac{\partial PR_N}{\partial y} & \frac{\partial PR_N}{\partial \rho} \end{pmatrix}. \quad (2.23)$$

The partial derivatives in Equation (2.23) are

$$\frac{\partial PR_i}{\partial x} = \frac{x - x_i}{d_i}, \quad \frac{\partial PR_i}{\partial y} = \frac{y - y_i}{d_i}, \quad \frac{\partial PR_i}{\partial \rho} = 1. \quad (2.24)$$

GDOP is finally calculated as

$$GDOP = \sqrt{G_{1,1} + G_{2,2}}, \quad (2.25)$$

with $G_{1,1}$ and $G_{2,2}$ being the two first diagonal elements of G

$$G = (H_{GDOP}^T H_{GDOP})^{-1}. \quad (2.26)$$

2.6 Orthogonality

When transmitting serial data, the conventional method is to sequentially transmit symbols bearing information. Each symbol's frequency spectrum occupies the entire available bandwidth [28]. The bandwidth itself is then divided into separate parallel frequency bands, or channels, onto which the different information streams are mapped. In order to reduce interference between adjacent frequency bands a frequency guard is introduced to separate them from each other. This well-known technique is a modulation scheme called *Frequency Division Multiplexing* (FDM) [16].

The concept of FDM can be extended to what is known as *Orthogonal Frequency Division Multiplexing* (OFDM). In OFDM the information is carried by multiple closely spaced orthogonal subcarriers with a guard interval between the symbols in the time domain instead of between the frequency bands in the frequency domain.

Each subcarrier will in the frequency domain result in a sinc function spectrum and the OFDM signal can be described as a signal consisting of a set of closely spaced subcarriers. The side lobes will overlap adjacent subcarriers and cause interference if the subcarrier spacing is not chosen wisely. In OFDM the subcarriers are orthogonally spaced which means that each individual peak of a

subcarrier is aligned with the zeros of any other subcarrier spectra, see Figure 2.1. The carefully chosen spacing prevents interference between overlapping subcarriers and results in an increased spectral efficiency by allowing a larger amount of subcarriers per bandwidth [16]. This is what is meant by having orthogonal signals in the frequency domain.

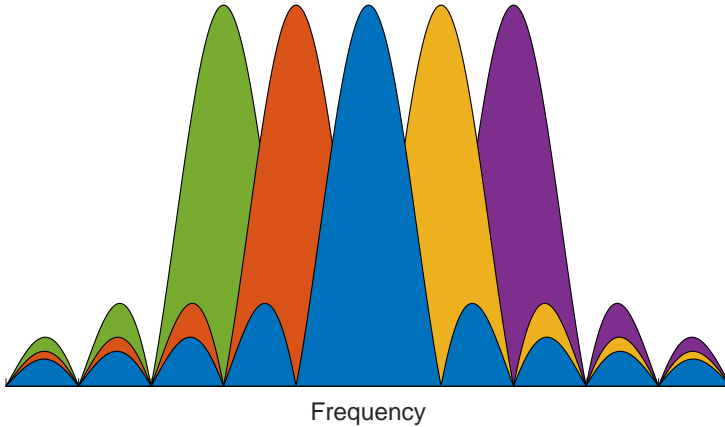


Figure 2.1: Example of OFDM signal spectrum.

When the orthogonal subcarriers fill the bandwidth an *Inverse Fast Fourier Transform* (IFFT) is performed to produce an OFDM signal in the time domain. As mentioned before, guard intervals are then inserted between the transmitted signals with the purpose of preventing inter-symbol interference. To recover the original data, a *Fast Fourier Transform* (FFT) is later performed at the receiver [16].

2.7 Positioning Reference Signal

The signal called PRS, which was referred to in Section 2.3.1, was introduced in 3GPP LTE Release 9 to improve the performance of OTDOA positioning by allowing proper timing measurements of the signals sent from multiple BSs to a UE. The downlink signals which were previously relied upon suffered from poor hearability, something that is crucial when using OTDOA positioning and when signals from multiple dispersed BSs have to be detected [10].

The PRS is allocated on resource elements and these are the smallest time-frequency resources available. One resource element corresponds to one subcarrier. Twelve resource elements make up a physical resource block of which there can be a maximum of 275 [7]. The number of resource blocks determines the PRS bandwidth.

A notation commonly used for describing the orthogonality of a signal is comb- X , where X is a number representing the frequency re-use. The frequency re-use specifies how many orthogonal signals can be generated. Comb-1 means only one orthogonal signal can be generated and comb-4 means four orthogonal

signals in total can be generated. The PRS in 5G supports multiple configurations and the one considered in this thesis is the standard staggered configuration which can be configured for comb factors ranging from 2 to 12. Figure 2.2 illustrates the standard staggered PRS configuration with comb-4 for one BS where the PRS is allocated on the orange blocks. The PRS sequence generation and mapping to physical resources are defined by 3GPP in accordance with TS 38.211 [5].

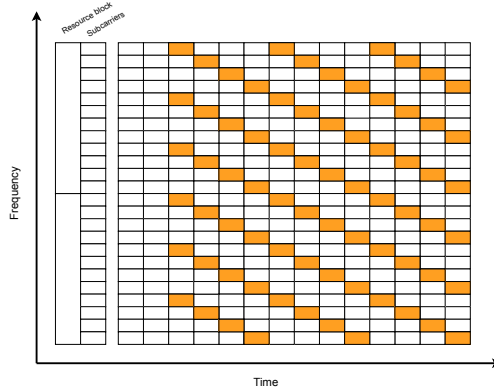


Figure 2.2: Example of comb-4 PRS configuration. The PRS is allocated on the orange blocks.

3

Methodology

The solution methodology of the thesis stated problem is presented in this chapter. First the MATLAB simulation tool is introduced followed by a summary of the deployment parameters. Moving on, the link level study is described and lastly the processes of studying the IOO and InF scenarios is explained.

3.1 Positioning Simulator

The positioning studies is performed using an internal simulation tool provided by Ericsson that supports timing measurements based on both uplink and downlink reference signals. The work flow when utilising the simulator is to first generate various data such as TOA estimates and LOS information to then be used for the position estimations. The simulation type can either be system level or link level. After the data is collected it is used in a position estimator which outputs various figures and data related to, for example, positioning accuracy. The two simulation types and how they affect the simulation will be explained below, as well as the TOA estimator, the position estimator and the newly implemented functionalities. The new functionalities are mainly visualisation options for use in this thesis.

3.1.1 System Level Simulation

A system level simulation means that a complete scenario with a set of UEs distributed geographically has been considered. The position estimation is done for all UEs in that scenario based on the obtained TOA estimates from all BSs. The output data consists, as mentioned before, of TOA and LOS information but also *Signal-to-Interference-plus-Noise Ratio* (SINR) and node information. The calculations are usually computationally heavy, hence they are carried out on a compute

cluster.

3.1.2 Link Level Simulation

In contrast to a system level simulation a link level simulation focuses on studying a single link between a BS and a UE. In this kind of simulation the purpose is to evaluate the performance of the TOA estimator when the *Signal-to-Noise Ratio* (SNR) of a link is changed. The output data consists of TOA errors and information about how many TOA estimation attempts failed.

3.1.3 Time of Arrival Estimator

The TOA estimator is called upon during the simulations in order to calculate TOA estimates needed by the position estimator. When a UE receives a PRS from a BS it performs a cross-correlation with an original copy of the PRS known to the UE. The cross-correlation will produce a *Power Delay Profile* (PDP) containing multiple peaks corresponding to different signal paths. Amongst all the paths, the TOA of the first path is of interest for positioning.

To determine the TOA of the first path, the peak corresponding to the first path needs to be detected. To do so, the TOA estimator relies on two threshold values. The first threshold value is defined as $-\log_2(p)$ to select the first peak that has probability $\leq p$ of being a noise sample. The second threshold value is defined as *Sidelobe Guard Fraction* to avoid detecting side lobes in the PDP as first path. For all system level and link level simulations, a set of *Sidelobe Guard Fraction* values as [0.15 0.22 0.30 0.35 0.40] and a set of $-\log_2(p)$ values as [2 3 30 40 50 100] are considered. TOA estimates are computed for all values and the combination yielding the most accurate estimates is chosen as the optimal parameter combination. The TOA estimates corresponding to this combination is later used for the position estimation.

3.1.4 Position Estimator

The position estimator uses the data generated in the system level simulation to compute position estimates of the UEs and returns the positioning error represented as a CDF. Sometimes the TDOA based algorithm cannot solve the position estimation problem and then falls back on a simple CID based positioning technique. This method estimates the position of a UE to the position of its serving cell. There exists a possibility to choose which TOA estimates to include when calculating position estimates, for example one can include all available estimates or only the ones which completely or partly satisfy the LOS conditions. Partly satisfying the LOS conditions implies that one can put a threshold on how much the TOA estimate is allowed to differ from its true value.

3.1.5 New Functionalities

Some new functionalities for post processing the results from the simulations is implemented in order to better analyse the data. The additions include visualisa-

tions of the following:

- LOS statistics — Presented in a histogram showing a distribution of how many UEs that have a certain number of LOS links. It is also possible to choose a selected number of UEs and obtain the same information, not in a figure but only as data.
- Positioning error of UEs inside and outside the area enclosed by BSs — Presented as CDF curves, one for each group of UEs.
- UEs with worst positioning error — Presented in a figure containing the boundaries of the deployment area with the UE locations plotted inside. The worst X percent of the UEs when considering positioning error are plotted, where X is a manually selected threshold.
- Average link strength — Presented in a bar graph showing the average SINR for the strongest to the weakest BS–UE link.

3.2 Deployment Parameters

Creating and simulating all deployments to be described in the following sections means adjusting a variety of parameters in the positioning simulator. As mentioned in Section 1.3, the two scenarios IOO and InF are considered in this thesis. Many of the scenario specific parameters are already pre-defined by 3GPP but some parameters are adjustable. The adjustable parameters can be referred to as deployment parameters and include, for instance, number of BSs, positions of BSs and if interference is present or not. The scenario specific parameters and deployment parameters for the system level and link level simulations are summarised and commented below.

3.2.1 System Level Simulation

The system level simulations cover the two indoor scenarios IOO and InF. The IOO scenario is defined as an open area of dimensions $120\text{ m} \times 50\text{ m} \times 3\text{ m}$ designed to capture typical indoor scenarios such as shopping malls or office environments. The BSs are in these cases often mounted either on the walls or on the ceiling at a height of approximately 2–3 m. The InF scenario is designed to represent factory halls of varying sizes containing different clutter densities, here meaning different distributions of machines, storage shelves, assembly lines, etc. The area is $120\text{ m} \times 60\text{ m}$ with a ceiling height of 5–25 m where the BSs can be mounted at any height. The presence of objects makes this scenario more challenging than IOO.

Pre-defined scenario parameters for IOO and InF, found in the 3GPP documents TR 38.855 [3] and TR 38.901 [4], are summarised in Table 3.1. In order to simulate and study all deployments presented in Sections 3.4 and 3.5 for the two environments, the different deployment parameters are changed according to what is listed in Table 3.2.

Table 3.1: Pre-defined scenario parameters for the IOO and InF scenarios.

Scenario parameter	IOO	InF
Room size	120 m × 50 m × 3 m	120 m × 60 m × 10 m
BS height	3 m	8 m
UE height	1.5 m	
Total BS transmission power	24 dBm	
BS antenna radiation pattern	Isotropic	
UE antenna radiation pattern	Isotropic	
UE mobility (2D)	3 km/h	
Minimum BS–UE distance	0 m	
UE distribution (2D)	Uniform	
Channel model	Indoor open office (according to TR 38.901 [4])	Indoor factory (according to TR 38.901 [4])
LOS/NLOS	LOS and NLOS	
Penetration loss	0 dB	

Table 3.2: Deployment parameters for the system level simulations of IOO and InF.

Deployment parameter	IOO	InF
Scenario	-	InF-SH, InF-DH (see Table 3.5)
No of UEs	1000	800
No of BSs	6, 12, 18, 24, 30, 36, 68 and 207	12, 36 and 91
BS positions	See Figure 3.1	See Figure 3.4
ISD	See Table 3.4	See Table 3.6
Interference	True/False	False
PRS frequency re-use	1, 4 and 12	-
Network direction	Downlink/Uplink	Downlink

3.2.2 Link Level Simulation

The different deployment parameters used in the link level simulation are presented in Table 3.3.

Table 3.3: Deployment parameters and their corresponding values for the link level simulation.

Deployment parameter	Value
Channel model	TDL-D (according to TR 38.901 [4])
No of UEs	1
No of BSs	1
No of time instants	1000
SNR	-20 dB to 20 dB
SNR step size	5 dB

3.3 Link Level Study

A link level simulation is carried out to evaluate the performance of the TOA estimator. A channel model called *TDL-D* representing LOS conditions is chosen and the link SNR ranges from -20 dB to 20 dB with a step size of 5 dB. This specific SNR interval is chosen since the coverage is rather good in indoor scenarios and therefore represents what one might expect. The channel behaviour is time-variant, making it different every time the channel is realised. To address the channel behaviour variation, numerous simulations at each SNR are made. The link level simulation results thus return the average error of the TOA estimates at a certain SNR level.

3.4 Indoor Open Office Study

The IOO environment is the main study item in this work and consequently the most covered scenario. All investigations are first done in this environment in order to collect results and reach conclusions to later be tested and confirmed in the InF environment. DL-TDOA is evaluated throughout all investigations but the positioning simulator does not completely support RTT. Due to the software constraint, RTT is only applied in the simulations performed in Section 3.4.1 and the CRLB study performed in Section 3.4.2. In this section the approach taken to answer the questions asked in the beginning of the report will be explained.

3.4.1 Deployment Scenarios

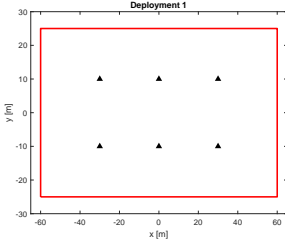
To be able to investigate the effect of different deployments on the positioning accuracy, various deployments are defined. As a starting point, the standard deployment for IOO defined by 3GPP in TR 38.901 [4] with two rows of six BSs is used, see Figure 3.1e. Alternative deployments are then designed by varying the number of BSs and their positions.

The number of BSs is both increased and decreased with multiples of six, spanning from 6–36 BSs, with the aim of exploring how densification affects the posi-

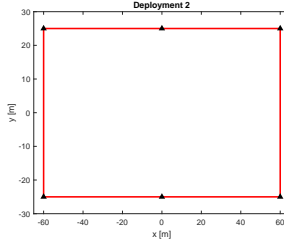
tion estimation and if the improvement in accuracy will eventually saturate. The saturation aspect is the reason why there are two extra deployments, number 22 and 23, having a significantly higher number of BSs compared to the rest, see Figures 3.1v and 3.1w.

To study the effect of BS geometry the positions of the BSs are changed. What follows are deployments with all BSs around the edges, all spread out in the middle and a mix of both types. Two types of geometry occur several times and these are referred to as the standard and the edge type. The standard type geometry is made up of rows of six BSs and is inspired by the 3GPP standard deployment, whereas the edge type geometry always has all BSs at the edges of the room. Why only these deployments are repeated with different number of BSs is because the edge type intuitively seems to have the best potential making it interesting to compare with deployments inspired by what initially had been agreed to and proposed by 3GPP.

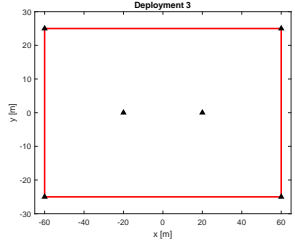
In total, 23 deployments are created and simulated in the positioning simulator. They are illustrated in Figure 3.1. Table 3.4 shows the number of BSs, deployment type and *Inter-Site Distance* (ISD) for every deployment. Sometimes there is not a common ISD for the entire deployment but instead it differs between BSs placed around the edges of the area and the BSs placed in the centre of the area. This is indicated in the table. In some deployments the ISD is expressed as X/Y m which in every case means that the ISD between a BS in the corner and the adjacent one is adjusted to X m in order for the others to have a constant ISD of Y m.



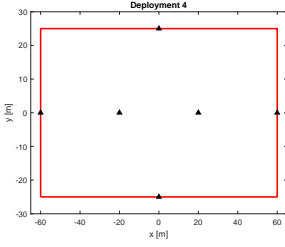
(a) IOO deployment 1.



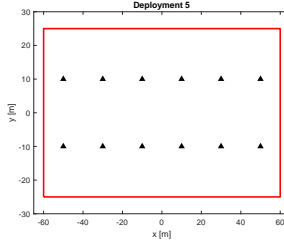
(b) IOO deployment 2.



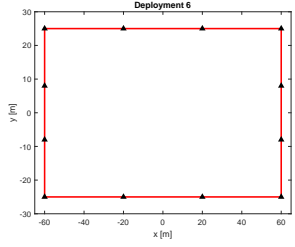
(c) IOO deployment 3.



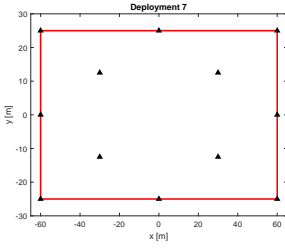
(d) IOO deployment 4.



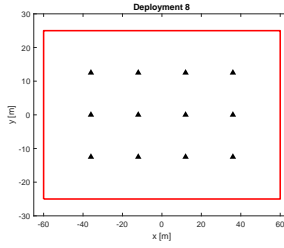
(e) IOO deployment 5.



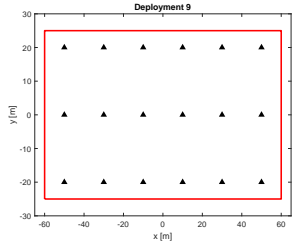
(f) IOO deployment 6.



(g) IOO deployment 7.

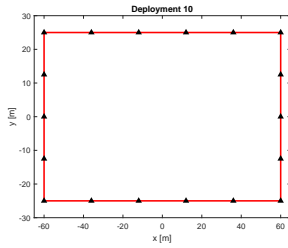


(h) IOO deployment 8.

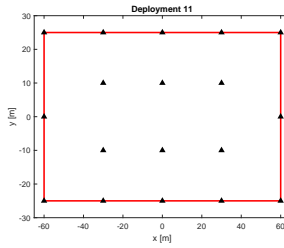


(i) IOO deployment 9.

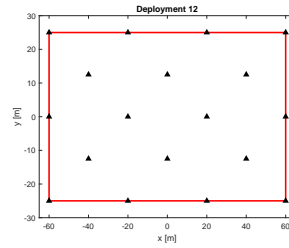
Figure 3.1: Every BS deployment studied in the IOO scenario. The red lines represent the 50 m × 120 m area and the black triangles represent the BSs.



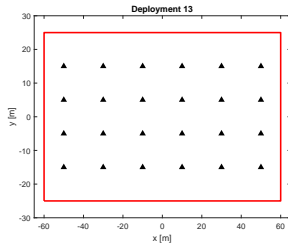
(j) IOO deployment 10.



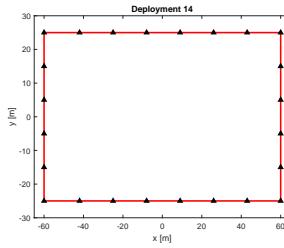
(k) IOO deployment 11.



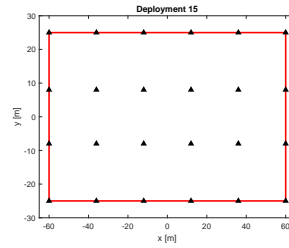
(l) IOO deployment 12.



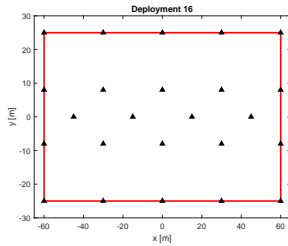
(m) IOO deployment 13.



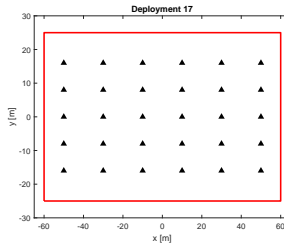
(n) IOO deployment 14.



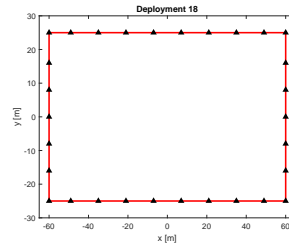
(o) IOO deployment 15.



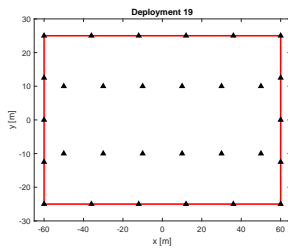
(p) IOO deployment 16.



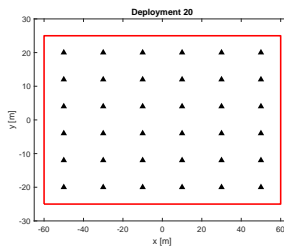
(q) IOO deployment 17.



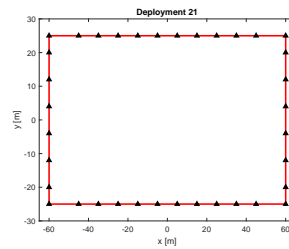
(r) IOO deployment 18.



(s) IOO deployment 19.

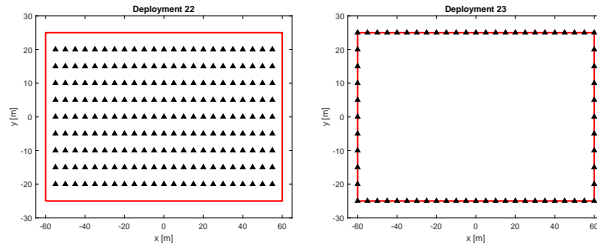


(t) IOO deployment 20.



(u) IOO deployment 21.

Figure 3.1: Continued.



(v) IOO deployment 22. (w) IOO deployment 23.

Figure 3.1: Continued.

Table 3.4: Number of BSs, type and ISD of the 23 investigated IOO deployments are presented in this table.

IOO deployment	No of BSs	Type	ISD
1	6	Standard	X-axis: 30 m Y-axis: 20 m
2	6	Edge	X-axis: 60 m Y-axis: 50 m
3	6	-	X-axis (edge): 120 m Y-axis (edge): 50 m X-axis (centre): 40 m
4	6	-	X-axis: 40 m Y-axis: 50 m
5	12	Standard	X-axis: 20 m Y-axis: 20 m
6	12	Edge	X-axis: 40 m Y-axis: 16/17 m
7	12	-	X-axis (edge): 60 m Y-axis (edge): 25 m X-axis (centre): 60 m Y-axis (centre): 25 m
8	12	-	X-axis: 12.5 m Y-axis: 24 m
9	18	Standard	X-axis: 20 m Y-axis: 20 m
10	18	Edge	X-axis: 24 m Y-axis: 12.5 m
11	18	-	X-axis (edge): 25 m Y-axis (edge): 25 m X-axis (centre): 25 m Y-axis (centre): 20 m

12	18	-	X-axis (edge): 40 m Y-axis (edge): 25 m X-axis (centre): 40 m Y-axis (centre): 25 m
13	24	Standard	X-axis: 20 m Y-axis: 10 m
14	24	Edge	X-axis: 17 m Y-axis: 10 m
15	24	-	X-axis (edge): 24 m Y-axis (edge): 16/17 m X-axis (centre): 24 m Y-axis (centre): 16/17 m
16	24	-	X-axis (edge): 30 m Y-axis (edge): 16/17 m X-axis (centre): 30 m Y-axis (centre): 16 m
17	30	Standard	X-axis: 20 m Y-axis: 8 m
18	30	Edge	X-axis: 11/14 m Y-axis: 8/9 m
19	30	-	X-axis (edge): 24 m Y-axis (edge): 12.5 m X-axis (centre): 20 m Y-axis (centre): 20 m
20	36	Standard	X-axis: 20 m Y-axis: 8 m
21	36	Edge	X-axis: 10/15 m Y-axis: 5/8 m
22	207	Standard	X-axis: 5 m Y-axis: 5 m
23	68	Edge	X-axis: 5 m Y-axis: 5 m

3.4.2 Cramér-Rao Lower Bound Investigation

During the CRLB investigation the theory presented in Section 2.4 is applied. To be able to make a comparison between the theoretical CRLB and the simulated positioning errors, a reasonable measurement noise level has to be chosen for the theoretical study. To decide what is a reasonable measurement noise level, meaning the variances of the noise terms in Equations (2.3) and (2.4), the distribution of the simulated TOA estimation errors is determined for DL-TDOA simulations. The difference between the true and the estimated TOA values is calculated for each deployment and results in a Gaussian distribution with a mean of 0.12 m and a variance of 0.53. These values are obtained when TOA estimation errors larger than 3 m are considered as outliers and filtered out. Since the theoretical

measurement model assumes AWGN with zero mean, an approximation is made considering a measurement model that follows a Gaussian distribution with zero mean and a variance of 0.53. The variance is assumed equal for all N measurement errors, meaning $\sigma_1^2 = \sigma_2^2 = \dots = \sigma_N^2 = 0.53$. These values are used when studying both DL-TDOA and RTT.

3.4.3 Geometry

One factor affecting the positioning error is the deployment geometry and it is analysed using the theory presented in Section 2.5. The theoretical GDOP is calculated for deployments 1, 2, 5, 6, 20 and 21, which are all of the edge and standard types. Deployments 1, 2, 20 and 21 are chosen with the purpose of having representatives with the fewest and most number of BSs. Deployments 5 and 6 are included since 3GPP specifies 12 BSs in their standard deployment. With this choice of deployments, it is possible to observe how the GDOP develops when the number of BSs increases while still using the same type of deployment.

Another geometry aspect is to investigate if the positioning error of UEs located inside and outside the convex hull of the BSs differs. The convex hull of the BSs is defined as the area enclosed by them. This is thought of as a way to confirm the results obtained by studying GDOP. Since the convex hull of an edge deployment is the whole area, only three standard deployments are used.

One last point of interest regarding deployment geometry is to find out where the 10% of the UEs with the worst positioning error are located and if this can be related to GDOP. This is examined for the deployments mentioned above.

3.4.4 Interference

The effect of interference on the positioning accuracy is investigated by performing simulations utilising different numbers of orthogonal signals. Deployments 5, 6, and 20 are studied with the same motivation as in the previous section and each deployment has three interference cases. Two of the cases correspond to the extremes where either no or all PRSSs interfere with each other. The third case corresponds to an intermediate one where three PRSSs interfere with each other. For deployments 5 and 6 this means two scenarios where the PRS is configured as comb-1 and comb-4 signals, and one scenario where interference is disabled. For deployment 20 it means two scenarios where the PRS is configured as comb-1 and comb-12, and one scenario where interference is disabled. Setting the frequency re-use equal to 4 and 12 when using 12 and 36 BSs, respectively, results in one BS interfering with two others. As mentioned in Section 2.6, 3GPP only allows up to twelve orthogonal signals, implicating that having deployment 20 with no signals interfering based on frequency re-use is impossible but still interesting to study.

Interfering BSs can be placed in different patterns when trying to minimise the effect of interference by virtue of network plannings. However, in this study we take no such considerations. The network planning used for comb-4 and comb-12 is here called *down up* planning. This planning means that the BSs are given an

ID starting from the BS that is located at the bottom left corner of the deployment and then increasing the ID by going down to up and continuing to the right. The ID count starts over when it becomes equal to the re-use factor. The allocated ID is then used to generate PRSS where $\text{mod}(\text{ID}, \text{re-use factor})$ determines the allocated frequency resources for the PRS transmission to that particular BS. The network planning when all PRSS interfere is called *all interfering* when no PRSS interfere with each other is called *no interference*. The latter represents the default simulation setup. The network planings *down up* and *all interfering* for all deployments are shown in Figures 3.2 and 3.3

When signals interfere with each other the SINR of each BS-UE link will most likely be affected. This phenomenon might have an impact on the positioning accuracy and therefore the link SINR is also examined for the different deployments.

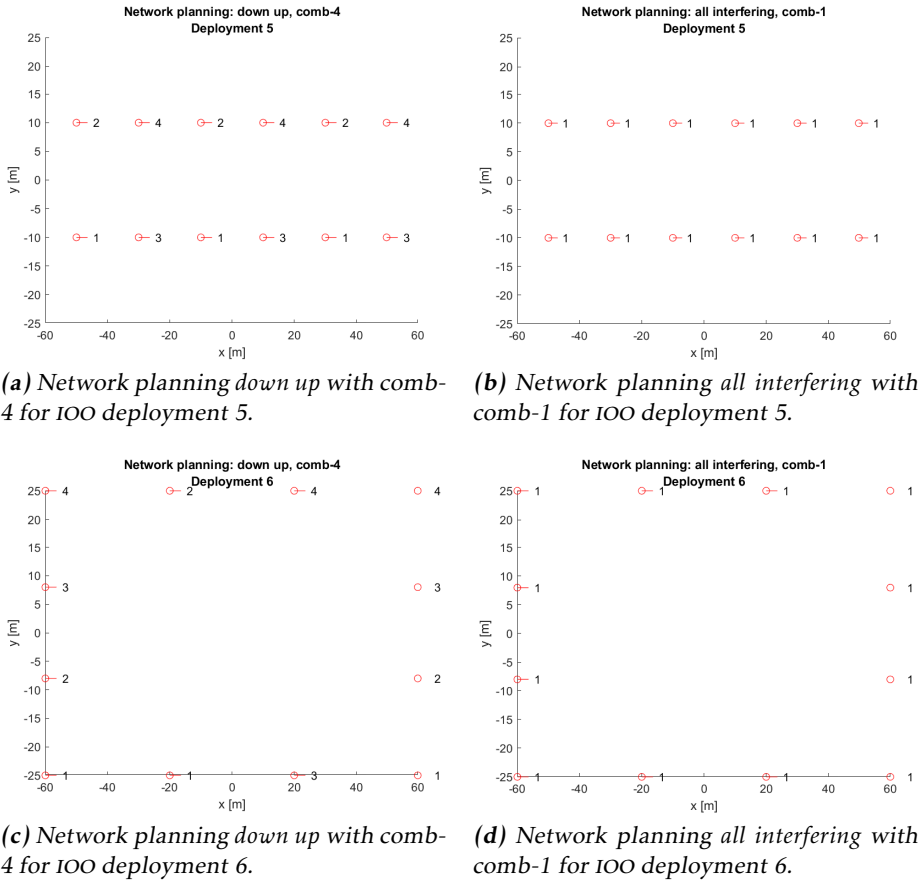
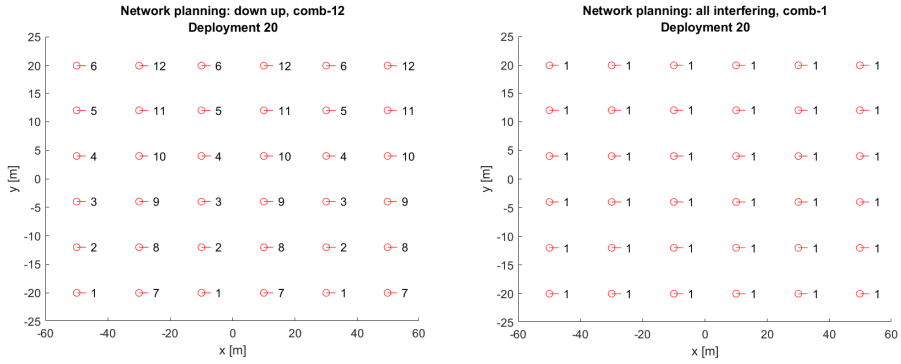


Figure 3.2: Two different network planings; *down up* and *all interfering* for 100 deployment 5 and 6, both with 12 BSs.



(a) Network planning down up with comb-12 for IOO deployment 20.

(b) Network planning all interfering with comb-1 for IOO deployment 20.

Figure 3.3: Two different network plannings; down up and all interfering for IOO deployment 20 with 36 BSs.

3.4.5 Line-Of-Sight

The last topic covered in the IOO study concerns the effect of LOS links on the positioning accuracy. Up until this point every investigation is described having in mind that all available measurements shall be used for the position estimation. The available measurements consist of both LOS and NLOS links. Instead of utilising all measurements when calculating the positioning accuracy it is interesting to examine if the accuracy improves or worsens when only using LOS measurements. This is applied for the simulation described in Section 3.4.1, for the investigation of the locations of UEs with worst positioning error and for the interference simulations. To be able to draw further conclusions about the effect of LOS conditions the number of LOS links for every UE in deployments 1–21 is studied as well.

3.5 Indoor Factory Study

After carrying out investigations in the IOO environment, focus turns to the InF scenario. This scenario has five different variants compared to the single variant in the IOO scenario. Out of the five, two variants named *Indoor Factory - Sparse High* (InF-SH) and *Indoor Factory - Dense High* (InF-DH) are chosen for the study as they depict InF scenarios with sparse and dense clutter. The sparse clutter option specifies a scenario with $< 40\%$ of the deployment area being covered by clutter and the dense clutter option specifies a scenario with $\geq 40\%$ of the deployment area being covered by clutter. Both scenarios have highly mounted BSs. Table 3.5 contains summarised descriptions of InF-SH and InF-DH.

The InF scenarios are supposed to function as environments where observations and conclusions from the IOO scenario can be further tested and validated,

therefore the scope of this study is not as large and extensive in comparison to the IOO scenario. Interference is not considered in these simulations and only DL-TDOA is applied.

Table 3.5: Descriptions of InF-SH and InF-DH.

InF scenario parameter	InF-SH	InF-DH
Effective clutter height	0–10 m	
External wall and ceiling type	Concrete or metal walls and ceiling with metal coated windows.	
Clutter type	Big machineries composed of regular metallic surfaces. For example: several mixed production areas with open spaces and storage/commissioning areas.	Small to medium metallic machinery and objects with irregular structure. For example: assembly and production lines surrounded by mixed small-sized machineries.
Typical clutter size	10 m	2 m
Clutter density	< 40%	≥ 40%

3.5.1 Deployment Scenarios

Based on the results of the IOO study seven deployments are created and simulated in the positioning simulator. Three deployments contain 12 BSs, three contain 36 BSs and one contains 91 BSs, all deployments are of the types standard, edge and a mix between them. The last deployment with 91 BSs is added with the purpose of analysing if a drastic increase in the number of BSs will yield significantly better positioning accuracy or not. All deployments are illustrated in Figure 3.4 and Table 3.6 shows the number of BSs, deployment type and ISD.

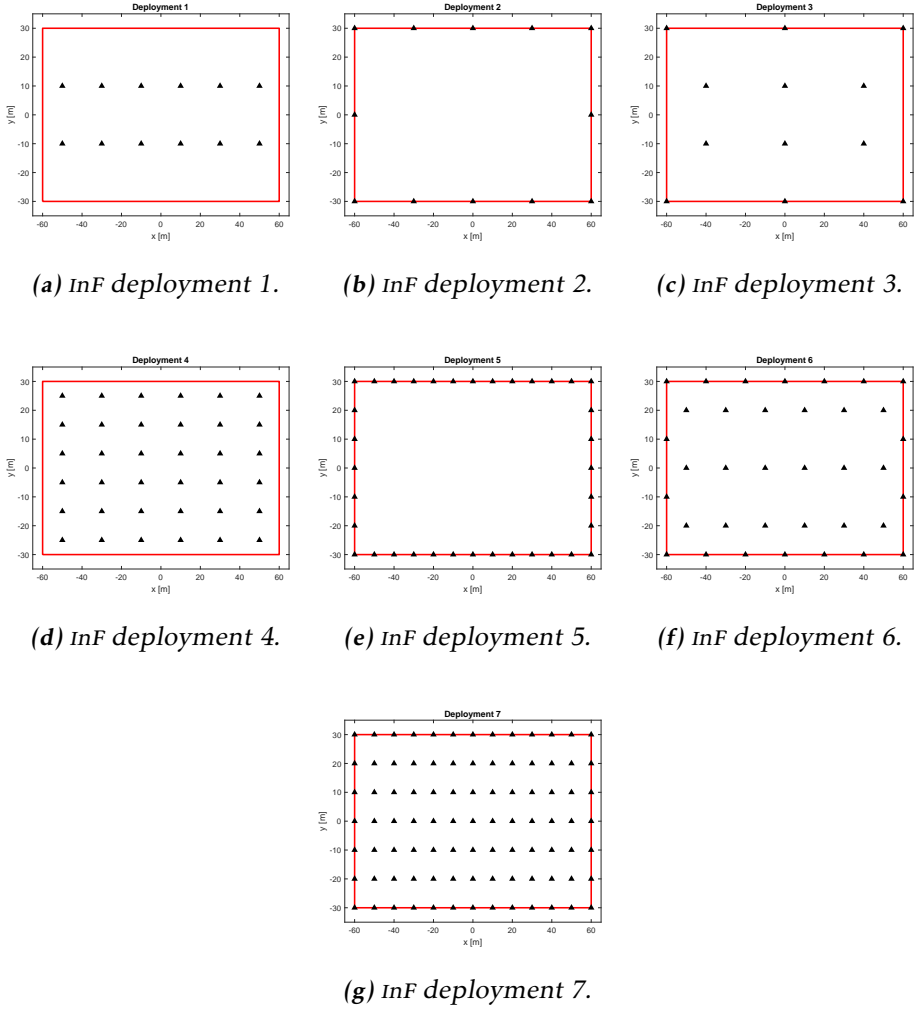


Figure 3.4: Every BS deployment studied in the InF scenarios. The red lines represent the $60\text{ m} \times 120\text{ m}$ area and the black triangles represent the BSs.

Table 3.6: Number of BSs, type and ISD of the seven investigated InF deployments.

InF deployment	No of BSs	Type	ISD
1	12	Standard	X-axis: 20 m Y-axis: 20 m
2	12	Edge	X-axis: 30 m

			Y-axis: 30 m
3	12	Mixed	X-axis (edge): 60 m Y-axis (edge): 60 m X-axis (centre): 40 m Y-axis (centre): 20 m
4	36	Standard	X-axis: 20 m Y-axis: 10 m
5	36	Edge	X-axis: 10 m Y-axis: 10 m
6	36	Mixed	X-axis (edge): 20 m Y-axis (edge): 20 m X-axis (centre): 20 m Y-axis (centre): 20 m
7	91	Mixed	X-axis (edge): 10 m Y-axis (edge): 10 m X-axis (centre): 10 m Y-axis (centre): 10 m

3.5.2 Geometry

As a result of how the InF scenarios of interest are defined, the BSs are mounted above the clutter at a higher height compared to IOO. Changing the BS height is not supported by the software and is therefore a geometric aspect that will not be investigated. Because other effects of deployment geometry has already been explored in the IOO scenario, the only geometry perspective taken with the InF scenario is to investigate where the UEs with the worst positioning error are located. This aspect is of interest since the presence of different amount of clutter can maybe impact the position estimation of these UEs and not stay in line with what might be suggested by GDOP. Only the deployments with 12 BSs are compared for this analysis.

Afterwards when the result is inspected, BSs are either moved or added to areas where the worst positioned UEs are located in order to observe if any change occurs.

3.5.3 Line-Of-Sight

The two different clutter density options make it interesting to study the number of LOS links for every UE. This is studied for all deployments. Additionally, as with IOO, the position accuracy is simulated when only LOS measurements are used when doing the positioning estimation.

3.5.4 Fallback Positioning Technique

As mentioned in Section 3.1.4, a CID based positioning method is used when it is impossible for the simulator to compute a TDOA or RTT position estimate of a UE. The InF scenario with dense clutter represents a very challenging environment

and therefore a performance comparison is made between using the default DL-TDOA algorithm and using only CID based UE position estimates.

4

Simulation Results

In this chapter the results from different simulations are presented. The link level results are followed by the system level results, all of which are performed with the same set of simulation parameters displayed in Table 4.1

Table 4.1: *Simulation parameters common for both link and system level simulations.*

Simulation parameter	Value
Carrier frequency	2 GHz
Subcarrier spacing	30 kHz
No of subcarriers	4096
PRS bandwidth	100 MHz

4.1 Link Level Study

The link level simulations are carried out according to Section 3.3. Figure 4.1a shows the RMSE of the TOA estimates when the SNR ranges from -10 dB to 20 dB. The performance of the TOA estimator is consistent for multiple parameter combinations in the SNR interval -5 dB to 20 dB. It means that equally accurate TOA estimates can be obtained when using one of those TOA estimator parameter combinations, described in Section 3.1.3, if the SNR values lie within this range.

At low SNR the TOA estimator sometimes fails to calculate TOA estimates, thus, only TOA estimates corresponding to SNR with a low failure ratio are considered when determining the best performing parameter combination. When $\text{SNR} = -20$ dB and $\text{SNR} = -15$ dB the failure ratio is always high, see Figure 4.2a, therefore the RMSE corresponding such SNR is omitted from the calculations. Taking

the above into consideration the parameter combination yielding the lowest average RMSE when $\text{SNR} \geq -10$ is visualised in Figure 4.1b. With the best parameter combination the RMSE is around 1 m at $\text{SNR} = -10$ dB but at $\text{SNR} = -5$ dB and onwards it decreases to a value just below 0.3 m and the TOA estimator performs consistently. At its best the TOA estimates include an error of at least 0.27 m and this result puts an upper limit on how well the TOA estimator can perform.

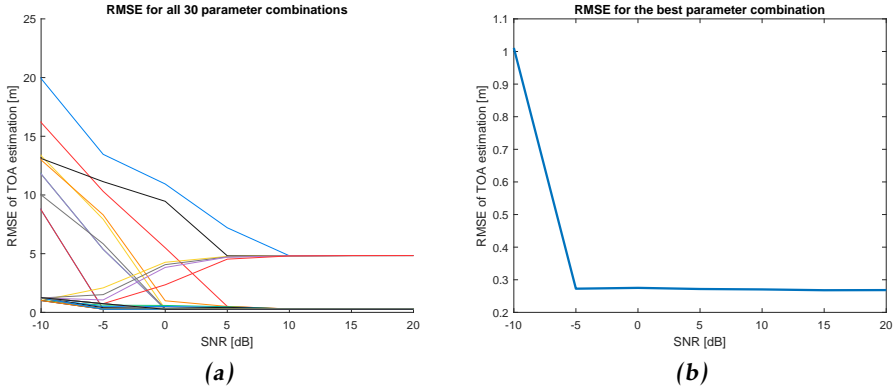


Figure 4.1: RMSE of the TOA estimates for (a) all 30 different parameter combinations and (b) the best combination.

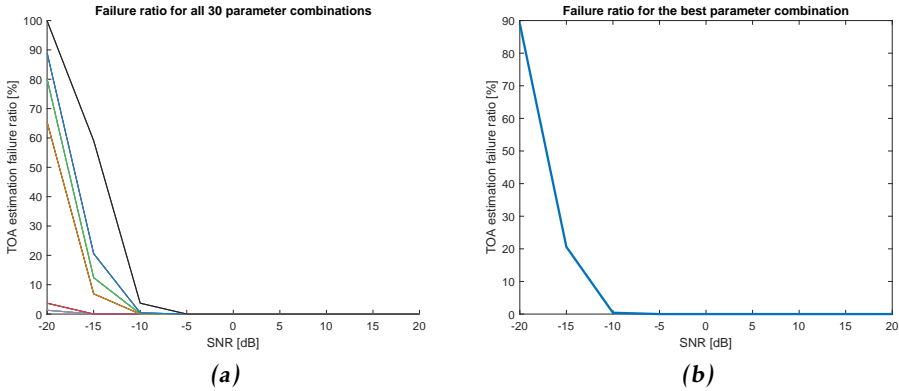


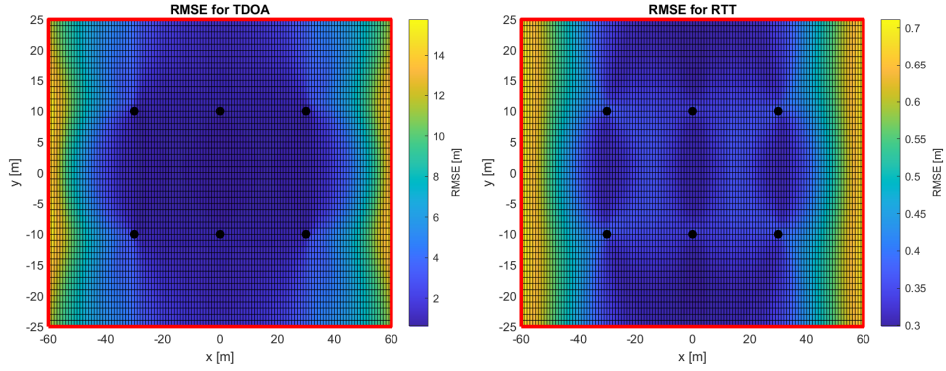
Figure 4.2: Failure ratio of the TOA estimates for (a) all 30 different parameter combinations and (b) the best combination.

4.2 Indoor Open Office Study

All theoretical and simulation results obtained when studying the IOO scenario are presented in this section. For a consistent behaviour of the TOA estimator, the same parameter combination, described in Section 3.1.3, was used throughout all IOO simulations, with two exceptions. The first exception is the investigation of the UEs with the worst positioning error in Section 4.2.4, where the optimal parameter index for each deployment was considered. The other exception is the study of positioning accuracy inside and outside the convex hull of the BSS in Section 4.2.3, where the optimal parameter index for each deployment was considered.

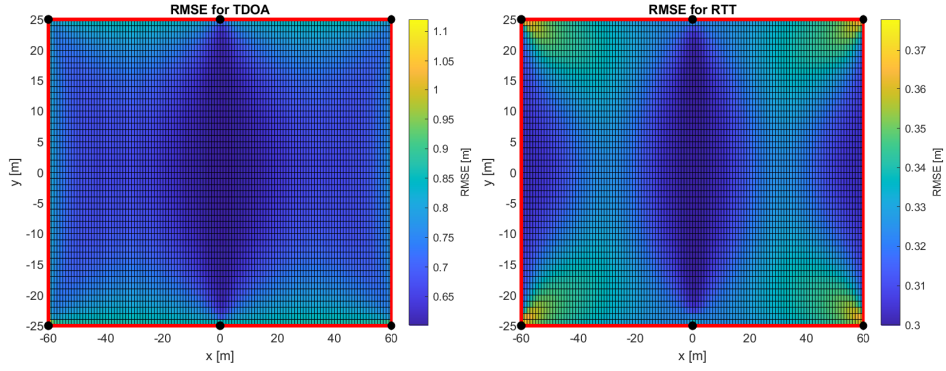
4.2.1 Theoretical and Simulated Positioning Accuracy

Deployments 1–21, presented in Section 3.4.1, were simulated when investigating the theoretical CRLB. The resulting heat maps representing the RMSE of the position estimates for deployments 1, 2, 5, 6, 20 and 21 are shown in Figures 4.3–4.5. These are standard and edge deployments containing 6, 12 and 36 BSSs. The black dots in the heat maps represent the location of BSSs and the red lines mark the boundaries of the deployment area. What can be noted is that the size of the RMSE of the position estimates is larger for TDOA than RTT in every deployment. There is also a much larger variation in RMSE for TDOA compared to RTT. The heat maps corresponding to the remaining deployments depict the same behaviour and can be seen in Appendix A.1.1.



(a) RMSE for TDOA in IOO deployment 1.

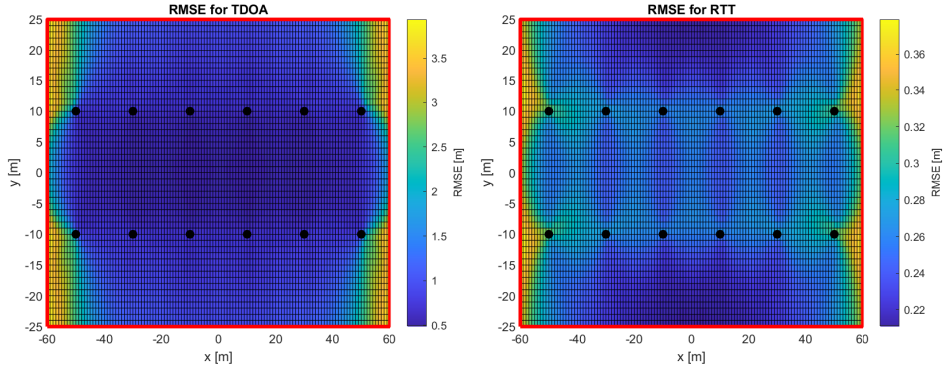
(b) RMSE for RTT in IOO deployment 1.



(c) RMSE for TDOA in IOO deployment 2.

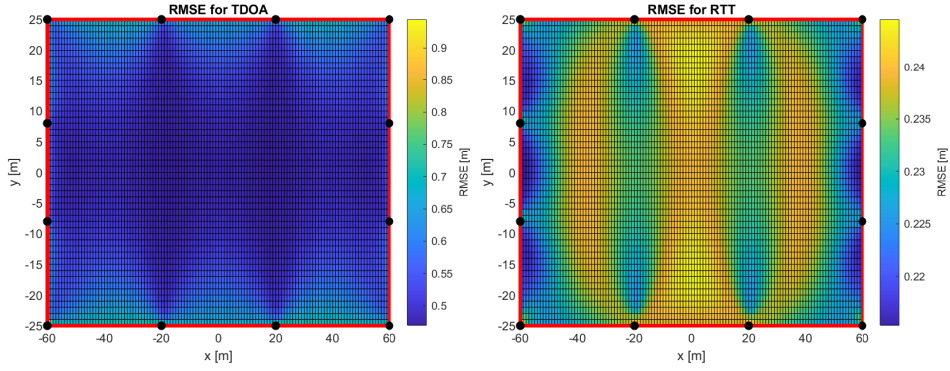
(d) RMSE for RTT in IOO deployment 2.

Figure 4.3: Heat maps showing the RMSE of the position estimates using TDOA and RTT for IOO deployments 1 and 2 with 6 BSs each.



(a) RMSE for TDOA in IOO deployment 5.

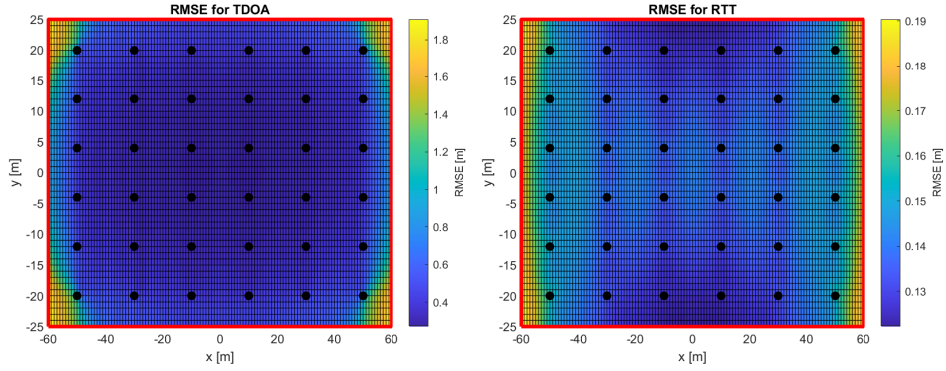
(b) RMSE for RTT in IOO deployment 5.



(c) RMSE for TDOA in IOO deployment 6.

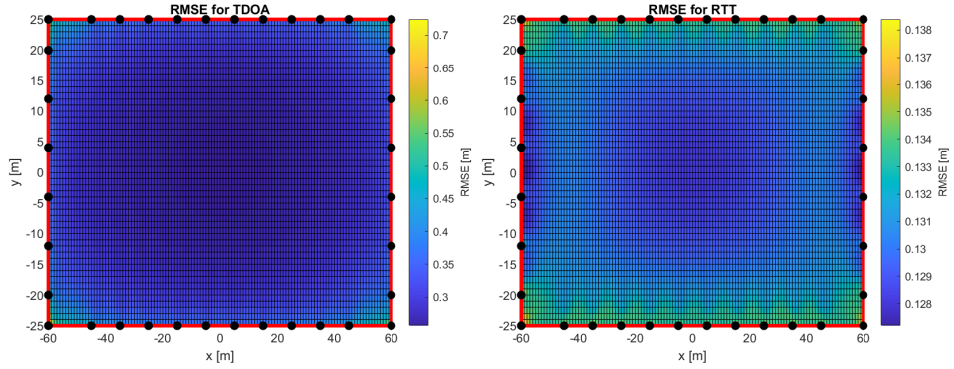
(d) RMSE for RTT in IOO deployment 6.

Figure 4.4: Heat maps showing the RMSE of the position estimates using TDOA and RTT for IOO deployments 5 and 6 with 12 BSs each.



(a) RMSE for TDOA in IOO deployment 20.

(b) RMSE for RTT in IOO deployment 20.

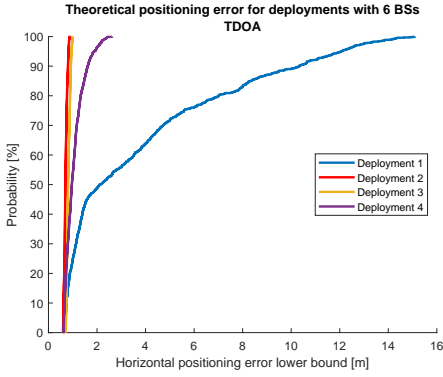


(c) RMSE for TDOA in IOO deployment 21.

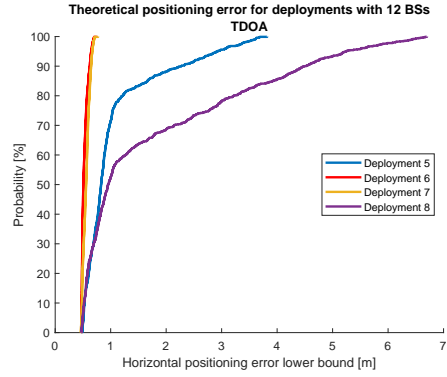
(d) RMSE for RTT in IOO deployment 21.

Figure 4.5: Heat maps showing the RMSE of the position estimates using TDOA and RTT for IOO deployments 20 and 21 with 36 BSs each.

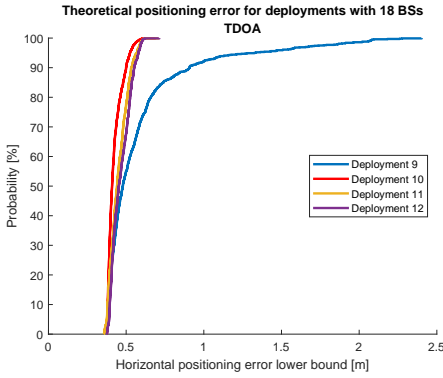
The theoretical RMSE of the position estimates for each of the 21 deployments is also visualised as a CDF, both for TDOA and RTT. CDFs produced from deployments with the same number of BSs are grouped together in one figure for easy comparison. The CDFs for TDOA can be seen in Figure 4.6 and for RTT in Figure 4.7. In these plots we can observe that the positioning accuracy is worse for the standard deployments as compared to the edge deployments with the exception of deployment 8 in Figures 4.6b and Figures 4.7b. The edge deployments always have the best positioning accuracy and the mixed deployments lie in between. This is true for both positioning techniques. It is also visible from the said figures that there is a decrement in positioning error as the number of BSs increases.



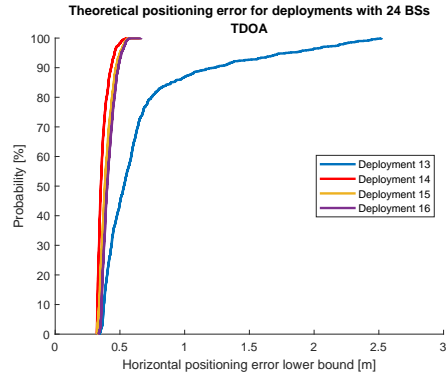
(a) 100 deployments 1–4 with 6 BSs.



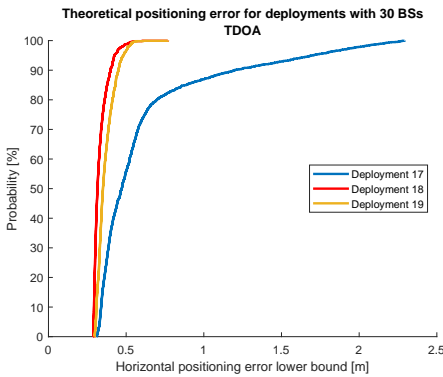
(b) 100 deployments 5–8 with 12 BSs.



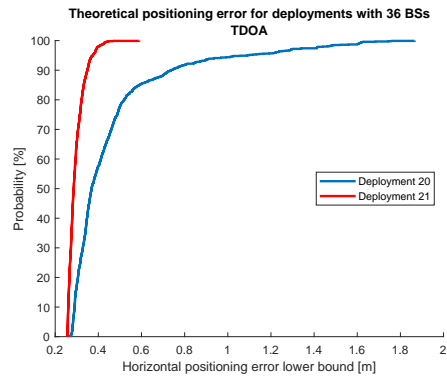
(c) 100 deployments 9–12 with 18 BSs.



(d) 100 deployments 13–16 with 24 BSs.

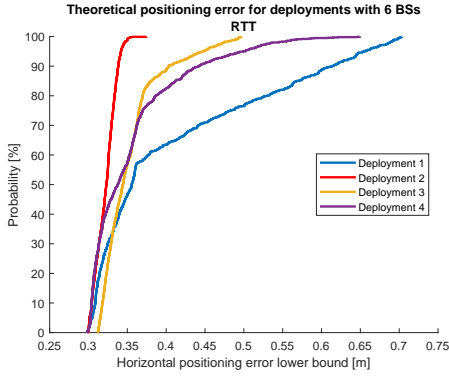


(e) 100 deployments 17–19 with 30 BSs.

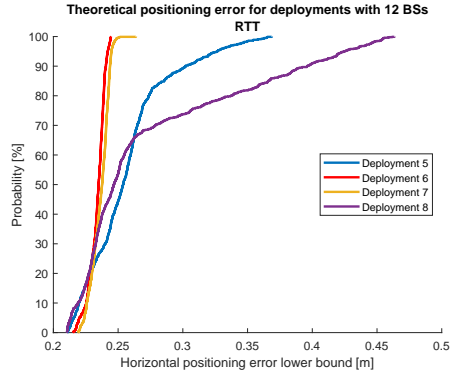


(f) 100 deployments 20–21 with 36 BSs.

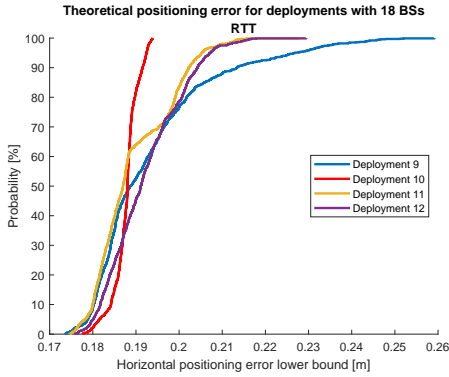
Figure 4.6: CDFs showing the theoretical lower bound of the horizontal positioning error using TDOA for 100 deployments 1–21.



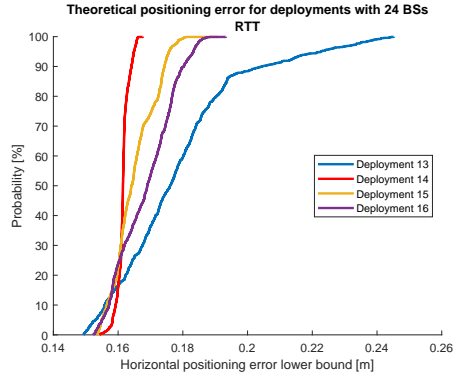
(a) 100 deployments 1–4 with 6 BSs.



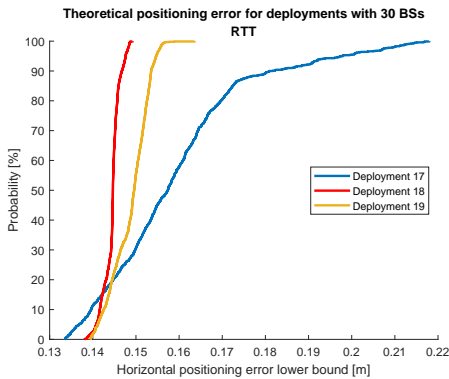
(b) 100 deployments 5–8 with 12 BSs.



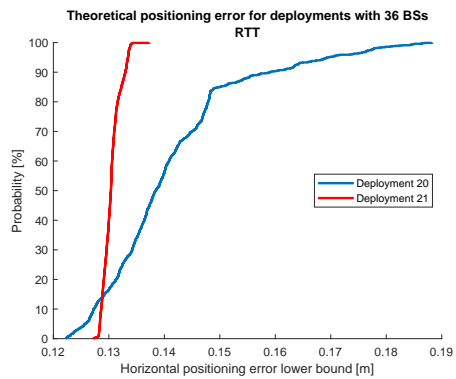
(c) 100 deployments 9–12 with 18 BSs.



(d) 100 deployments 13–16 with 24 BSs.



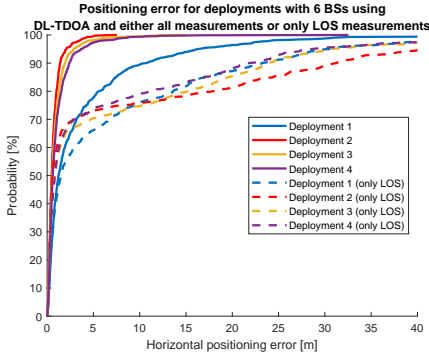
(e) 100 deployments 17–19 with 30 BSs.



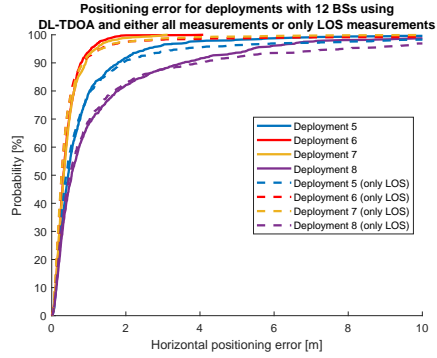
(f) 100 deployments 20–21 with 36 BSs.

Figure 4.7: CDFs showing the theoretical lower bound of the horizontal positioning error using RTT for 100 deployments 1–21.

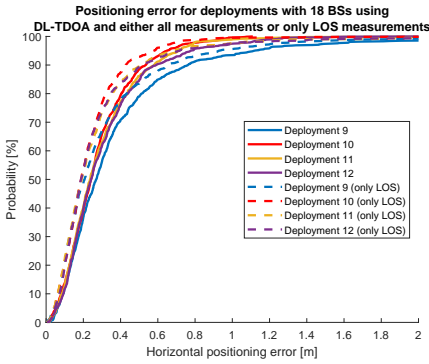
The simulated positioning errors for deployments 1–21 are visualised as CDFs for DL-TDOA and RTT in Figures 4.8 and 4.9, respectively. For DL-TDOA the solid lines represent positioning errors where all available measurements are used in the estimation and the dashed lines represent positioning errors where only measurements from LOS links are used. The simulation results for both positioning techniques follow a similar pattern concerning the performance of the different deployments as observed in the theoretical results. The positioning accuracy improves as the number of BSs increases for both positioning techniques but the difference in positioning error between them is very small. When only LOS measurements are used when estimating the position, the accuracy increases compared to utilising all available measurements. This holds when the number of BSs is at least 18, otherwise the accuracy becomes better when all measurements are included.



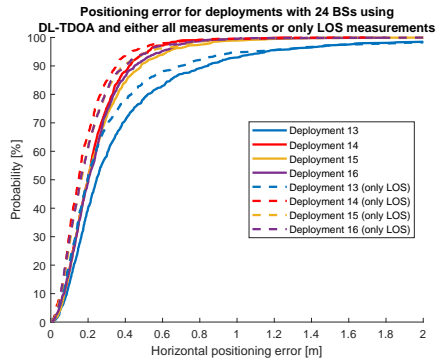
(a) 100 deployments 1–4 with 6 BSs.



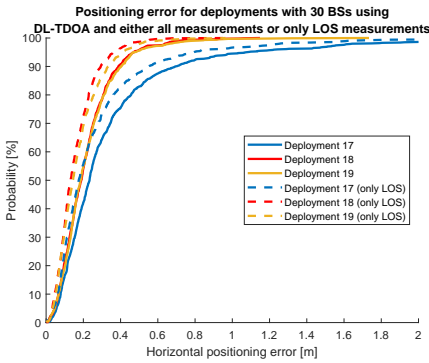
(b) 100 deployments 5–8 with 12 BSs.



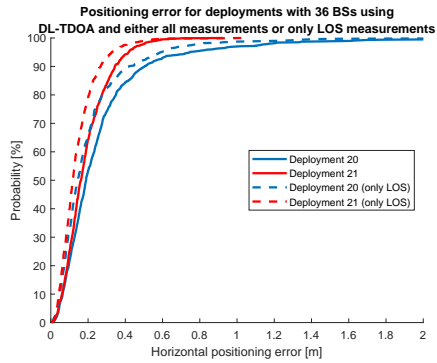
(c) 100 deployments 9–12 with 18 BSs.



(d) 100 deployments 13–16 with 24 BSs.

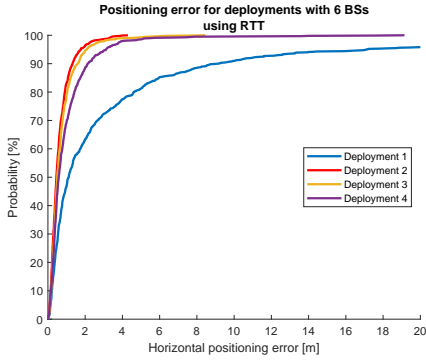


(e) 100 deployments 17–19 with 30 BSs.

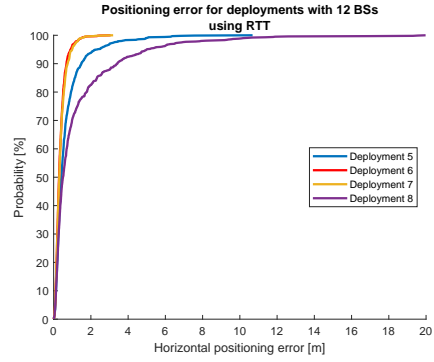


(f) 100 deployments 20–21 with 36 BSs.

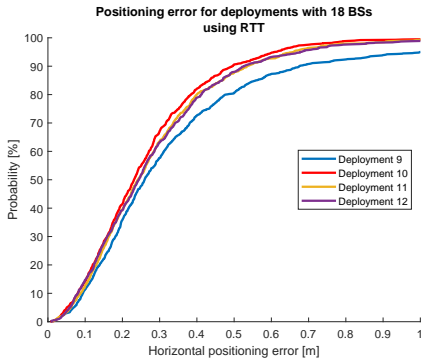
Figure 4.8: CDFs showing the simulated positioning error using DL-TDOA for 100 deployments 1–21 using either all measurements or only LOS measurements.



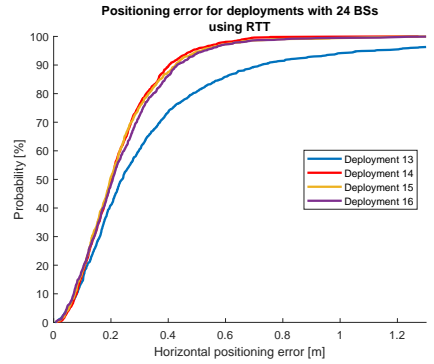
(a) 100 deployments 1–4 with 6 BSs.



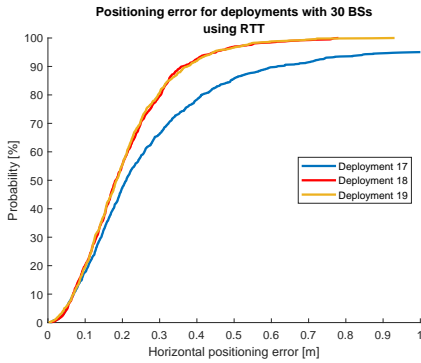
(b) 100 deployments 5–8 with 12 BSs.



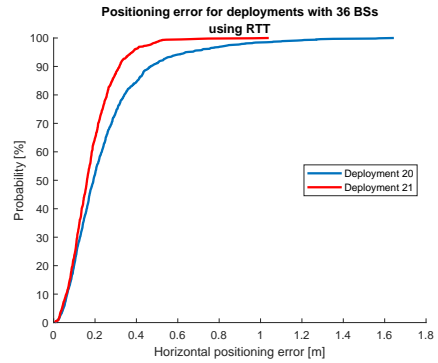
(c) 100 deployments 9–12 with 18 BSs.



(d) 100 deployments 13–16 with 24 BSs.



(e) 100 deployments 17–19 with 30 BSs.



(f) 100 deployments 20–21 with 36 BSs.

Figure 4.9: CDFs showing the simulated positioning error using RTT for 100 deployments 1–21 using all available measurements.

For all deployments, the positioning error at the 80, 90 and 95 percentiles are presented in Table 4.2. The best result is obtained for deployment 21 with a

positioning error of 0.28 m at the 80 percentile, 0.34 m at the 90 percentile and 0.42 m at the 95 percentile.

Table 4.2: Positioning error at the 80, 90, and 95 percentiles using DL-TDOA for 100 deployments 1–21.

100 deployment	Positioning error [m]		
	80%	90%	95%
1	5.59	10.68	16.31
2	1.01	1.40	2.06
3	1.25	1.94	2.86
4	1.55	2.37	3.70
5	1.02	1.78	2.58
6	0.61	0.79	1.06
7	0.60	0.92	1.19
8	1.79	3.53	5.42
9	0.51	0.76	1.12
10	0.40	0.53	0.65
11	0.44	0.58	0.71
12	0.44	0.59	0.78
13	0.52	0.84	1.15
14	0.33	0.42	0.52
15	0.36	0.48	0.62
16	0.34	0.45	0.59
17	0.46	0.69	1.08
18	0.31	0.39	0.47
19	0.31	0.40	0.47
20	0.35	0.51	0.75
21	0.28	0.34	0.42

In Figure 4.10, the position estimation accuracy for the standard and edge deployments are plotted as the number of BSs increases and when DL-TDOA is used. In the figures, the # symbolises the word *number*. The solid lines represent positioning accuracy when all available measurements are used in the estimation and the dashed lines represent positioning errors when only measurements from LOS links are used. In general the position estimation accuracy increases as the number of BSs increases. The subfigures indicate a saturation of the accuracy when the number of BSs exceeds 18 or 24. This is the case both when all measurements are used and when only LOS measurements are used.

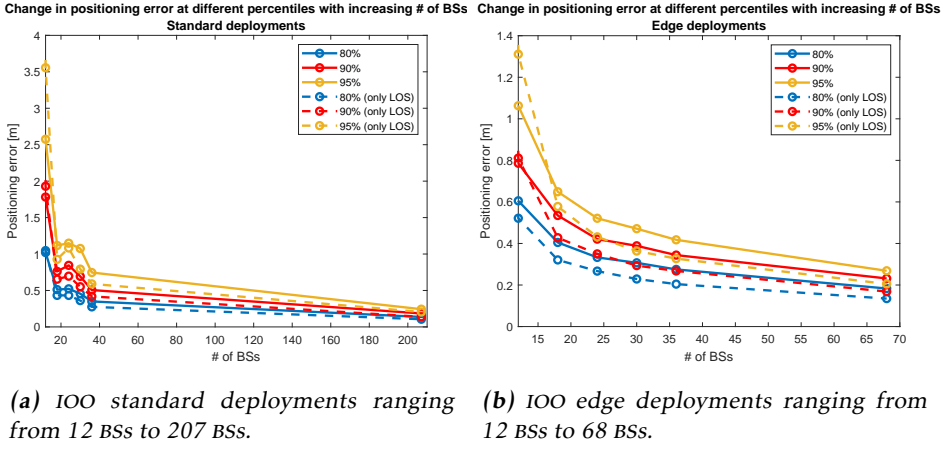


Figure 4.10: Curves showing the change in positioning error at different percentiles with increasing number of BSs, starting at 12 BSs. The standard and edge deployments are presented when DL-TDOA is the method used.

In Table 4.3, the positioning error at the 80, 90 and 95 percentiles is presented for the standard deployments when all measurements are used. The percentage change in positioning error between two consecutive deployments is also shown. The largest improvement in performance occurs at the increment from 6 BSs to 12 BSs, where the positioning error decreases with more than 80 %. Table 4.4 presents the corresponding information for the edge deployments. Also amongst the edge deployments the largest improvement in performance occurs at the increment from 6 BSs to 12 BSs, where the positioning error decreases with more than 40 %.

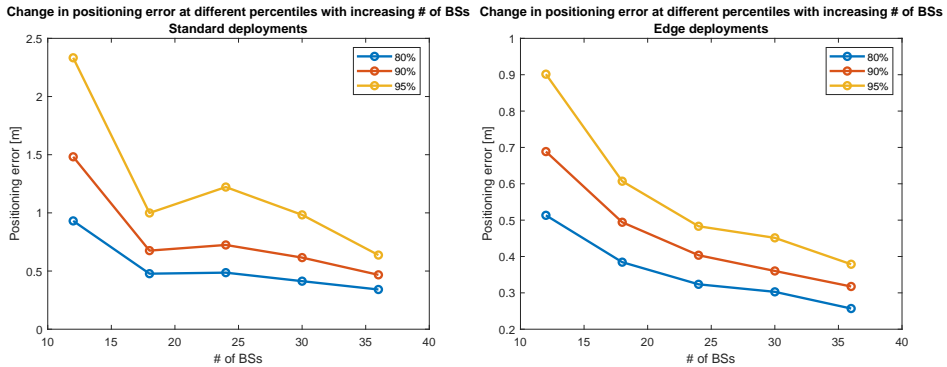
Table 4.3: Positioning error and percentage change in positioning error between two consecutive deployments for all IOO standard deployments when DL-TDOA and all measurements are used.

No of BSs	Positioning error [m]			Percentage change [%]		
	80%	90%	95%	80%	90%	95%
6	5.59	10.68	16.31	-	-	-
12	1.02	1.79	2.58	81.8	83.3	84.2
18	0.51	0.76	1.12	49.8	57.3	56.6
24	0.52	0.84	1.15	-2.1	-11.0	-2.9
30	0.46	0.69	1.08	12.7	17.9	6.4
36	0.35	0.51	0.75	23.4	27.1	30.7
207	0.14	0.18	0.24	60.8	63.6	67.4

Table 4.4: Positioning error and percentage change in positioning error between two consecutive deployments for all IOO standard deployments when RTT and all measurements are used.

No of BSs	Positioning error [m]			Percentage change [%]		
	80%	90%	95%	80%	90%	95%
6	1.01	1.40	2.06	-	-	-
12	0.61	0.79	1.06	40.0	44.0	48.4
18	0.40	0.53	0.65	33.1	32.0	39.0
24	0.33	0.42	0.52	17.8	21.2	19.7
30	0.31	0.39	0.47	7.8	7.7	9.6
36	0.28	0.34	0.42	10.4	11.5	11.4
68	0.18	0.23	0.27	33.4	32.7	35.7

In Figure 4.11, the position estimation accuracy for the IOO standard and edge deployments are plotted as the number of BSs increases and when RTT is used. In general the position estimation accuracy increases as the number of BSs increases. Figure 4.11a indicates a saturation of the accuracy when the number of BSs exceeds 18 or 24. A clear saturation is not seen in Figure 4.11b. The best accuracy in the tested intervals is obtained when the number of BSs is 36, i.e. deployment 21. In this deployment the positioning error is 0.13 m at the 80 percentile, 0.17 m at the 90 percentile and 0.21 m at the 95 percentile.



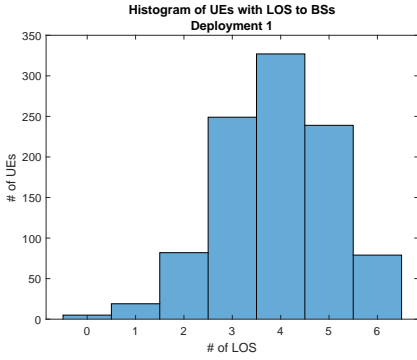
(a) IOO standard deployments ranging from 12 BSs to 36 BSs.

(b) IOO edge deployments ranging from 12 BSs to 36 BSs.

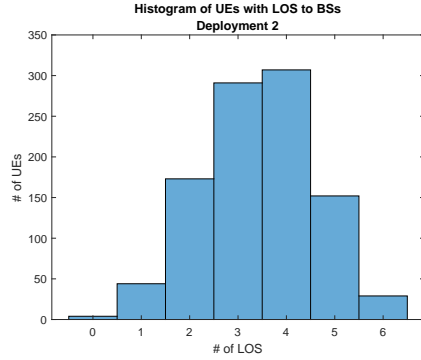
Figure 4.11: Curves showing the change in positioning error at different percentiles with increasing number of BSs, starting at 12 BSs. The standard and edge deployments are presented when RTT is the method used.

4.2.2 Line-Of-Sight

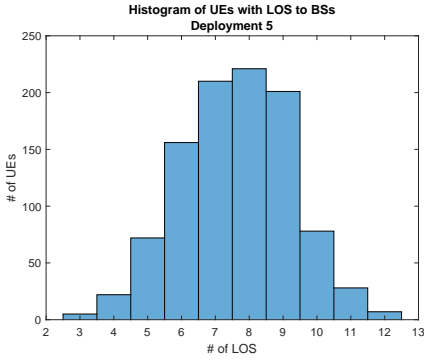
In IOO there is a probability of having a LOS link between a BS and a UE. This probability only depends on the 2D distance between the BS and the UE. In Figure 4.12, LOS statistics are presented for the IOO deployments 1, 2, 5, 6, 20 and 21. The histograms show the number of UEs that have a certain number of LOS links to BSs and more BSs are shown to increase the number of LOS links. The corresponding histograms for the remaining IOO deployments are shown in Appendix A.1.2.



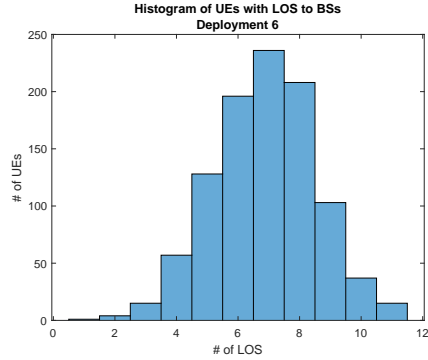
(a) 100 deployment 1.



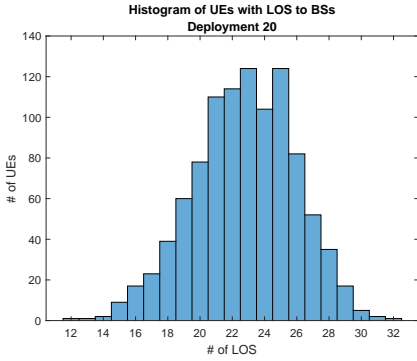
(b) 100 deployment 2.



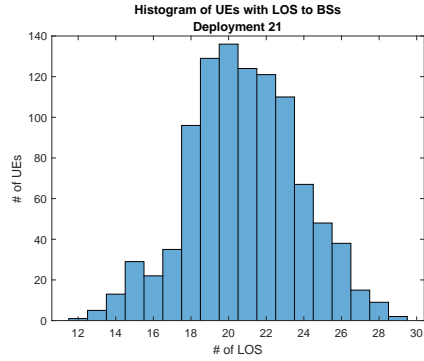
(c) 100 deployment 5.



(d) 100 deployment 6.



(e) 100 deployment 20.

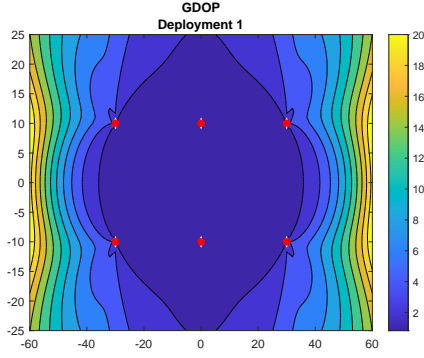


(f) 100 deployment 21.

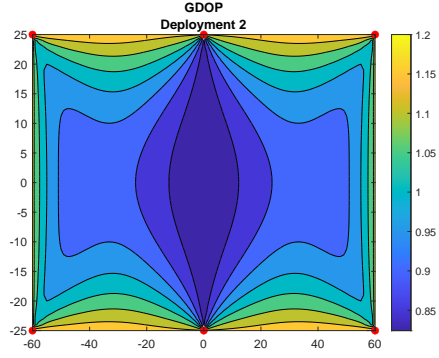
Figure 4.12: Histograms showing the number of UEs with a certain number of LOS links to BSs for 100 deployments 1, 2, 5, 6, 20 and 21.

4.2.3 Geometry

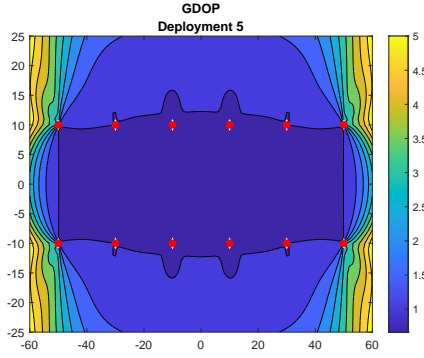
In Figure 4.13, contour plots of the GDOP, as a result from Equation (2.25), for deployments 1, 2, 5, 6, 20 and 21 are presented. In general, the GDOP is lower in the edge deployments compared to the standard deployments. The corners and edges exhibit the highest GDOP. Increasing the number of BSs leads to lower GDOP for both deployment types. The best GDOP is obtained in deployment 21.



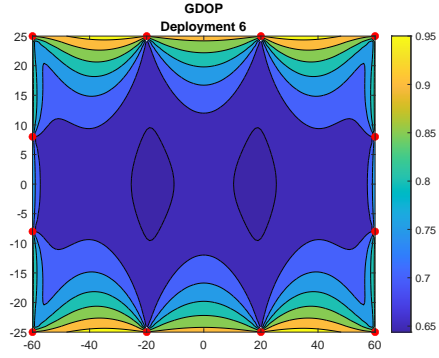
(a) IOO deployment 1.



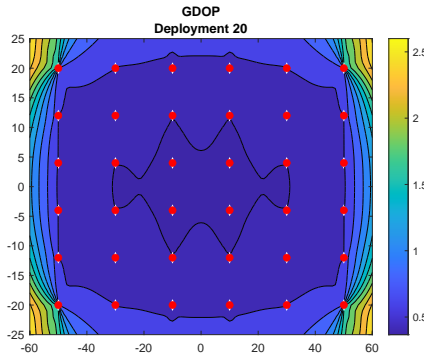
(b) IOO deployment 2.



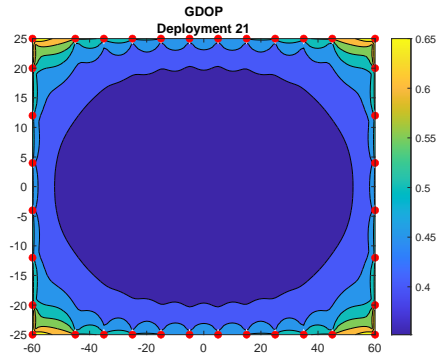
(c) IOO deployment 5.



(d) IOO deployment 6.



(e) IOO deployment 20.



(f) IOO deployment 21.

Figure 4.13: Contour plots showing the GDOP for IOO deployments 1, 2, 5, 6, 20 and 21. The deployment area is $120 \text{ m} \times 50 \text{ m}$ and the red dots represent the BSs.

The positioning error for UEs located inside and outside the convex hull of the BSs is visualised in Figure 4.14 for deployments 1, 5 and 20. DL-TDOA is considered. An observation to be made is that the position estimation of UEs located inside the convex hull is more accurate in comparison to the position estimation of UEs located outside the convex hull.

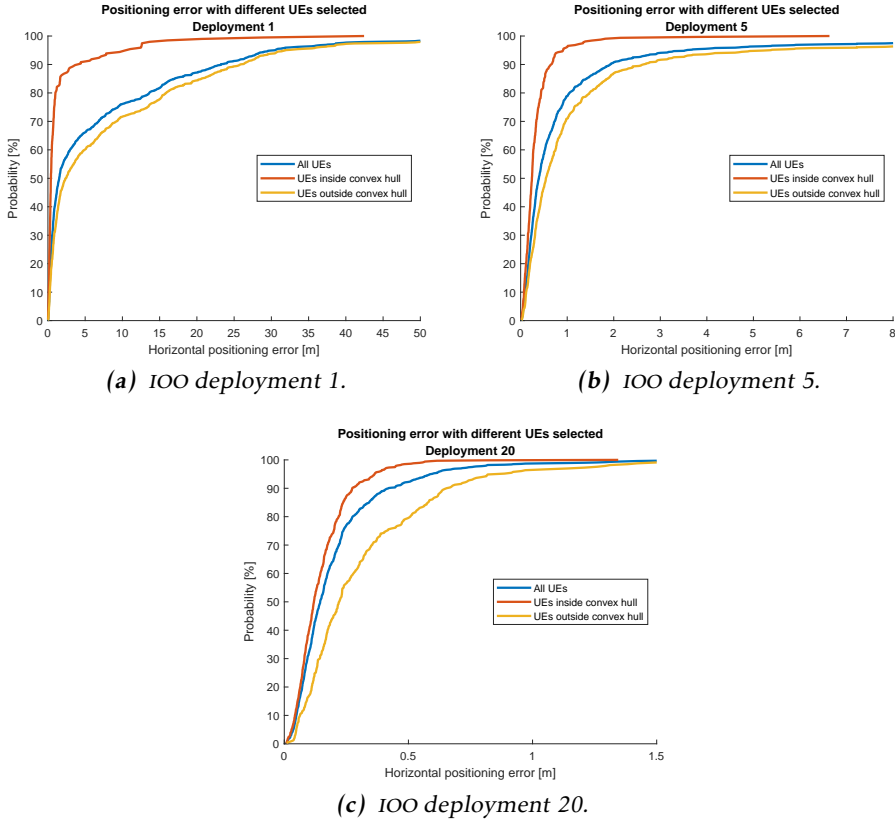


Figure 4.14: CDFs showing the positioning error for IOO deployment 1, 5 and 20 for all UEs, only UEs inside the convex hull and only UEs outside the convex hull selected.

4.2.4 Worst Position Estimates

For IOO deployments 5 and 6, Figure 4.15 illustrates the locations of the worst 10% of the UEs when considering positioning error. Results are shown for both cases when using all measurements in the position estimation and when only using LOS measurements. In the figures, the red dots illustrate the UEs and the black dots represent the BSs. In Figures 4.15a and 4.15c the positioning error at the 90 percentile is 1.77 m and 0.85 m, respectively, when all measurements are used. In Figures 4.15b and 4.15d the positioning error at the 90 percentile is

1.93 m and 0.88 m, respectively, when only LOS measurements are used.

In the edge deployment the worst 10% of the UEs seem to be randomly distributed inside the whole deployment area. This is independent of if all measurements or only LOS measurements are used during the position estimation. In the standard deployment the worst 10% of the UEs tend to be located around the corners and the short sides of the deployment area, but with some outliers. This is also independent of which measurements are used during the position estimation. The corresponding figures for IOO deployments 1, 2, 20 and 21 can be seen in Appendix A.1.3. The different deployments follow the same pattern as previously described, thus are not shown here, but when more BSs are added to the standard deployment, a larger amount of UEs are located along the sides of the deployment area.

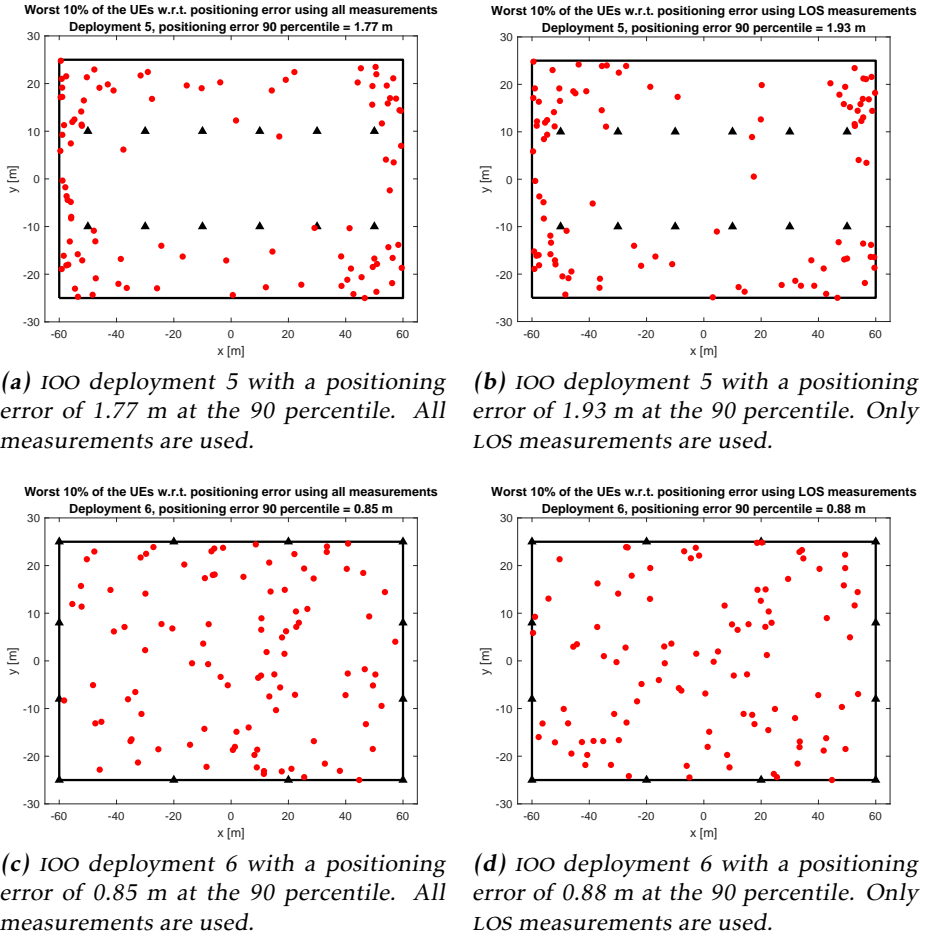


Figure 4.15: Plots showing the positions of the worst 10% of the UEs with respect to positioning error, either using all measurements or only LOS measurements, for IOO deployments 5 and 6 with 12 BSs each.

4.2.5 Interference

The network planning and different interference scenarios were previously presented in Section 3.4.4. Positioning error results from the interference investigation are shown as CDFs in Figure 4.16. The results concern the network planning *no interference*, *down-up* and *all interfering* for deployments 5, 6 and 20. The order from best to worst performance regarding accuracy is for deployments 5 and 6 *no interference*, *down up* and finally *all interfering*. For deployment 20, the order from best to worst performance is *no interference* and *down up* with similar performance and then *all interfering*. The performance is better in the edge deployment compared to the standard deployments when the number of BSs is 12.

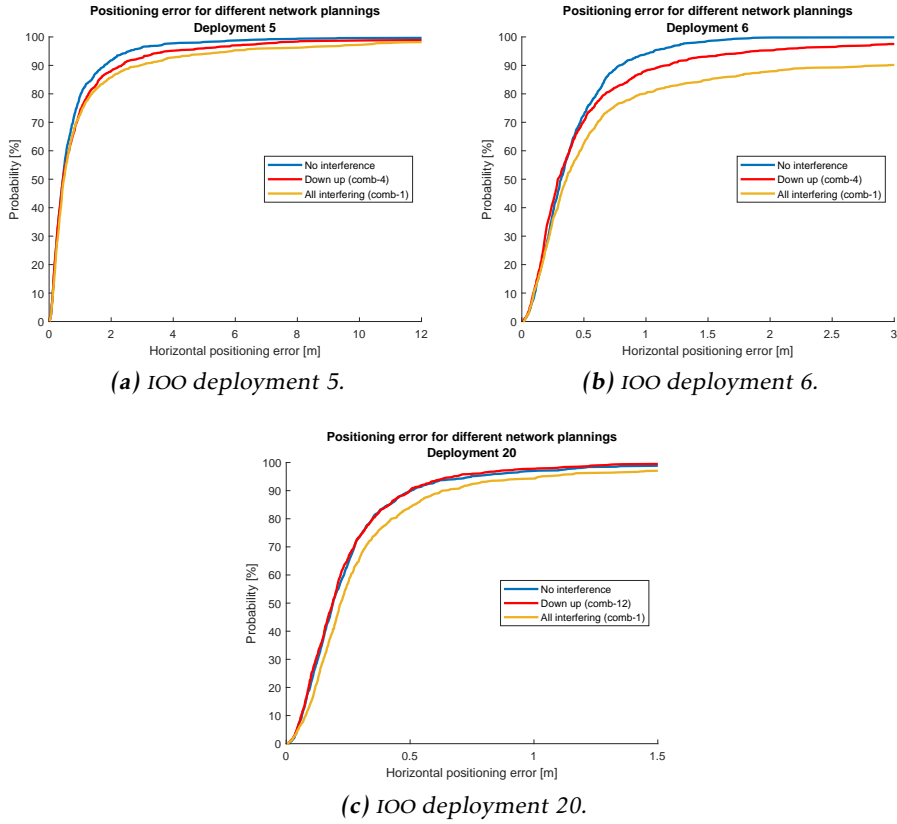


Figure 4.16: CDFs showing the positioning error for 100 deployments 5, 6 and 20 when interference is disabled as well as when interference is present.

Figure 4.17 presents the CDFs for 100 deployment 5 when interference is present and either all measurements or only LOS measurements are used in the position estimation. What can be observed is that there is no significant difference whether all measurements are used or not. The corresponding figures for 100 deployments 6 and 20 exhibit the same behaviour and can be seen in Figure A.15 in Appendix A.1.4.

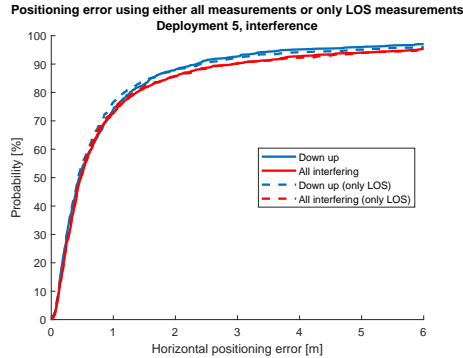


Figure 4.17: CDFs showing the positioning error for IOO deployment 5 using the two different network plannings down up and all interfering.

The positioning error at the 80, 90 and 95 percentiles for the different deployments with different network plannings is presented in Table 4.5. One can notice that deployment 20 has the best performance in terms of positioning accuracy and that *down up* leads to a lower position estimation error than *all interfering*.

Table 4.5: Positioning error in meters for three different percentiles for the network plannings down up and all interfering.

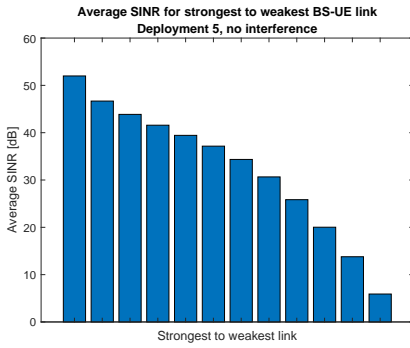
IOO deployment	Network planning					
	Down up [m]			All interfering [m]		
	80%	90%	95%	80%	90%	95%
5	1.28	2.34	3.82	1.37	2.92	5.89
6	0.67	1.17	1.87	0.98	2.95	6.49
20	0.35	0.50	0.67	0.43	0.63	1.03

The best performing network planning when interference is present is for all deployments *down up*. In Table 4.6, the positioning error at the 90 percentile for *down up* is compared to the positioning error of *no interference* where interference is disabled. Also presented is the percentage change in positioning error between *down up* and *no interference*.

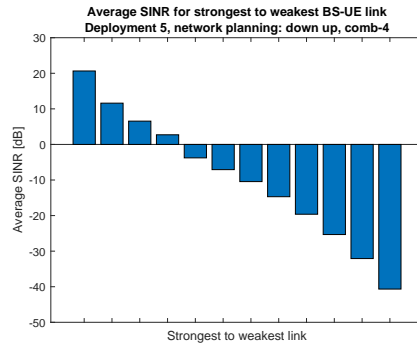
Table 4.6: Positioning error at the 90 percentile for the network plannings *no interference* and *down up*. The percentage change in positioning error is also shown.

IOO deployment	Positioning error		
	No interference [m]	Down up [m]	Percentage change [%]
5	1.78	2.34	31.3
6	0.79	1.17	48.2
20	0.56	0.50	-1.2

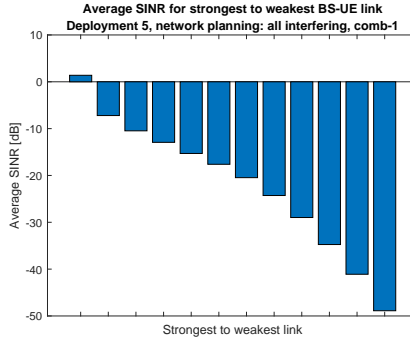
Histograms visualising the average link SINR for strongest to weakest link are presented in Figure 4.18 for 100 deployment 5 and includes the three network plannings. The corresponding figures for 100 deployments 6 and 20 are shown in Figures A.16 and A.17 in Appendix A.1.4. With no interference the SINR is positive for all links between a BS and a UE. Deployment 20 has one link with negative SINR. When all signals are interfering, the link SINR is always negative. One exception is the strongest link for deployments 5 and 6. In the intermediate case, meaning network planning *down up*, the SINR is partly positive and partly negative for the links, though a majority of the links have negative SINR. In the figures it can clearly be seen that less interference results to higher link SINR.



(a) 100 deployment 5 with network planning no interference.



(b) 100 deployment 5 with network planning down up.



(c) 100 deployment 5 with network planning all interfering.

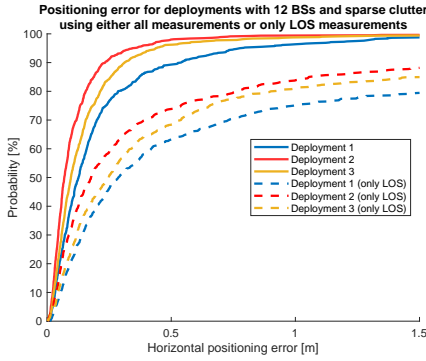
Figure 4.18: Bar graphs showing average SINR for strongest to weakest BS-UE link for 100 deployment 5 when interference is disabled as well as when interference is present.

4.3 Indoor Factory Study

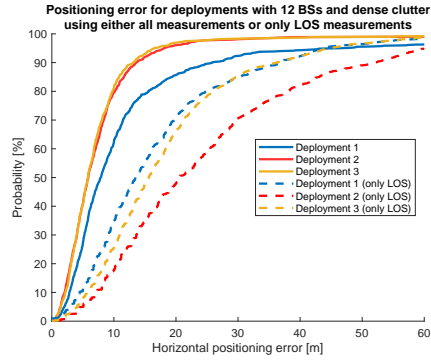
All simulation results obtained when studying the InF scenario are presented in this section. The same parameter combination chosen in the IOO simulations was used in the InF simulations.

4.3.1 Simulated Positioning Accuracy

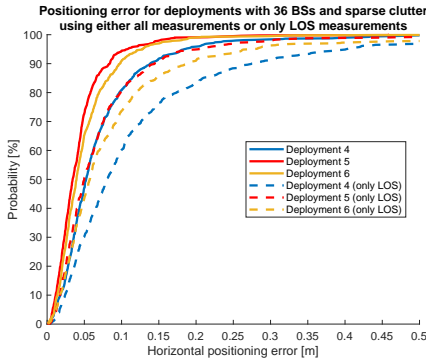
The simulated positioning errors for deployments 1–6 in InF-SH and InF-DH are visualised as CDFs in Figure 4.19. The solid lines represent positioning errors where all available measurements are used in the position estimation and the dashed lines represent positioning errors where only measurements from LOS links are used. The positioning accuracy is better in the sparsely cluttered environment compared to the densely cluttered environment and in both cases it improves when increasing the number of BSs. The standard deployments always have the worst performance. In the sparsely cluttered environment, the edge deployments perform better but in the densely cluttered environment the edge and mixed deployments perform equally good. The accuracy decreases when only LOS measurements are used for the position estimation compared to when all available measurements are utilised.



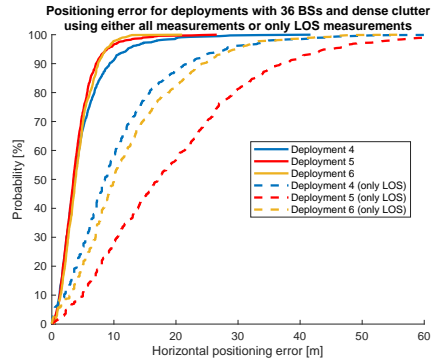
(a) InF deployments 1–3 with 12 BSs in InF-SH.



(b) InF deployments 1–3 with 12 BSs in InF-DH.



(c) InF deployments 4–6 with 36 BSs in InF-SH.



(d) InF deployments 4–6 with 36 BSs in InF-DH.

Figure 4.19: CDFs showing the positioning error for InF deployments 1–6 in the InF scenarios InF-SH and InF-DH.

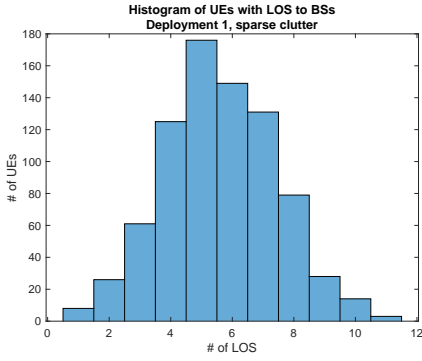
Table 4.7 shows the positioning error at the 80, 90 and 95 percentiles for deployments 1–7 in the sparsely and densely cluttered environments when all measurements are used in the position estimation. Deployment 7 was only simulated in InF-DH because of the overall bad accuracy in the densely cluttered environment.

Table 4.7: Positioning error at the 80, 90 and 95 percentiles for InF deployments 1–7 in InF-SH and InF-DH.

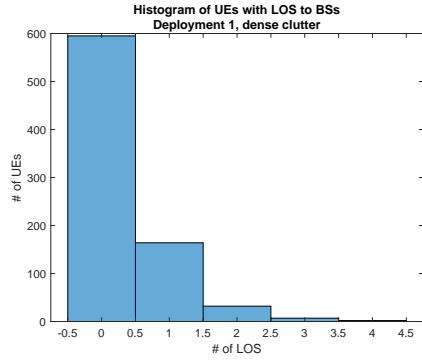
InF deployment	Positioning error [m]					
	InF-SH			InF-DH		
	80%	90%	95%	80%	90%	95%
1	0.29	0.54	0.78	15.59	25.83	46.47
2	0.16	0.23	0.34	10.18	13.56	18.04
3	0.21	0.31	0.44	9.77	13.11	16.48
4	0.10	0.14	0.18	6.87	9.32	12.22
5	0.06	0.08	0.11	5.70	7.11	8.89
6	0.07	0.10	0.13	6.12	7.47	8.69
7	-	-	-	4.63	5.93	7.52

4.3.2 Line-Of-Sight

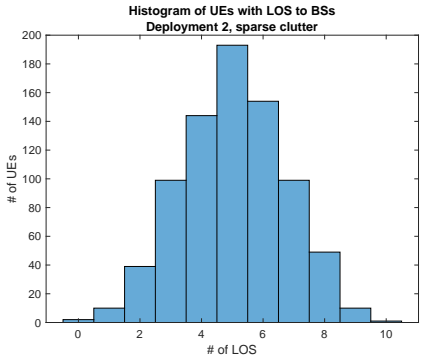
The LOS probability in InF depends on the placement and size of the clutter, as well as the BS and UE heights. The histograms in Figures 4.20 and 4.21 show the LOS statistics for deployments 1, 2, 4 and 5 in the two InF scenarios. The LOS statistics display a significantly higher number of LOS links in InF-SH compared to InF-DH. This relationship also applies for the mixed deployments, which can be seen in Figures A.18 and A.19 in Appendix A.2.1.



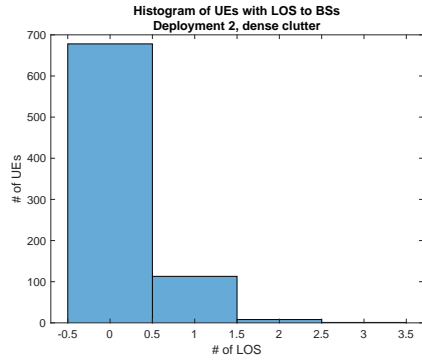
(a) InF deployment 1 in InF-SH.



(b) InF deployment 1 in InF-DH.



(c) InF deployment 2 in InF-SH.



(d) InF deployment 2 in InF-DH.

Figure 4.20: Histograms showing the number of UEs with a certain number of LOS links to BSs for InF deployments 1 and 2 with 12 BSs each in InF-SH and InF-DH.

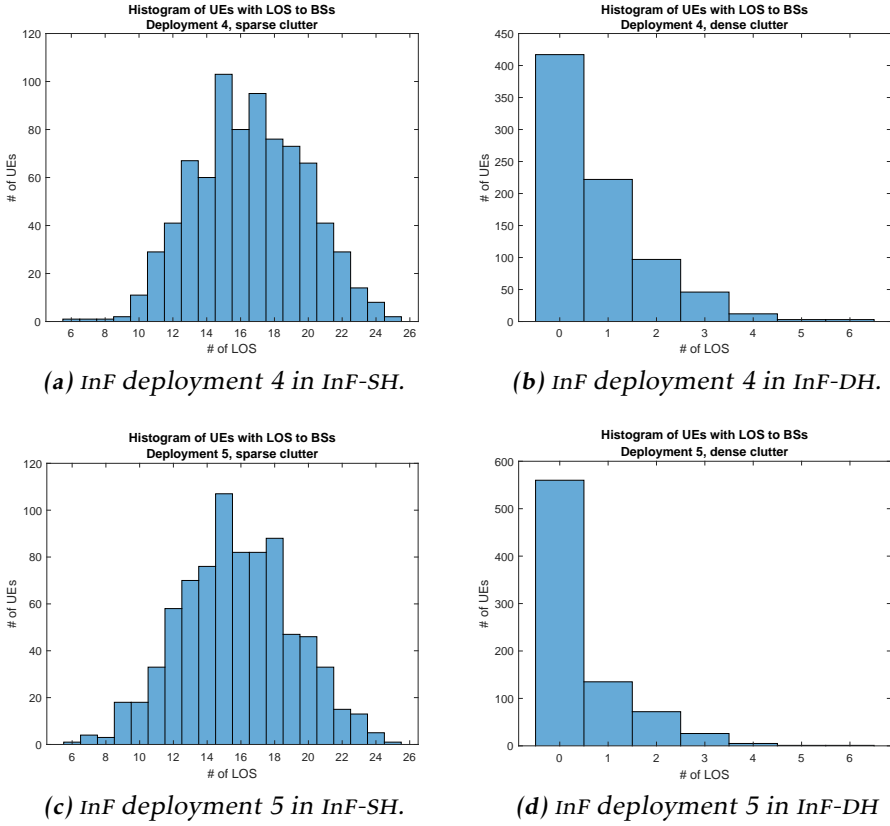
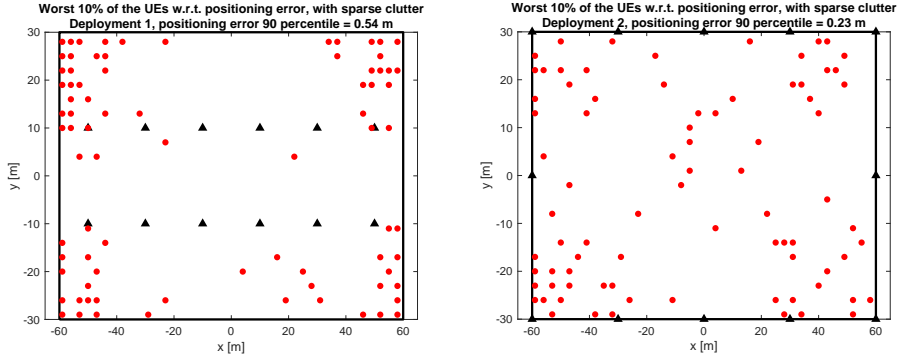


Figure 4.21: Histograms showing the number of UEs with a certain number of LOS links to BSs for InF deployments 4 and 5 with 36 BSs each in InF-SH and InF-DH.

4.3.3 Worst Position Estimates

The worst 10% of the UEs with respect to positioning error for deployments 1 and 2 in InF-SH are visualised in Figure 4.22. For the standard deployment, seen in Figure 4.22a, the worst 10% of the UEs are located around the corners and along the short sides, with some additional outliers. The positioning error at the 90 percentile is 0.54 m. The edge deployment, seen in Figure 4.22a, has a positioning error of 0.23 m at 90 percentile and does not have any clear pattern regarding the UE positions. The distribution appears to be mostly random. The same holds for the mixed deployment in InF-SH. In InF-DH the UEs with the worst position estimates for the standard and edge deployments are mostly placed in groups, around what might be clutter, inside the deployment area. The corresponding figures representing deployment 3 in InF-SH and deployments 1-3 in InF-DH can be seen in Appendix A.2.2.

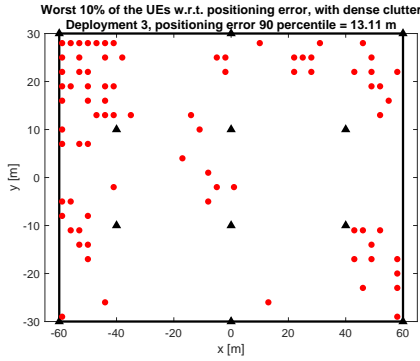


(a) InF deployment 1 with a positioning error of 0.54 m at the 90 percentile.

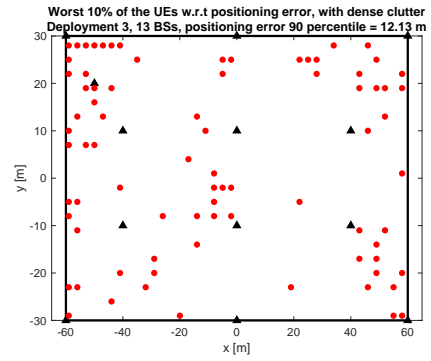
(b) InF deployment 2 with a positioning error of 0.23 m at the 90 percentile.

Figure 4.22: Plots showing the positions of the worst 10% of the UEs with respect to positioning error for InF deployments 1 and 2 with 12 BSS each in InF-SH.

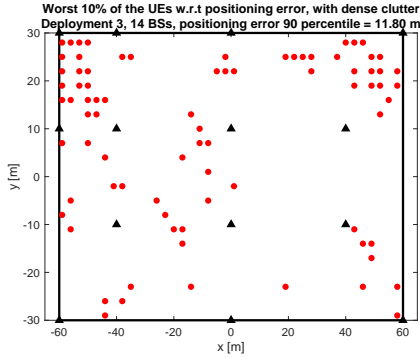
The 10% of the UEs with worst position estimates in deployment 3 in InF-DH, which is the mixed deployment, is plotted in Figure 4.23a. A large share of the visualised UEs are located in the upper left corner. Figures 4.23b–4.23d illustrate modifications of the mixed deployment where BSSs have been added in the UE dense corner. The figures show that adding BSSs decreases the number of poorly positioned UEs located in the upper left corner, furthermore the positioning error at the 90 percentile decreases. The CDFs of deployment 3 and its modifications are presented in Figure 4.24. The overall positioning accuracy slightly improves when adding BSS.



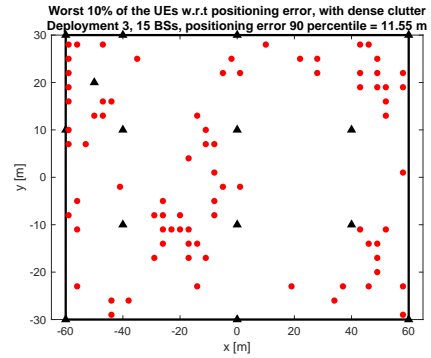
(a) Original InF deployment 3 with a positioning error of 13.11 m at the 90 percentile.



(b) InF deployment 3 with one additional BS and a positioning error of 12.13 m at the 90 percentile.



(c) InF deployment 3 with two additional BSs and a positioning error of 11.80 m at the 90 percentile.



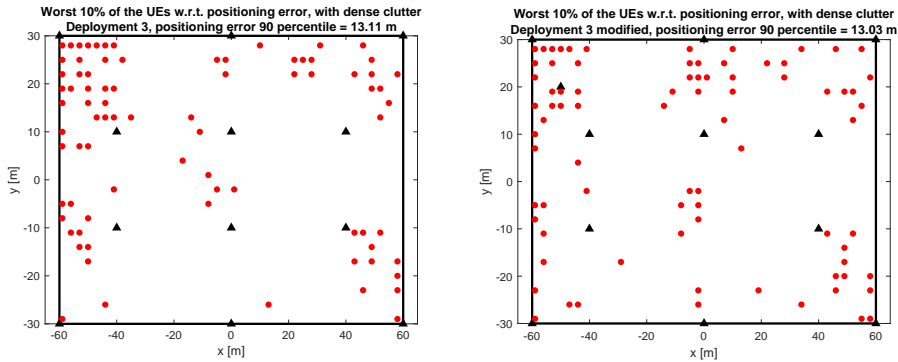
(d) InF deployment 3 with three additional BSs and a positioning error of 11.55 m at the 90 percentile.

Figure 4.23: Plots showing the positions of the worst 10% of the UEs with respect to positioning error for InF deployment 3 and the modifications where 1–3 BSs are added in InF-DH.



Figure 4.24: CDFs showing the positioning error for InF deployment 3 and the modifications where 1–3 BSs are added in InF-DH.

Instead of only adding BSs, the effect of moving BSs was examined as well. In Figure 4.25, representing deployment 3, one BS is moved to the top left corner, which contains many poorly positioned UEs, from a spot where few poorly positioned UEs are located. The positioning error at the 90 percentile slightly decreases but there is no significant difference in accuracy in total, see Figure 4.26.



(a) Original InF deployment 3 with a positioning error of 13.11 m at the 90 percentile.

(b) InF deployment 3 with one BS moved and a positioning error of 13.03 m at the 90 percentile.

Figure 4.25: Plots showing the positions of the worst 10% of the UEs with respect to positioning error for InF deployment 3 and the modification where one BS is moved in InF-DH.

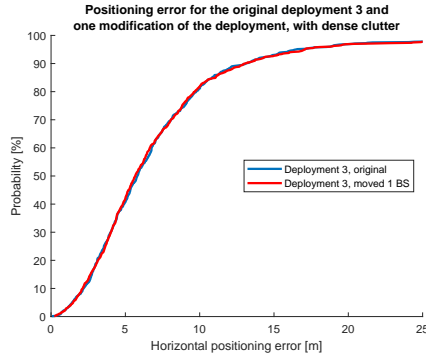


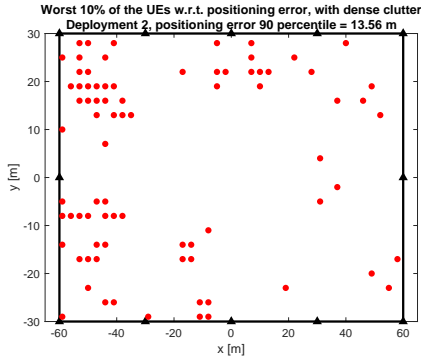
Figure 4.26: CDFs showing the positioning error for InF deployment 3 and the modification where one BS is moved.

Table 4.8 shows the positioning error at the 90 and 95 percentiles for InF deployment 3 and the modifications where BSs are added or moved. Also included is the number of UEs with a positioning error greater than 10 m. As can be seen, this number decreases when BSs are added but when one BS is moved the difference is minimal.

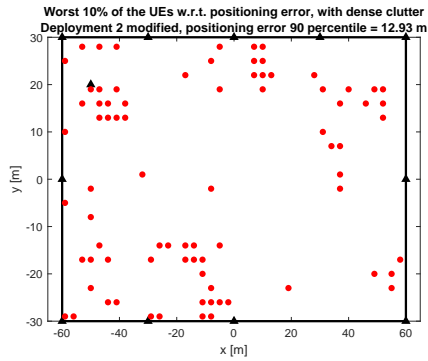
Table 4.8: Positioning error at the 90 and 95 percentile for InF deployment 3 and the modifications where 1–3 BSs are added or one BS is moved. The scenario is InF-DH.

InF deployment 3	Positioning error [m]		No of UEs with positioning error > 10 m
	90%	95%	
Original	13.11	16.48	151
Added 1 BS	12.13	15.80	133
Added 2 BSs	11.80	14.73	129
Added 3 BSs	11.55	14.12	114
Moved 1 BS	13.03	17.09	146

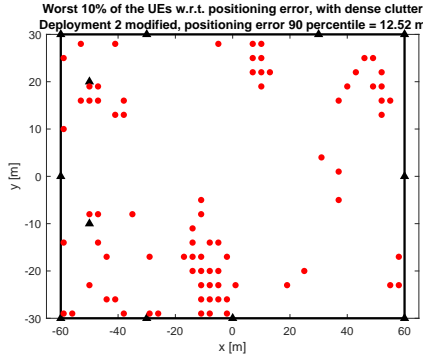
Moving one BS in deployment 3 does not display a large difference in positioning accuracy, thus, the same investigation is made for deployment 2 which is an edge type deployment, to observe if the effect is similar or not. Figure 4.27 illustrates the locations of the 10% of the UEs with the worst positioning error for the original deployment 2 and the modifications where one and two BSs are moved. The corresponding BSs are presented in Figure 4.28. Table 4.9 shows the position error at the 90 and 95 percentile and also the number of UEs with a positioning error greater than 10 m. The results show that moving one or two BSs only contribute with a very small improvement in positioning accuracy.



(a) Original InF deployment 2 with a positioning error of 13.56 m at the 90 percentile.



(b) InF deployment 2 with one BS moved with a positioning error of 12.93 m at the 90 percentile.



(c) InF deployment 2 with two BSs moved with a positioning error of 12.52 m at the 90 percentile.

Figure 4.27: Plots showing the positions of the worst 10% of the UEs with respect to positioning error for InF deployment 2 and the modifications where one and two BSs are moved in InF-DH.

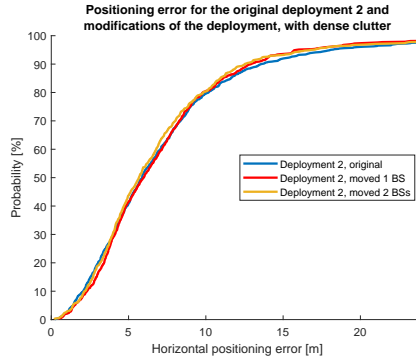


Figure 4.28: CDFs showing the positioning error for InF deployment 2 and the modifications where one and two BSs are moved, respectively.

Table 4.9: Positioning error at the 90 and 95 percentile for InF deployment 2 and the modifications where one and two BSs are moved, respectively. The scenario is InF-DH.

InF deployment 2	Positioning error [m]		No of UEs with positioning error > 10 m
	90%	95%	
Original	13.56	18.04	163
Moved 1 BS	12.93	15.85	156
Moved 2 BSs	12.52	16.76	156

Results from simulating deployment 7 with 91 BS located around the edges and in the center, meaning a mixed deployment, in InF-DH can be seen in Figure 4.29. The LOS statistics are slightly improved in comparison to previous deployments and the 10% of the worst UEs with respect to positioning error are clearly grouped together. The CDF for deployment 7 is compared to the CDF for deployment 5 in Figure 4.29c and what can be noticed is an improvement in positioning accuracy. The positioning error at the 90 percentile is now 5.93 m which is an improvement of around 1 m, i.e. a percentage change of 16.5%. The difference in number of BSs is 55.

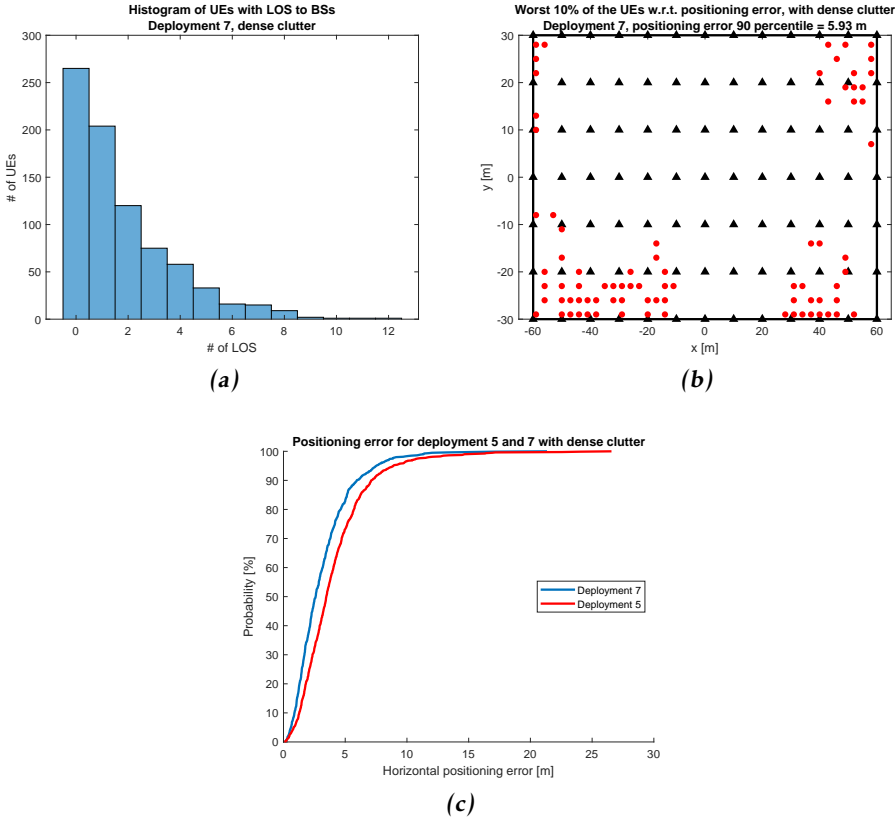
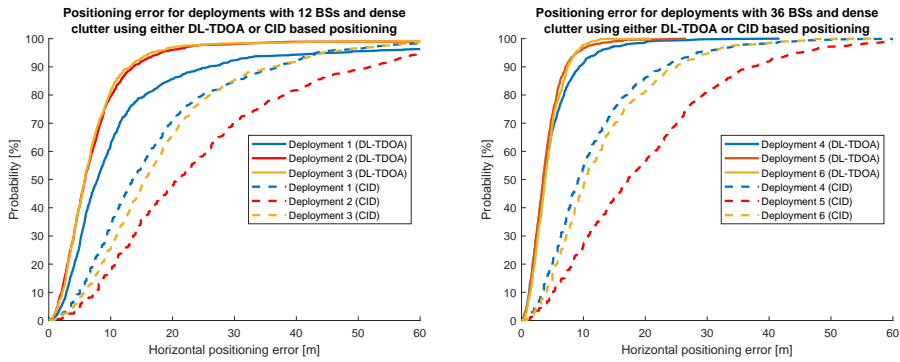


Figure 4.29: (a) LOS statistics for InF deployment 7. (b) Positions of the worst 10% of the UEs with respect to positioning error for InF deployment deployment 7. The positioning error at the 90 percentile is 5.93 m. (c) Positioning error for InF deployment 5 and 7.

4.3.4 Fallback Positioning Technique

Figure 4.30 presents the positioning error for deployments 1–6 in InF-DH when either DL-TDOA or CID based positioning is used. Clearly observable is that DL-TDOA leads to better positioning accuracy compared to CID based positioning.



(a) InF deployments 1–3 with 12 BSs.

(b) InF deployments 4–6 with 36 BSs.

Figure 4.30: CDFs showing the positioning error for InF deployments 1–6 in InF-DH using either DL-TDOA or CID based positioning.

5

Discussion and Analysis

A discussion of the results presented in Chapter 4 is given in this section. First IOO is analysed, followed by InF and afterwards some comments about general deployment strategies are mentioned.

5.1 Indoor Open Office

In this section the results from the IOO study is discussed and analysed. The theoretical and simulated performances of the different deployments and positioning techniques are compared and the impact of BS geometry, LOS links and interference is evaluated.

5.1.1 Theoretical and Simulated Positioning Accuracy

Some figures showing the theoretical RMSE of the position estimates for RTT, for example Figures 4.3d and 4.4b, may be interpreted as having large variations in RMSE but the scale to the right of the heat maps show a very limited range with small values. When using RTT the deployments then have notably low RMSE throughout all deployments compared to using TDOA.

The theoretical CDFs representing the RMSE of the position estimates in Figure 4.6 show the lower bound of the position estimation accuracy when TDOA is used. If these are compared to the corresponding CDFs with simulated positioning errors in Figure 4.8, it can be seen that the simulated CDFs show a slightly higher RMSE than the theoretical one. One reason for such good alignment is that the measurement noise variance utilised in the theoretical study was set to the measurement noise variance estimated from the simulations, making the theory better represent the reality.

Using RTT, the CDFs presenting the theoretical and simulated positioning errors for the different deployments show a behaviour resembling that of TDOA. The difference between the theoretical and simulated accuracy is slightly larger for RTT in comparison to TDOA. The theoretical investigation for both TDOA and RTT assumes perfect synchronisation between BSs and also between BS and UE, which in the end means no synchronisation errors but only measurement errors in each case. In the simulation tool the synchronisation error between BS and UE is incorporated, thereby resulting in slightly worse positioning error for TDOA. The RTT simulations are performed in the simulation tool designed for TDOA calculations, hence the RTT technique is not applied exactly as described by the theory. Moreover, the synchronisation error between BS and UE will be accounted for. The two error sources will together contribute to a greater difference in the positioning error between theory and simulation for RTT as opposed to TDOA. Furthermore, in the RTT method one downlink and one uplink signal measurement are added and then divided by two to obtain an RTT measurement, meaning the total error will be halved. This is a reason why the simulated positioning accuracy is better when using RTT than using TDOA. Still, the theoretical results suggest that RTT can lead to even better positioning accuracy.

When using DL-TDOA the improvement in positioning accuracy saturates at around 18 or 24 BSs for both the standard and edge deployments. The positioning error continues to decrease with additional BSs, but the improvements are very small relative to the total positioning error. Tables 4.3 and 4.4 indicate a large relative change in positioning error when increasing the number of BSs from 36 to 207 in the standard deployment and from 36 to 68 in the edge deployment. Taking into account the significant change in the number of BSs the positioning error does not decrease considerably in relation to the number of added BSs. For the standard deployments, when going from 18 to 24 BSs, the error in fact increases. This is however not related to the number of BSs in the different deployments, but rather to their geometry. Deployment 9 seen in Figure 3.1i, has its 18 BSs enclosing a larger area than deployment 13 with 24 BSs, see Figure 3.1m. The effect of geometry is further discussed in Section 5.1.2. For RTT the positioning error saturates at around 18 or 24 BSs for the standard deployment but there is no clear saturation visible for the edge deployments. The explanation for the increment in positioning error when going from 18 to 24 BSs in the standard deployments is the same as for DL-TDOA.

5.1.2 Geometry

The GDOP plots in Figure 4.13 reveal that deployments with BSs around the edges create more favourable positioning conditions compared to deployments with BSs placed evenly inside the deployment area. The GDOP is considerably smaller and more consistent throughout the whole deployment area in the edge deployments and lower GDOP implies better positioning accuracy according to Equation (2.21). In the standard deployments the GDOP is best inside the convex hull of the BSs and worsens quickly outside. This effect of GDOP on positioning accuracy is validated in Figure 4.14 where UEs inside the convex hulls have smaller positioning

errors in comparison to the UEs outside the convex hulls. In the same figure, the curves named *All UEs* and *UEs outside convex hull* lie close to each other for deployments 1 and 5. The reason is that these deployments have convex hulls enclosing small areas relative to the total deployment area, see Figures 3.1a and 3.1e. The improvement in GDOP is larger if a standard deployment is changed to an edge deployment with the same number of BSs as opposed to if six additional BSs are included in the standard deployment. This indicates that changing BS positions could be a cheaper solution to improve the positioning performance instead of adding BSs. To conclude, according to the GDOP plots, the edge deployments should be the best performing ones, which they are if we look at the simulated CDFs in Figure 4.8.

When using all available measurements during the position estimation, the locations of the UEs with the worst positioning error are justified by GDOP in both the standard and edge deployments. In the standard deployments the poorly estimated UEs are located along the short sides and in the corners, exactly what is anticipated by GDOP. The seemingly random UE distribution in the edge deployments is logical since GDOP is fairly homogenous over the whole deployment area. Some outliers are present in all the deployments and the explanation to these is related to the TOA estimator. The arbitrarily chosen combination of $-\log_2(p)$ and *Sidelobe Guard Fraction* for the TOA estimator might have resulted in a particularly bad fit for the outlier UEs regarding TOA estimation. When only LOS measurements are used in the position estimation, the locations of the worst UEs concerning position accuracy are justified by GDOP. The same reasoning about the cause of the outliers also holds. However, in deployment 1 containing 6 BSs, there exists another explanation to the outlier UEs. Some of them do not have above three LOS links, which is needed to calculate a position estimate. The UEs are then estimated with the generally more inaccurate CID based positioning method instead.

5.1.3 Line-Of-Sight

The results in Figure 4.8 clearly shows that deployments with 6 BSs perform better when all measurements are used in the position estimation compared to when only LOS measurements are used. When utilising DL-TDOA at least four TOA measurements are needed in order to calculate three hyperbolas. The intersection point between these hyperbolas is the estimated position of the UE. When only 6 BSs are deployed and only LOS measurements are used in the position estimation, there are many UEs with less than four LOS links according to the LOS statistics. Estimating the positions of those UEs with DL-TDOA is impossible due to the lack of measurements and CID based positioning is then instead applied as a fallback positioning method. For the deployments with 12 BSs, the difference in positioning accuracy is not significantly large when utilising either all measurements or only LOS measurements. This is justified by the LOS statistics which show very few UEs with less than four LOS links. When the number of BSs is 18 or higher, the positioning accuracy is better when only LOS measurements are used when estimating the UE positions. There are now enough LOS measurements to calcu-

late good position estimates without involving the less preferable NLOS measurements.

The LOS statistics in Figure 4.12 indicate that deployments with all or some BSs placed inside the deployment area have more UEs with a larger number of LOS links than deployments with BSs only placed around the edges. In terms of LOS statistics, the standard deployments then outperform the edge deployments. Given this, the edge deployments still yield the best position estimation accuracy and the standard deployments yield the worst accuracy, regardless of the number of BSs. What can be concluded is that good BS geometry has a bigger impact on the positioning accuracy than the number of LOS links in the studied scenarios.

5.1.4 Interference

Comparing deployments 5 and 6, which are standard and edge deployments with 12 BSs respectively, shows that the standard deployment is slightly less affected by interference. The same comparison is not possible to make for deployments 20 and 21 since we do not have any data from deployment 21. The effect of interference decreases in the standard deployments when increasing the number of BSs. We are not able to comment if the same effect is seen for the edge deployments. However, when inspecting Figure 4.16, none of the deployments are greatly affected by interference. In deployment 5, the network planning *no interference* results in the best positioning accuracy but when interference is present there is not a large difference between *down up* and *all interfering*. In deployment 20, *down up* even shows similar performance as *no interference*. The difference in accuracy between the network plannings is a bit more distinct in deployment 6. In total, the interference does not seem to have a significant impact on the positioning accuracy with a robust positioning algorithm, provided a proper network planning is done. From a positioning perspective one can get a cheaper deployment considering resource consumption by allowing some degree of interference and having a clever network planning. By allocating resources to gain orthogonality the accuracy may improve marginally but it might not be worth the cost.

The link level study reveals in Figure 4.1, an RMSE just below 0.3 m for SNR = -5 dB and higher. Below -5 dB the RMSE is worse. This implies that in system level simulations the best TOA estimates will be obtained when the link SNR \geq -5 dB. Some parameter combinations result in curves where higher SNR results in higher RMSE. The reason is that every parameter combination is not optimal for detecting the first path in the PDP. Interference is somewhat affecting the positioning accuracy and by using the information in Figure 4.1 and Figure 4.18 an explanation can be given. In the network planning *no interference* the average link SINR is always greater than -5 dB, meaning the TOA estimator will compute every TOA estimate with the smallest error possible. In *down up* a majority of the links are subject to SINR below -5 dB implicating more TOA estimates containing a larger error. When all signals are interfering every link except one have an SINR below -5 dB. The same reasoning is valid for the remaining deployments in the interference investigation. This is a justification to why the simulations with interference result in larger positioning errors.

When there is interference involved and only LOS measurements are used in the position estimation, there is no obvious difference in positioning accuracy compared to when all measurements are used, see Figure 4.16. The same result can be seen for the rest of the investigated deployments. This differs from the case with no interference because then the choice of measurements to include in the position estimation affected the positioning accuracy. With and without interference the LOS links correspond to the best measurements but when interference is present even the signals with LOS will interfere. Only utilising the LOS measurements when doing the position estimation will therefore not improve the accuracy when having interfering signals. In this case one might as well use both the LOS and NLOS measurements.

5.2 Indoor Factory

The results from the InF simulations is discussed in this section. The simulated positioning accuracy is evaluated and parallels to the IOO scenario are made. The last part contains an analysis of the impact of various amount of clutter on the positioning accuracy and if it can be improved by changing the BS deployment.

5.2.1 Simulated Positioning Accuracy

A first remark to be made concerning the InF study is that the behaviour of the different kinds of deployments follow the pattern as observed in IOO. With the same amount of BSs the standard deployments always result in the worst positioning accuracy, the edge deployment result in the best accuracy and the mixed deployment lie in between or perform equally good as the edge deployments. What also agrees is that increasing the number of BSs improves the positioning accuracy, but to a limited extent. The CDFs in Figure 4.29c show that the positioning accuracy is better in deployment 7, with 91 BSs, compared to deployment 5, with 36 BSs. At the 90 percentile the improvement in accuracy is a bit over 1 m, or 16.5% decrease in the horizontal positioning error, while the increment in number of BSs is 55, meaning more than twice as many. This tells us that the improvement in positioning accuracy will eventually saturate and the cost of adding BS will not lead to much better accuracy if a good BS geometry is chosen from the start.

It is clearly seen in Figure 4.19 that when only LOS measurements are used in the position estimation, the accuracy is significantly worse compared to when all measurements are used. This can be explained by a lack of UEs with a sufficient amount of LOS links and the analysis goes in line with the discussion held in Section 5.1.3. By looking at Figures 4.20 and 4.21 one can see a huge difference in the LOS statistics between InF-SH and InF-DH. In InF-DH, a majority of the UEs in both the standard and edge deployments do not have a single LOS link to a BS. As mentioned before, this will lead to a lot of CID based positioning which, in Figure 4.30, is proven to perform worse than DL-TDOA for every InF deployment. If the serving BS of a UE is not the closest one, the position estimate will be more inaccurate. This might be the case in InF-DH because of many clutters but since

the models are stochastic, and the clutters are not visualised, this could not be verified.

As in IOO, the standard deployments exhibit better LOS statistics than the edge deployments but the standard deployments still result in worse positioning accuracy compared to the edge deployments. This confirms that even in a more challenging environment the BS geometry has a bigger impact on the positioning accuracy than the number of LOS links.

5.2.2 Worst Position Estimates

The locations of the 10% of the UEs with largest positioning error for deployment 1–3 in InF-SH follow the same pattern as was discovered in the IOO study, meaning it is closely related to GDOP. In the standard deployment, with a large GDOP variation, they are located around the corners and along the short sides of the deployment area while in the edge and mixed deployments, with a more equal and consistent GDOP, they are distributed seemingly random. In InF-DH on the other hand, the worst UEs with respect to positioning error are distinctly located in groups, with some outliers, for all three deployments. Now the high clutter density plays a more important role than GDOP. This can be stated because deployment 1, for instance, has UEs with large positioning errors mostly concentrated to only one corner instead of all four corners as GDOP suggests.

To investigate if the positioning accuracy could be improved in InF-DH, additional BSs were deployed in a region in deployment 3 where multiple UE positions had been poorly positioned, see Figure 4.23. According to Table 4.8 it only resulted in modest improvements. Instead of being added, BSs were also moved in both deployments 2 and 3, see Figures 4.25 and 4.27. Table 4.28, presenting the results related to deployment 2, shows even less improvements when BSs are only moved. Based on these studies it can be said that a densely cluttered indoor environment is significantly more problematic from a positioning perspective.

5.3 Deployment Strategies for Positioning Accuracy and Availability

What has been observed during the IOO and InF investigations is that when the positioning accuracy improves, the availability generally improves as well, but there is a small trade-off between the two. A simple or sparsely cluttered environment does not pose as big of a problem in this aspect as opposed to a densely cluttered environment. In the latter case one deployment might, for example, have better positioning accuracy at the 90 percentile than another deployment, while on the other hand the last 10% of the UEs in the first deployment might have much larger positioning errors than the last 10% of the other. Here, one has to choose between providing higher positioning accuracy for a majority of the UEs or guaranteeing a smaller upper limit of the positioning error.

Given this, a deployment strategy to achieve both high positioning accuracy and availability in a simple environment is to deploy the BSs evenly around the

edges of the deployment area. Since there are not many obstacles inside the deployment area, a good BS geometry is of most importance and an edge deployment will fulfil this condition. In a more densely cluttered environment, and therefore increasingly problematic, the approach will differ somewhat. The best strategy is in this case to identify and strategically place some BSs in the most cluttered areas but still place a majority of the BSs around the edges of the deployment area. In this way, it is guaranteed to at least slightly improve both the positioning accuracy and availability.

6

Conclusions and Future Work

This chapter presents the final conclusions and topics for future work within this area.

6.1 Conclusions

In this thesis we have designed and investigated different network deployments in indoor environments in order to analyse their effect on position estimation accuracy and availability. Two questions were asked at the beginning of the thesis and the answers follow below.

1. *How does network deployment affect the position estimation accuracy and availability in two standard 3GPP scenarios when considering a limited number of deployments?*

By studying the IOO scenario we have been able to observe effects of various strength coming from number of BSs in the deployment, deployment geometry, LOS conditions and interference. An increasing number of BSs proved to always improve the positioning accuracy and availability. The deployment geometry is of surprisingly high importance and could, if planned well, achieve equal or better positioning accuracy than other deployments with a larger number of BSs. Better LOS conditions are favourable from a positioning perspective and improve the positioning accuracy. A final interesting finding is that if one has to choose between two deployments, one promoting deployment geometry and one promoting the number of LOS links, the choice should fall on the first option.

The study of the two InF scenarios highlighted the difficulty in achieving high accuracy and availability indoor positioning in a densely cluttered deployment area compared to a sparsely cluttered deployment area. The vital

factor was an immense lack of the number of LOS links which proved that decent LOS conditions are necessary for accurate positioning.

In the end, two deployment strategies are proposed. In order to achieve both high positioning accuracy and availability in a simple, sparsely cluttered environment, the strategy will be to deploy the BSs evenly around the edges of the deployment area. In a more problematic, densely cluttered environment, the approach will differ somewhat. The strategy will now be to identify and strategically place some BSs in the most cluttered areas but still place a majority of the BSs around the edges of the deployment area.

2. *How does orthogonality and resource consumption affect the position estimation accuracy and availability?*

In a simple, sparsely cluttered environment the position estimation accuracy and availability are affected by interference, but not necessarily to a great extent. With a robust DL-TDOA algorithm interference is handled well in a simple environment. The gain in positioning accuracy when allocating all available resources to obtain the maximum number of orthogonal PRSS is expensive compared to the slightly worse positioning accuracy obtained when some interference is allowed.

6.2 Future work

The work in this thesis put emphasis on finding factors affecting the positioning accuracy and availability, and then general deployment strategies were stated based on what was discovered. Only statistical models were considered but it would be interesting to study deterministic models as well, meaning, for instance, that clutter sizes and positions are known. This knowledge about the deployment area would enable investigations concerning how to deploy BSs in problematic areas where clutter creates unfavourable LOS conditions. It might, for example, be interesting to place different BSs at different heights within the deployment since all of them in this report had equal height.

In this thesis the main focus was on DL-TDOA positioning rather than RTT positioning since the simulation software did not completely support it. Another area of interest for future work would therefore be to further study RTT, and maybe additional positioning techniques as well, to determine if there are other alternative high performing positioning techniques available. Some positioning methods can possibly prove to be preferable in certain conditions.

The effect of interference was only briefly examined in the not so challenging IOO scenario where it showed to have limited impact on the positioning accuracy. Future work could include research on interference in different types of environments and to design clever network plannings allowing less number of orthogonal signals without a significant loss in positioning accuracy.

Constructing deployment strategies for different scenarios and environments can be seen as huge optimisation problems which have to be solved. Further work could involve developing tools and algorithms able to accept various deployment

related inputs, which then output BS positions yielding the best positioning accuracy and/or availability for the specific scenario.

Appendix

A

Additional Results

A.1 Indoor Open Office

A.1.1 Cramér-Rao Lower Bound

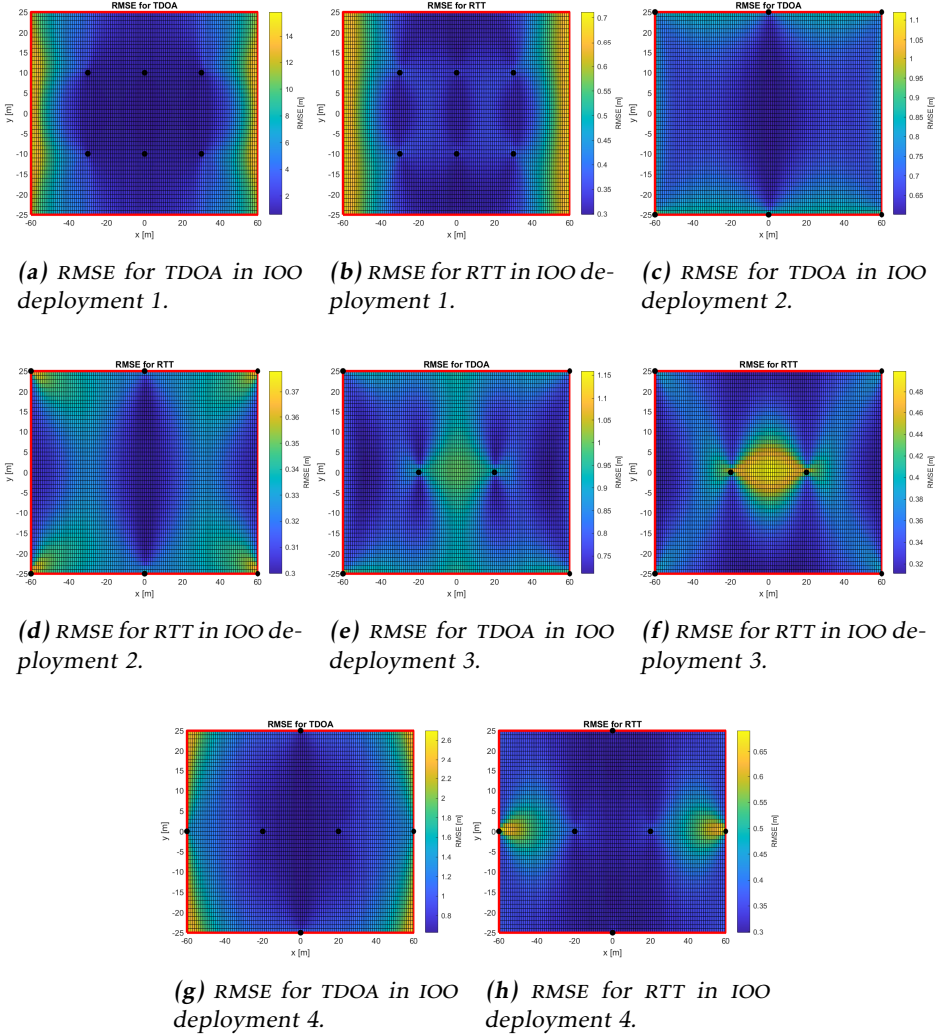


Figure A.1: Heat maps showing the RMSE of the position estimates using TDOA and RTT for IOO deployments 1–4 with 6 BSs each. The black dots represent the BSs and the red lines mark the boundaries of the deployment area.

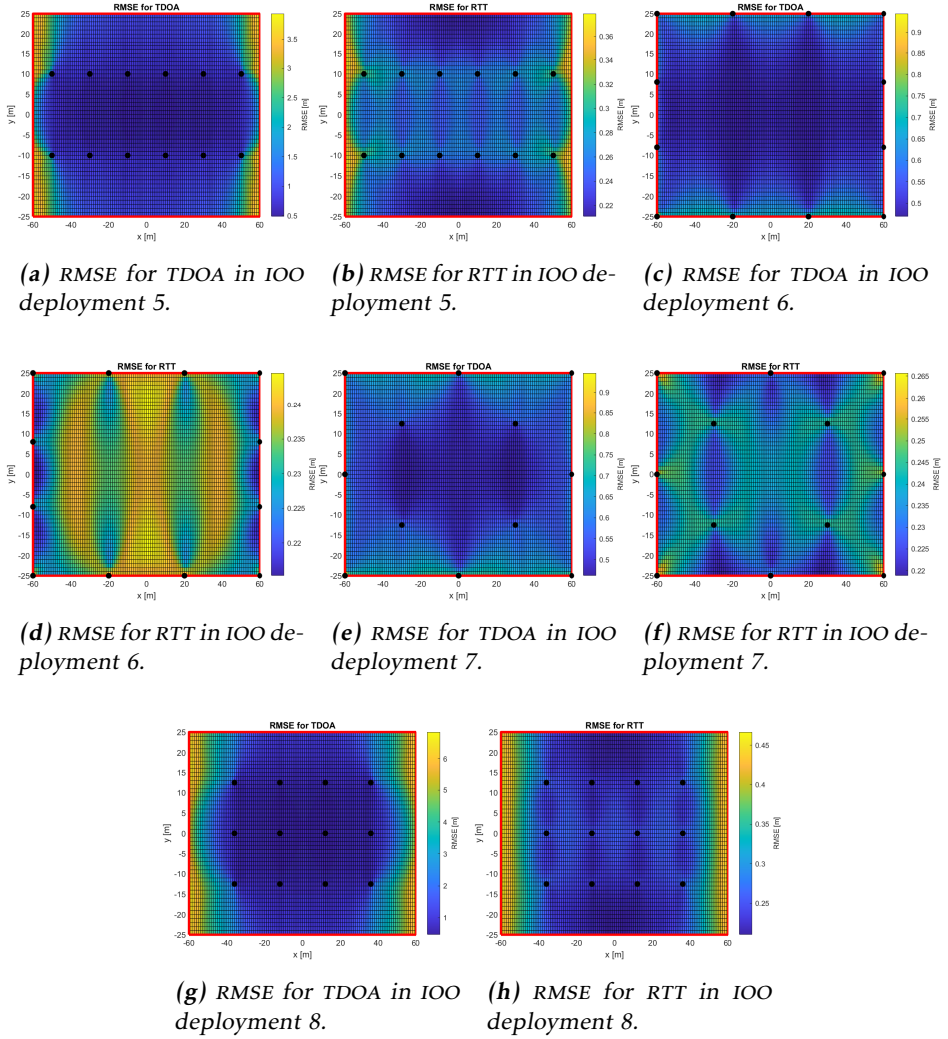


Figure A.2: Heat maps showing the RMSE of the position estimates using TDOA and RTT for IOO deployments 5–8 with 12 BSS each. The black dots represent the BSS and the red lines mark the boundaries of the deployment area.

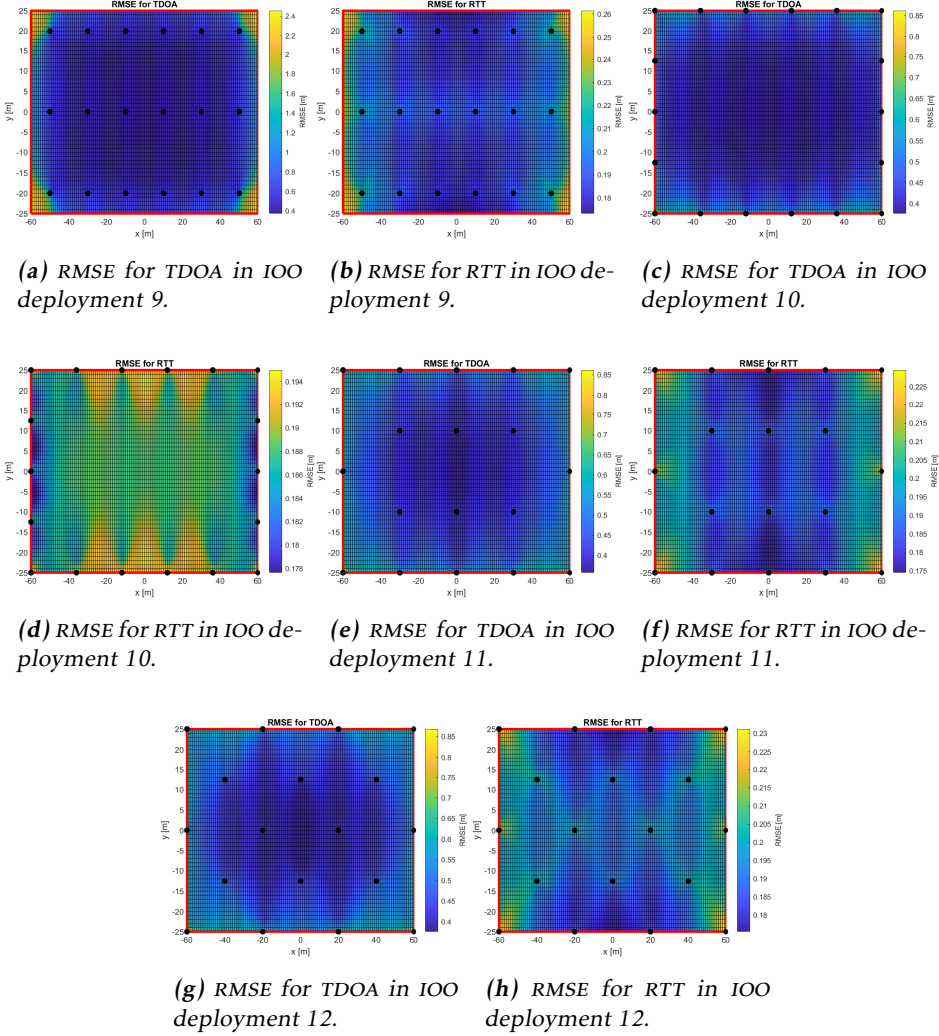


Figure A.3: Heat maps showing the RMSE of the position estimates using TDOA and RTT for IOO deployments 9–12 with 18 BSS each. The black dots represent the BSS and the red lines mark the boundaries of the deployment area.

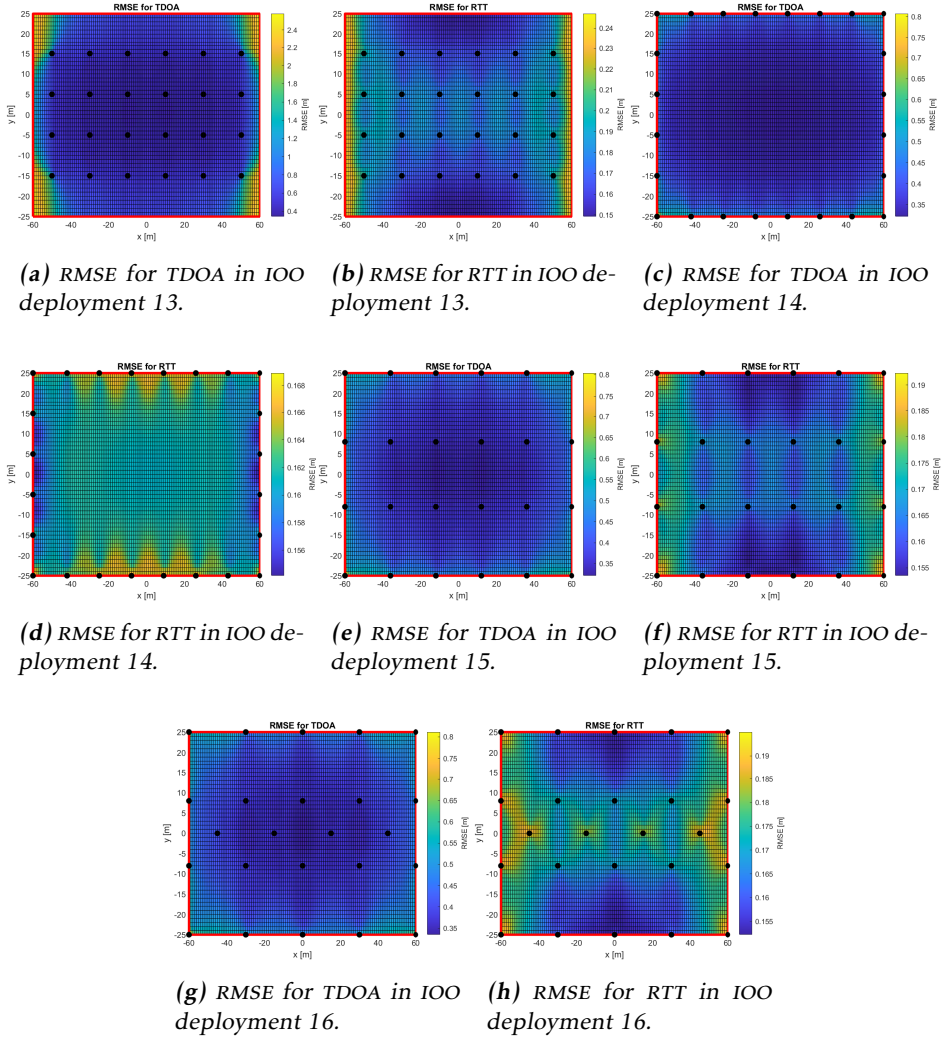


Figure A.4: Heat maps showing the RMSE of the position estimates using TDOA and RTT for IOO deployments 13–16 with 24 BSs each. The black dots represent the BSs and the red lines mark the boundaries of the deployment area.

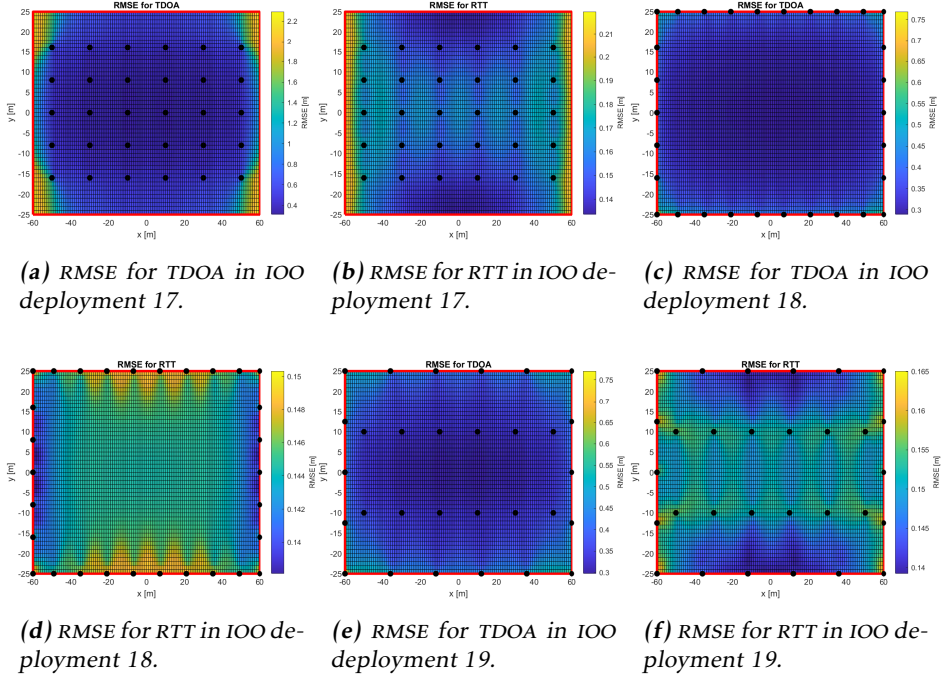


Figure A.5: Heat maps showing the RMSE of the position estimates using TDOA and RTT for IOO deployments 17–19 with 30 BSS each. The black dots represent the BSS and the red lines mark the boundaries of the deployment area.

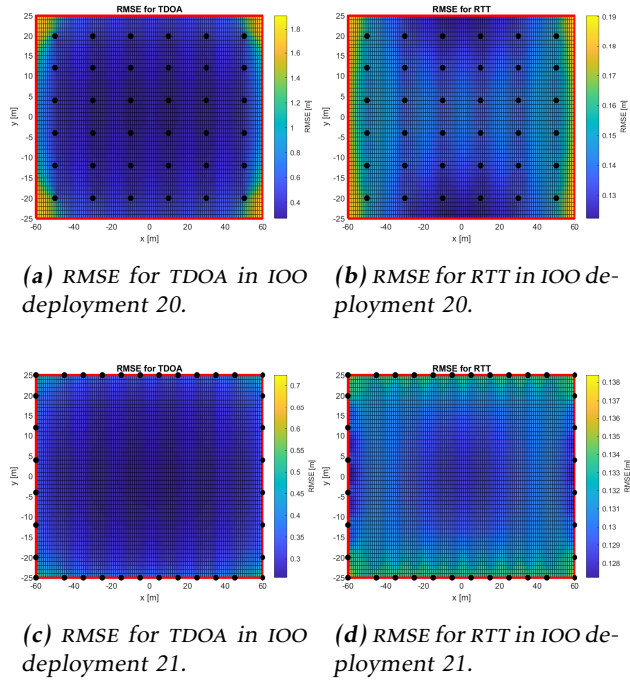
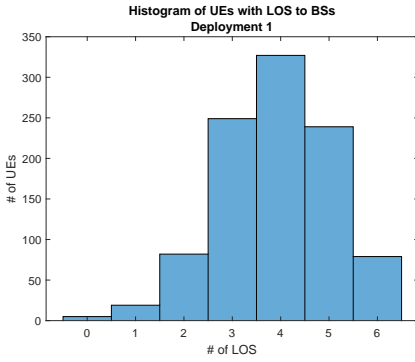
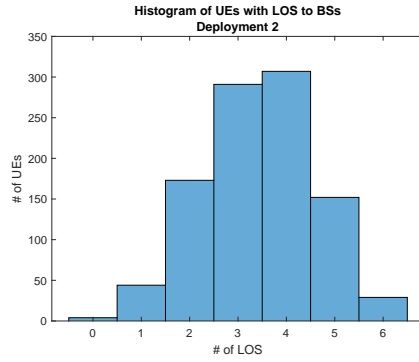


Figure A.6: Heat maps showing the RMSE of the position estimates using TDOA and RTT for IOO deployments 20–21 with 36 BSs each. The black dots represent the BSs and the red lines mark the boundaries of the deployment area.

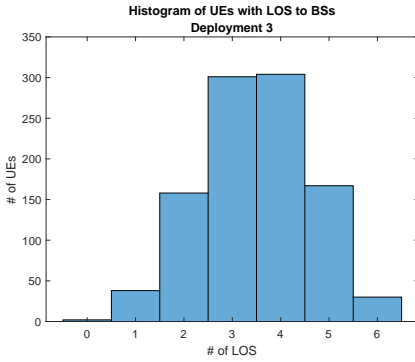
A.1.2 Line-Of-Sight



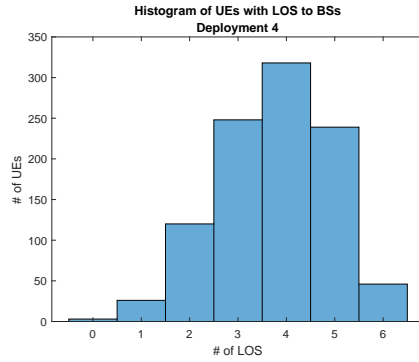
(a) IOO deployment 1.



(b) IOO deployment 2.

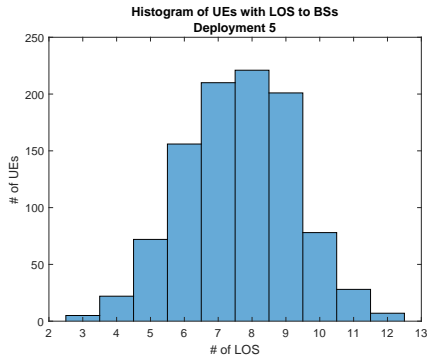


(c) IOO deployment 3.

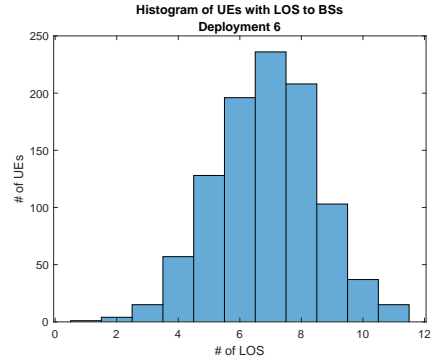


(d) IOO deployment 4.

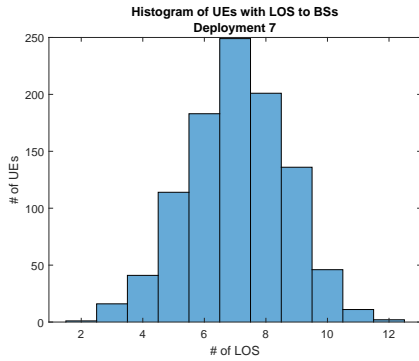
Figure A.7: Histograms showing the number of UEs with a certain number of LOS links to BSs for IOO deployments 1–4 with 6 BSs each.



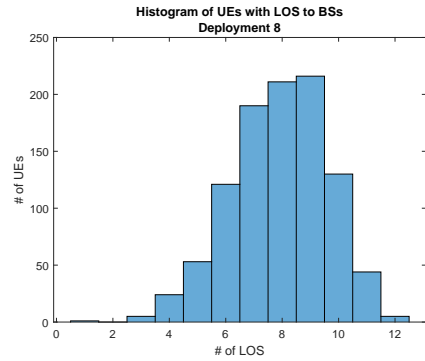
(a) 100 deployment 5.



(b) 100 deployment 6.

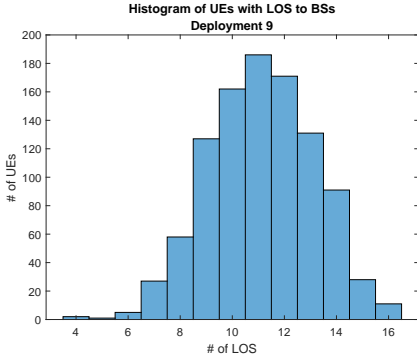


(c) 100 deployment 7.

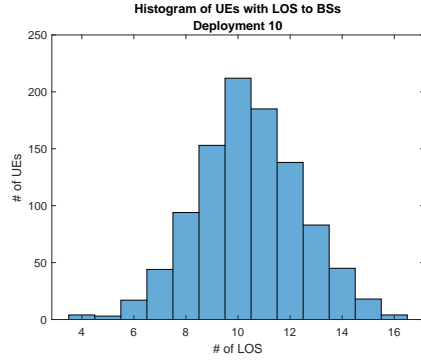


(d) 100 deployment 8.

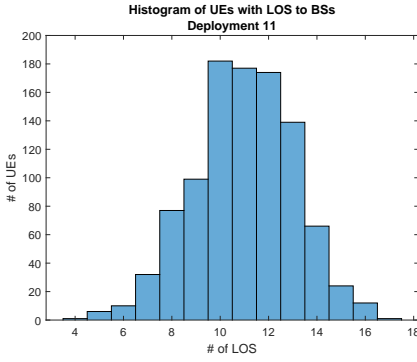
Figure A.8: Histograms showing the number of UEs with a certain number of LOS links to BSs for 100 deployments 5–8 with 12 BSs each.



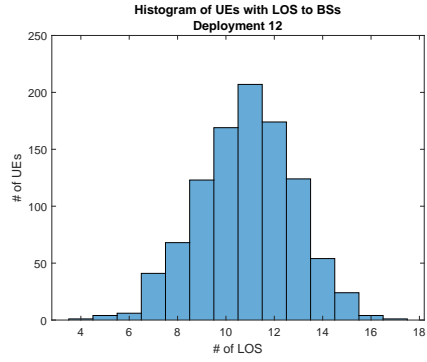
(a) IOO deployment 9.



(b) IOO deployment 10.

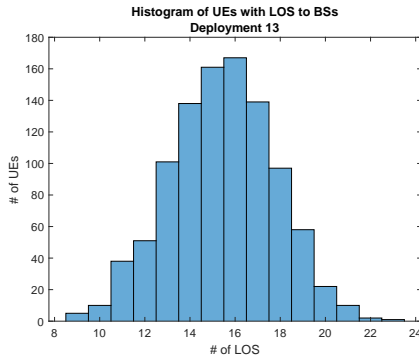


(c) IOO deployment 11.

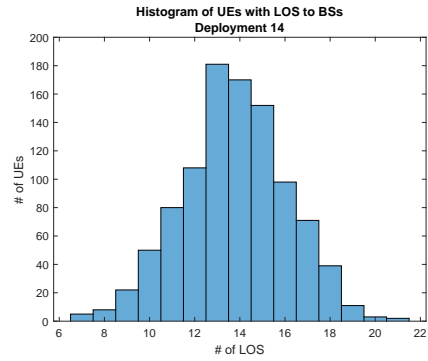


(d) IOO deployment 12.

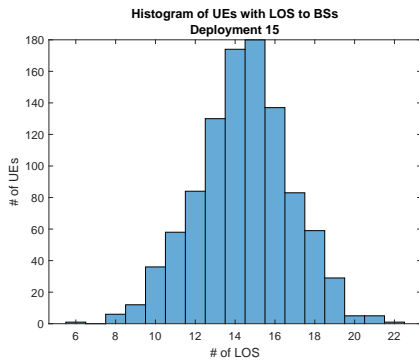
Figure A.9: Histograms showing the number of UEs with a certain number of LOS links to BSs for IOO deployments 9–12 with 18 BSs each.



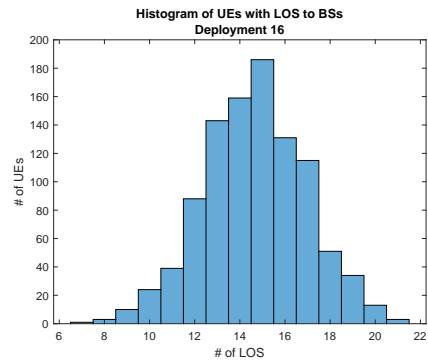
(a) IOO deployment 13.



(b) IOO deployment 14.



(c) IOO deployment 15.



(d) IOO deployment 16.

Figure A.10: Histograms showing the number of UEs with a certain number of LOS links to BSs for IOO deployments 13–16 with 24 BSs each.

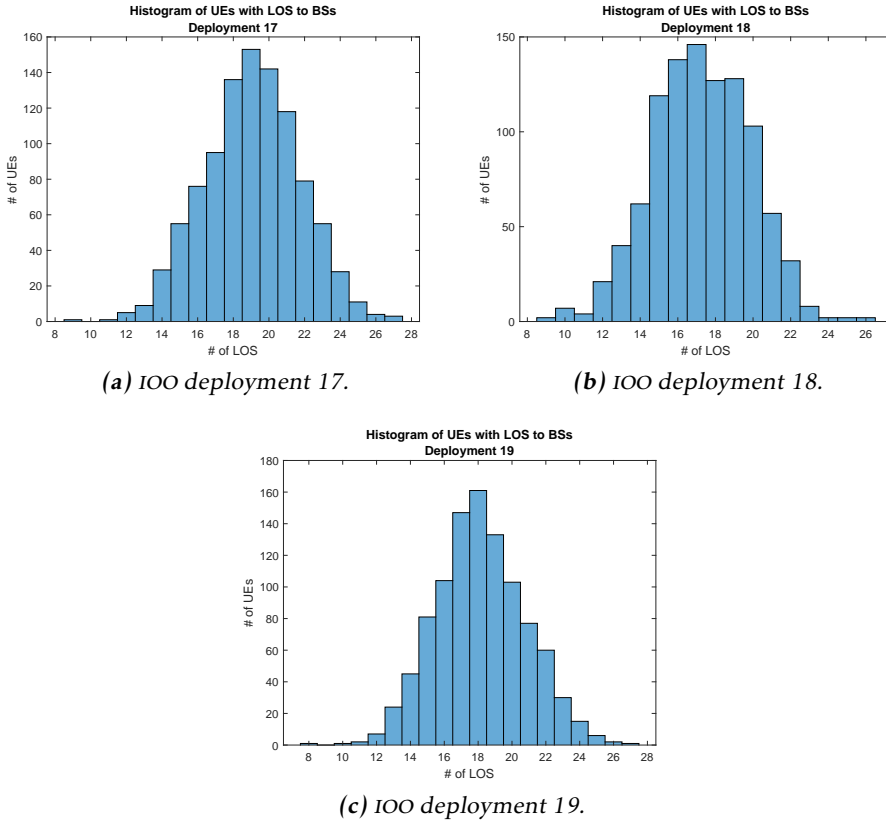


Figure A.11: Histograms showing the number of UEs with a certain number of LOS links to BSs for IOO deployments 17–19 with 30 BSs each.

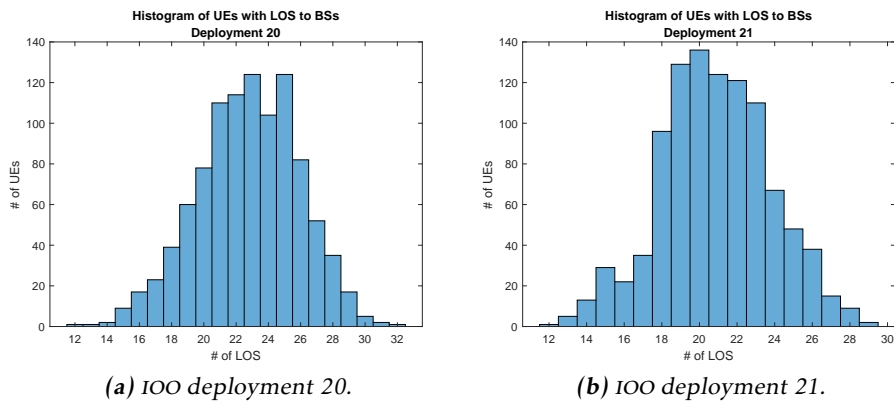
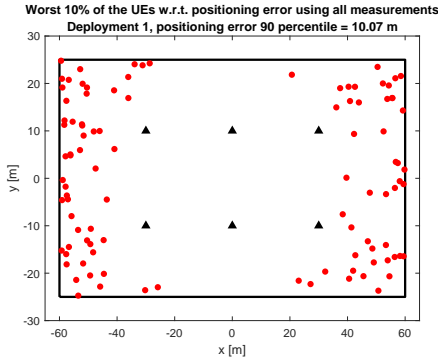
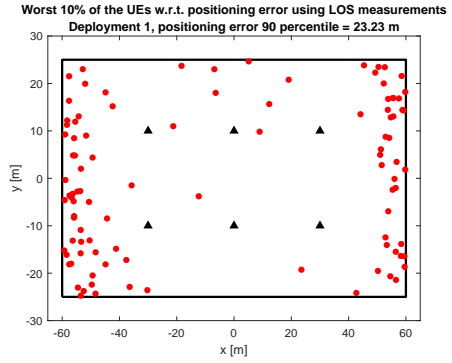


Figure A.12: Histograms showing the number of UEs with a certain number of LOS links to BSs for IOO deployments 20–21 with 36 BSs each.

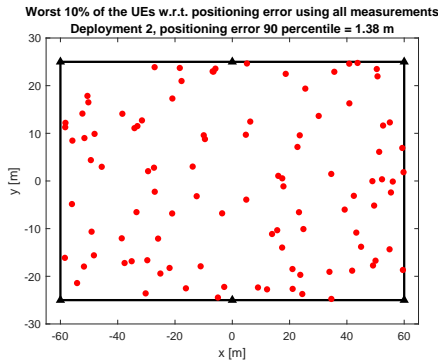
A.1.3 Worst Position Estimates



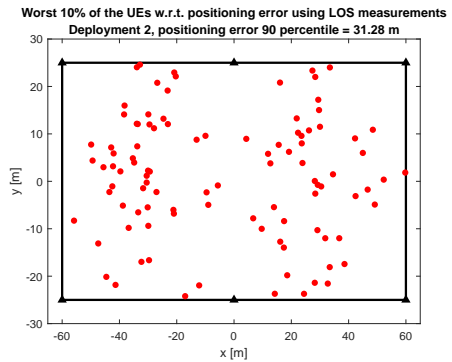
(a) IOO deployment 1 with a positioning error of 10.07 m at the 90 percentile. All measurements are used.



(b) IOO deployment 1 with a positioning error of 23.23 m at the 90 percentile. Only LOS measurements are used.

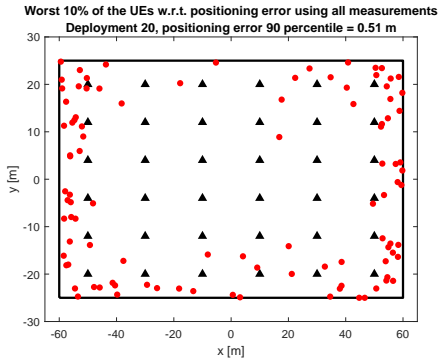


(c) IOO deployment 2 with a positioning error of 1.376 m at the 90 percentile. All measurements are used.

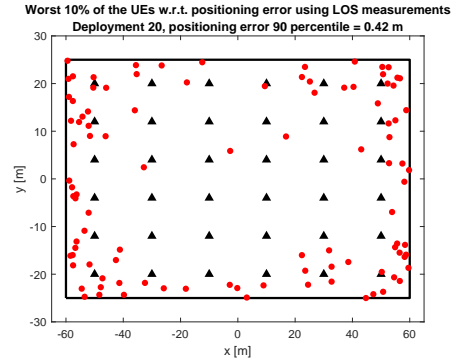


(d) IOO deployment 2 with a positioning error of 31.28 m at the 90 percentile. Only LOS measurements are used.

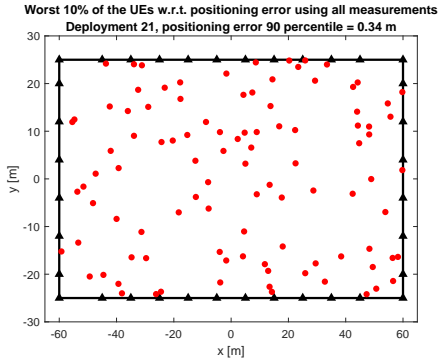
Figure A.13: Plots showing the positions of the worst 10% of the UEs with respect to positioning error, either using all measurements or only LOS measurements, for IOO deployments 1 and 2 with 6 BSs each. The red dots illustrate the UEs and the black dots represent the BSs.



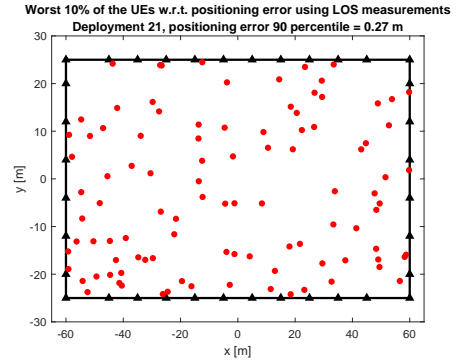
(a) 100 deployment 20 with a positioning error of 0.5057 m at the 90 percentile. All measurements are used.



(b) 100 deployment 20 with a positioning error of 0.4187 m at the 90 percentile. Only LOS measurements are used.



(c) 100 deployment 21 with a positioning error of 0.342 m at the 90 percentile. All measurements are used.



(d) 100 deployment 21 with a positioning error of 0.2677 m at the 90 percentile. Only LOS measurements are used.

Figure A.14: Plots showing the positions of the worst 10% of the UEs with respect to positioning error, either using all measurements or only LOS measurements, for 100 deployment 20 and 21 with 36 BSs each. The red dots illustrate the UEs and the black dots represent the BSs.

A.1.4 Interference

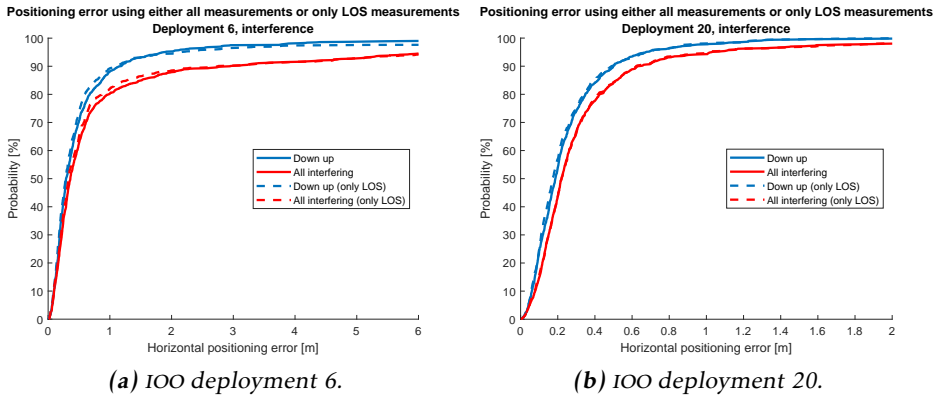
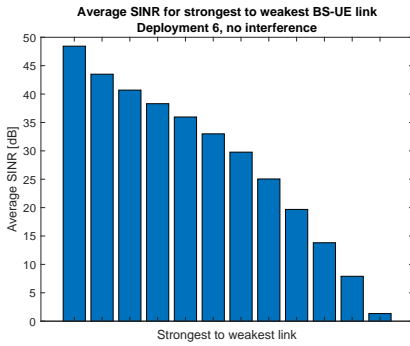
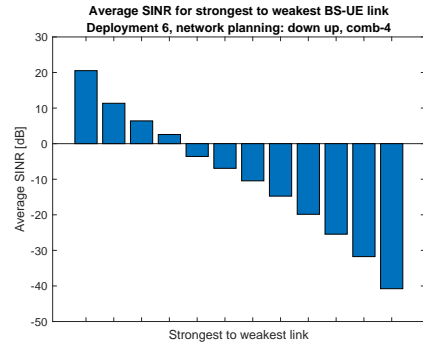


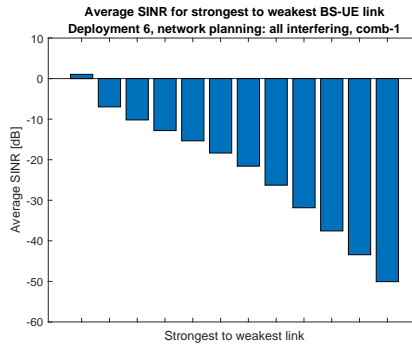
Figure A.15: CDFs showing the positioning error for 100 deployments 6 and 20 using the two different network planning down up and all interfering and either all measurements or only LOS measurements.



(a) 100 deployment 6 with network planning no interference.

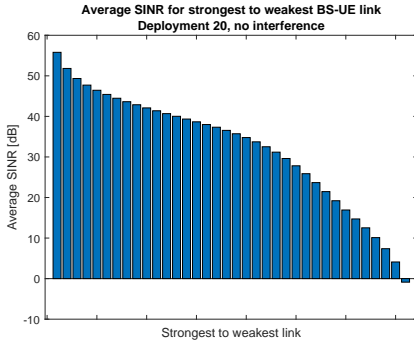


(b) 100 deployment 6 with network planning down up.

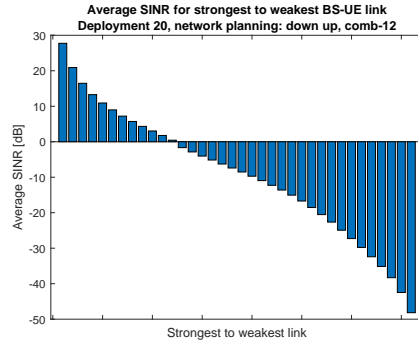


(c) 100 deployment 6 with network planning all interfering.

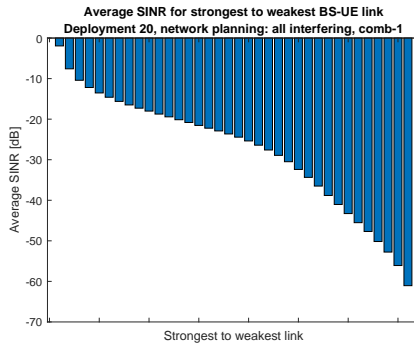
Figure A.16: Bar graphs showing average SINR for strongest to weakest BS-UE link for 100 deployment 6 when interference is disabled as well as when interference is present. The different network plans are no interference, down up and all interfering.



(a) 100 deployment 20 with network planning no interference.



(b) 100 deployment 20 with network planning down up.

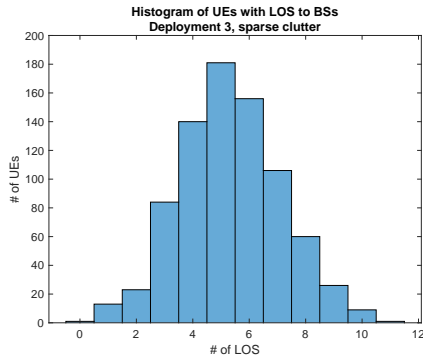


(c) 100 deployment 20 with network planning all interfering.

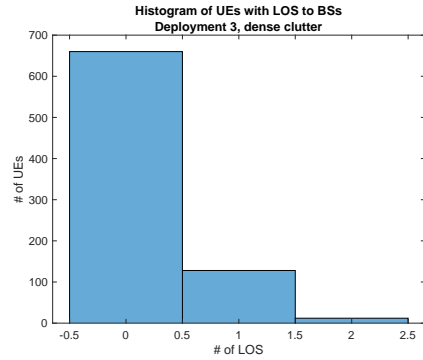
Figure A.17: Bar graphs showing average SINR for strongest to weakest BS-UE link for 100 deployment 20 when interference is disabled as well as when interference is present. The different network plannings are no interference, down up and all interfering.

A.2 Indoor Factory

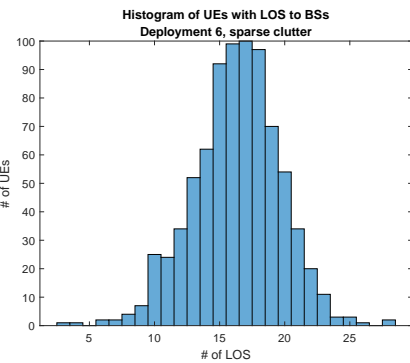
A.2.1 Line-Of-Sight



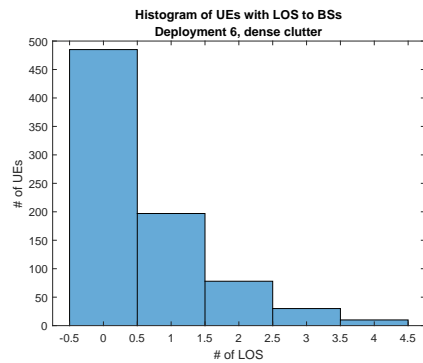
(a) InF deployment 3 in InF-SH.



(b) InF deployment 3 in InF-DH.



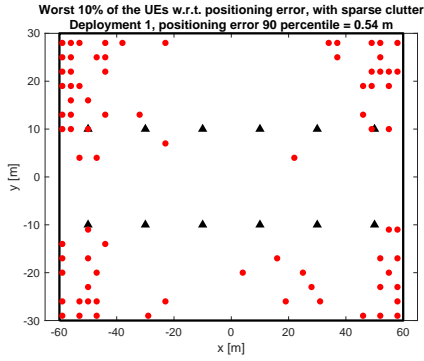
(a) InF deployment 6 in InF-SH.



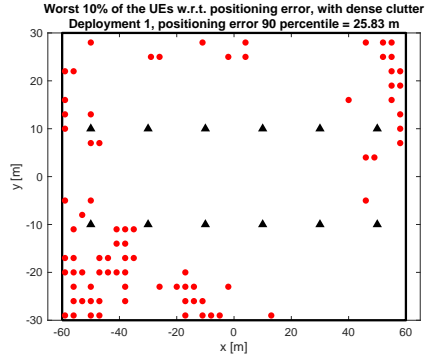
(b) InF deployment 6 in InF-DH.

Figure A.19: Histograms showing the number of UEs with a certain number of LOS links to BSs for InF deployment 6 in InF-SH and InF-DH.

A.2.2 Worst Position Estimates

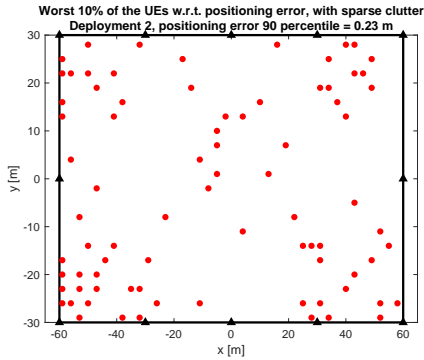


(a) InF deployment 1 in InF-SH with a positioning error of 0.54 m at the 90 percentile.

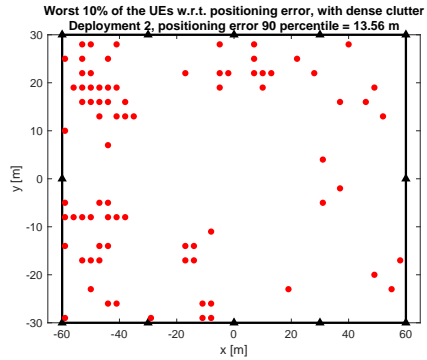


(b) InF deployment 1 in InF-DH with a positioning error of 25.83 m at the 90 percentile.

Figure A.20: Plots showing the positions of the worst 10% of the UEs with respect to positioning error, for InF deployment 1 in InF-SH and InF-DH. The red dots illustrate the UEs and the black dots represent the BSs.

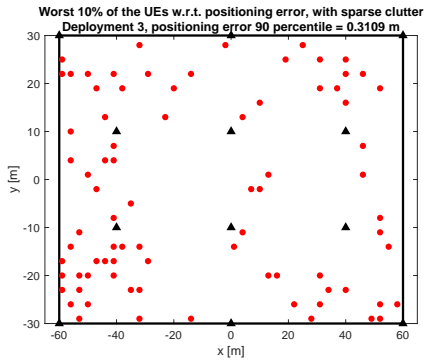


(a) InF deployment 2 in InF-SH with a positioning error of 0.23 m at the 90 percentile.

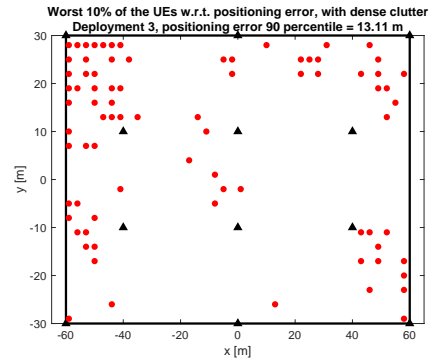


(b) InF deployment 2 in InF-DH with a positioning error of 13.56 m at the 90 percentile.

Figure A.21: Plots showing the positions of the worst 10% of the UEs with respect to positioning error, for InF deployment 2 in InF-SH and InF-DH. The red dots illustrate the UEs and the black dots represent the BSs.



(a) InF deployment 3 in InF-SH with a positioning error of 0.31 m at the 90 percentile.



(b) InF deployment 3 in InF-DH with a positioning error of 13.11 m at the 90 percentile.

Figure A.22: Plots showing the positions of the worst 10% of the UEs with respect to positioning error, for InF deployment 3 in InF-SH and InF-DH. The red dots illustrate the UEs and the black dots represent the BSs.

Bibliography

- [1] FCC 15-9. *Wireless E911 Location Accuracy Requirements*. fourth report and order. January 2015.
- [2] 3GPP TS 29.572. Location Management Services. Technical specification, March 2020.
- [3] 3GPP TR 38.855. Study on NR positioning support. Technical report, March 2019.
- [4] 3GPP TR 38.901. Study on channel model for frequencies from 0.5 to 100 GHz. Technical report, December 2019.
- [5] 3GPP TS 38.211. Physical channels and modulation. Technical specification, March 2020.
- [6] R. F. Brena, J. García-Vázquez, C. E. Galván-Tejada, D. Muñoz-Rodríguez, C. Vargas-Rosales, J. Fangmeyer Jr, and A. J. Palma. Evolution of Indoor Positioning Technologies: A Survey. *Journal of Sensors*, 2017, 03 2017. doi: 10.1155/2017/2630413.
- [7] J. Campos. Understanding the 5G NR Physical Layer. https://www.keysight.com/upload/cmc_upload/All/Understanding_the_5G_NR_Physical_Layer.pdf, 2017. Accessed: 2020-05-04.
- [8] J. A. del Peral-Rosado, J. A. López-Salcedo, G. Seco-Granados, F. Zanier, and M. Crisci. Analysis of Positioning Capabilities of 3GPP LTE. 2012.
- [9] J. A. del Peral-Rosado, R. Raulefs, J. A. López-Salcedo, and G. Seco-Granados. Survey of Cellular Mobile Radio Localization Methods: From 1G to 5G. *IEEE Communications Surveys Tutorials*, 20(2):1124–1148, Secondquarter 2018. ISSN 2373-745X. doi: 10.1109/COMST.2017.2785181.
- [10] S. Fischer. Observed Time Difference of Arrival (OTDOA) Positioning in 3GPP LTE. <https://www.qualcomm.com/media/documents/files/otdoa-positioning-in-3gpp-lte.pdf>, June 2014. Accessed: 2020-04-27.

- [11] S. Gezici, Z. Tian, G. B. Giannakis, H. Kobayashi, A. F. Molisch, H. V. Poor, and Z. Sahinoglu. Localization via Ultra-Wideband Radios: A look at positioning aspects for future sensor networks. *IEEE Signal Processing Magazine*, 22(4):70–84, July 2005. ISSN 1558-0792. doi: 10.1109/MSP.2005.1458289.
- [12] F. Gustafsson. *Statistical Sensor Fusion*. Studentlitteratur AB, third edition, 2018. ISBN 9789144127248.
- [13] F. Gustafsson and F. Gunnarsson. Mobile Positioning Using Wireless Networks: Possibilities and fundamental limitations based on available wireless network measurements. *IEEE Signal Processing Magazine*, 22(4):41–53, July 2005. ISSN 1558-0792. doi: 10.1109/MSP.2005.1458284.
- [14] S. M. Kay. *Fundamentals of Statistical Signal Processing: Estimation Theory*. Prentice-Hall, Inc., 1993. ISBN 0133457117.
- [15] R. Keating, M. Säily, J. Hulkkonen, and J. Karjalainen. Overview of Positioning in 5G New Radio. In *2019 16th International Symposium on Wireless Communication Systems (ISWCS)*, pages 320–324, 2019.
- [16] Inc. Keysight Technologies. Concepts of Orthogonal Frequency Division Multiplexing (OFDM) and 802.11 WLAN. http://rfmw.em.keysight.com/wireless/helpfiles/89600b/webhelp/subsystems/wlan-ofdm/Content/ofdm_basicprinciplesoverview.htm. Accessed: 2020-03-19.
- [17] N. Levanon. Lowest GDOP in 2-D scenarios. *Radar, Sonar and Navigation, IEE Proceedings -*, 147:149 – 155, 07 2000. doi: 10.1049/ip-rsn:20000322.
- [18] H. Liu, H. Darabi, P. Banerjee, and J. Liu. Survey of Wireless Indoor Positioning Techniques and Systems. *IEEE Transactions on Systems, Man, and Cybernetics, Part C (Applications and Reviews)*, 37(6):1067–1080, Nov 2007. ISSN 1558-2442. doi: 10.1109/TSMCC.2007.905750.
- [19] C. Mensing and S. Plass. Positioning Algorithms for Cellular Networks Using TDOA. In *2006 IEEE International Conference on Acoustics Speech and Signal Processing Proceedings*, volume 4, pages IV–IV, May 2006. doi: 10.1109/ICASSP.2006.1661018.
- [20] K. Radnosrati, F. Gunnarsson, and F. Gustafsson. New Trends In Radio Network Positioning. In *2015 18th International Conference on Information Fusion (Fusion)*, pages 492–498, July 2015.
- [21] S. M. Razavi, F. Gunnarsson, H. Rydén, Å. Busin, X. Lin, X. Zhang, S. Dwivedi, I. Siomina, and R. Shreevastav. Positioning in Cellular Networks: Past, Present, Future. In *2018 IEEE Wireless Communications and Networking Conference (WCNC)*, pages 1–6, April 2018. doi: 10.1109/WCNC.2018.8377447.

- [22] H. Rydén, S. M. Razavi, F. Gunnarsson, S. M. Kim, M. Wang, Y. Blankenship, A. Grövlén, and Å. Busin. Baseline Performance of LTE Positioning in 3GPP 3D MIMO Indoor User Scenarios. In *2015 International Conference on Localization and GNSS (ICL-GNSS)*, pages 1–6, June 2015. doi: 10.1109/ICL-GNSS.2015.7217158.
- [23] H. Rydén, A. A. Zaidi, S. M. Razavi, F. Gunnarsson, and I. Siomina. Enhanced Time of Arrival Estimation and Quantization for Positioning in LTE Networks. In *2016 IEEE 27th Annual International Symposium on Personal, Indoor, and Mobile Radio Communications (PIMRC)*, pages 1–6, Sep. 2016. doi: 10.1109/PIMRC.2016.7794634.
- [24] I. Sharp, K. Yu, and Y. J. Guo. GDOP Analysis for Positioning System Design. *IEEE Transactions on Vehicular Technology*, 58(7):3371–3382, 2009.
- [25] H. Soganci, S. Gezici, and H. V. Poor. Accurate Positioning in Ultra-Wideband Systems. *IEEE Wireless Communications*, 18(2):19–27, April 2011. ISSN 1558-0687. doi: 10.1109/MWC.2011.5751292.
- [26] D. J. Torrieri. Statistical theory of passive location systems. *IEEE Transactions on Aerospace and Electronic Systems*, AES-20(2):183–198, 1984.
- [27] J. Wennervirta and T. Wigren. RTT Positioning Field Performance. *IEEE Transactions on Vehicular Technology*, 59(7):3656–3661, Sep. 2010. ISSN 1939-9359. doi: 10.1109/TVT.2010.2054843.
- [28] Y. Wu and W. Y. Zou. Orthogonal frequency division multiplexing: a multi-carrier modulation scheme. *IEEE Transactions on Consumer Electronics*, 41(3):392–399, Aug 1995. ISSN 1558-4127. doi: 10.1109/30.468055.